

AD-A111 066

VIRGINIA POLYTECHNIC INST AND STATE UNIV BLACKSBURG D--ETC F/S 17/1
ADAPTIVE TARGET TRACKING OF UNDERWATER MANEUVERING TARGETS USIN--ETC(U)
DEC 81 R L MOOSE, T E DAILY, P M GODIWALA N00019-77-C-0164

UNCLASSIFIED

NL

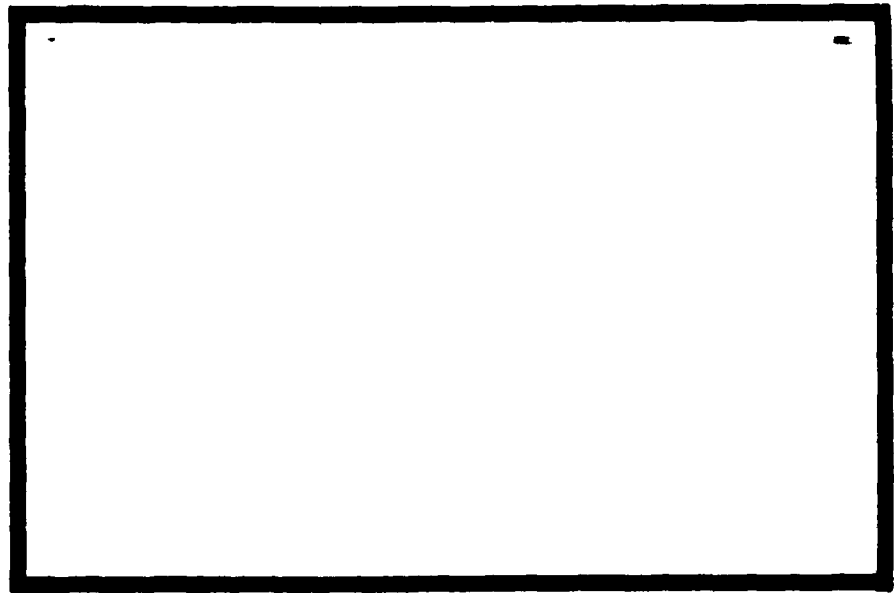
1 of 1
ADA
111066

END
DATE
FILMED
03-82
DTIC

2

LEVEL # ju

AD A111066



DTIC
ELECTE
FEB 18 1982

DTIC FILE COPY

DISTRIBUTION STATEMENT A
Approved for public release;
Distribution Unlimited

Virginia Polytechnic Institute and State University

Electrical Engineering
BLACKSBURG, VIRGINIA 24061

82 02 17067

ju

②

LEVEL III

Adaptive Target Tracking of Underwater
Maneuvering Targets Using
Passive Measurements (U)

Richard L. Moose
Principal Investigator

Research Assistants
Timothy E. Daily
Pankaj M. Godiwala

Sponsor: Naval Analysis Program, Office of Naval Research

ONR Contract Number N00014-77-C-0164

ONR Task Number NR 277-224

December 1981

Department of Electrical Engineering
Virginia Polytechnic Institute
and State University
Blacksburg VA 24061

DTIC
ELECTE
FEB 18 1982

B

Reproduction in whole or in part is permitted for any purpose of
the United States Government.

Approved for Public Release: Distribution Unlimited

Abstract

This report examines the problem of adaptively tracking a maneuvering target in two dimensional space using passive time delay measurements. The target is free to maneuver in velocity and to make depth changes at times unknown to the observer.

Tracking is accomplished by using the basic polar model of target and observer motion previously developed, and included in this report for the convenience of the reader. However, the important distinction is that now a nonlinear prefilter has been added to the tracking system. This leads to two major benefits: the first, is that the need for extended Kalman filters is completely eliminated which gives the tracking system a much larger degree of robustness than it previously had. The second benefit is a decoupling of the depth estimator from the polar range estimator, which considerably reduces the computational level of the adaptive tracking system.

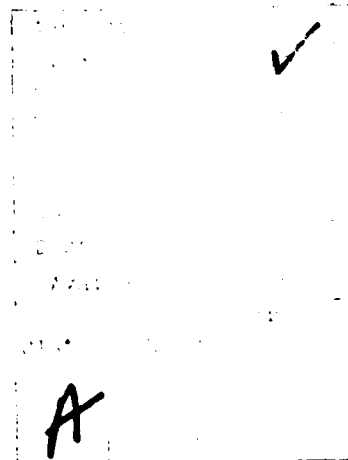


TABLE OF CONTENTS

CHAPTER 1	INTRODUCTION AND BASIC TARGET MODELING
CHAPTER 2	TWO DIMENSIONAL SYSTEM ANALYSIS AND DEVELOPMENT OF THE NONLINEAR PREFILTER
CHAPTER 3	STATISTICAL ANALYSIS OF THE LINEARIZED RANGE AND DEPTH MEASUREMENT ERRORS
CHAPTER 4	DEVELOPMENT AND SIMULATION RESULTS OF ADAPTIVE DEPTH ESTIMATOR
CHAPTER 5	DEVELOPMENT AND SIMULATION RESULTS OF ADAPTIVE RANGE ESTIMATOR
CHAPTER 6	CONCLUSION

Chapter 1

1.1 Introduction to Target Tracking

During the past several years much effort has been spent in the development of sophisticated digital filtering algorithms for tracking maneuvering targets. A common method has been to model the target dynamics in a rectangular coordinate system which results in a linear set of state equations, but forces the measurements to be nonlinear functions of the state variables. With this model an extended Kalman filtering algorithm is frequently used both to provide current state variable estimates and, by a one-step prediction process, to linearize the next measurement vector. This method works moderately well until the target makes an abrupt change in its trajectory in response to pilot or missile-guidance program commands. In this situation the velocity and position estimates can, and often do, diverge from the true unknown values. The inherent problems of this approach can lead to large bias errors and sometimes complete filter divergence.

Earlier work on the maneuvering target tracking problem includes Jazwinski's limited memory filtering [1], in which the filter gains are prevented from decaying to zero. Another technique, described by Thorp [2], involves switching between two Kalman filters in response to a detected maneuver. A third approach, due to Singer [3], models the target trajectory as a response of the target model to a time-correlated random acceleration. With this method additional

state variables are used to generate the correlated forcing functions which, in turn, increase the dimension of the Kalman filtering algorithm. In this manner the technique provides the filter with statistical information concerning target maneuvers based on an assumed range of possible accelerations. Singer's method was subsequently extended by many others.

Parallel to the effort was the method of modeling major changes in target trajectories by a semi-Markov process. An application of this approach to tracking maneuvering targets in two-dimensions by Moose [4] was successfully extended by Gholson and Moose [5] to three-dimensional tracking.

The general approach which uses the "adaptive semi-Markov maneuver model" of [4] and [5] implies a discretization of possible vehicle accelerations or velocities. The estimation algorithm then views the maneuvering vehicle as if it is responding to commands which are modeled by a semi-Markov process, i.e., a random process with a finite number of "states" (commands) which are selected according to the transition probabilities of a Markov process. A semi-Markov process differs from a Markov process in that the duration of time in one state prior to switching to another state is itself a random variable [6]. Incorporating the semi-Markov concept into a Bayesian estimator was done in [4] and [5]. This estimation algorithm provides a substantial improvement in filter stability, which means that large bias errors are prevented from being built up due to unmodeled target accelerations. An important aspect of this adaptive estimation algorithm is its elimination of a "growing memory" which is prevalent in many adaptive filters.

1.2 Target Modeling

With the brief history of the maneuvering target tracking problem presented in the previous section, we see a general progression in the sophistication of tracking filter design stemming primarily from the method in which the unknown target accelerations are modeled. This trend is graphically outlined in Figure 1.

Initially, target maneuvers were modeled as the response to uncorrelated, zero-mean variations about a nonaccelerating target, shown in Figure 1(A). As a result, the estimation algorithm could follow only those maneuvers which were comparable with the input noise level. Furthermore, the filtering results during nonmaneuvering situations were seriously degraded due to the uncorrelated input noise. As shown in Figure 1(B), Singer [3] attempted to model large-scale maneuvers by assuming a time-correlated input process and incorporating the statistics into the subsequent filter design. In Figure 1(C) large-scale target maneuvers were modeled as a stochastic process whose mean-value switched randomly from among a finite set of predetermined values. The adaptive estimation algorithm mentioned in the previous section could then be used to track the maneuvering target. This method was seriously restricted, however, by the requirement of a large number of preselected mean values in order to ensure convergence of the estimation process. It has been shown (6) that by combining the concepts illustrated in Figure 1(B) and Figure 1(C) the number of mean values required to prevent filter divergence is greatly reduced. This combination is illustrated in Figure 1(D). The primary benefit of this approach is the large saving in computational effort. An additional benefit, at least from a subjective viewpoint, is that the

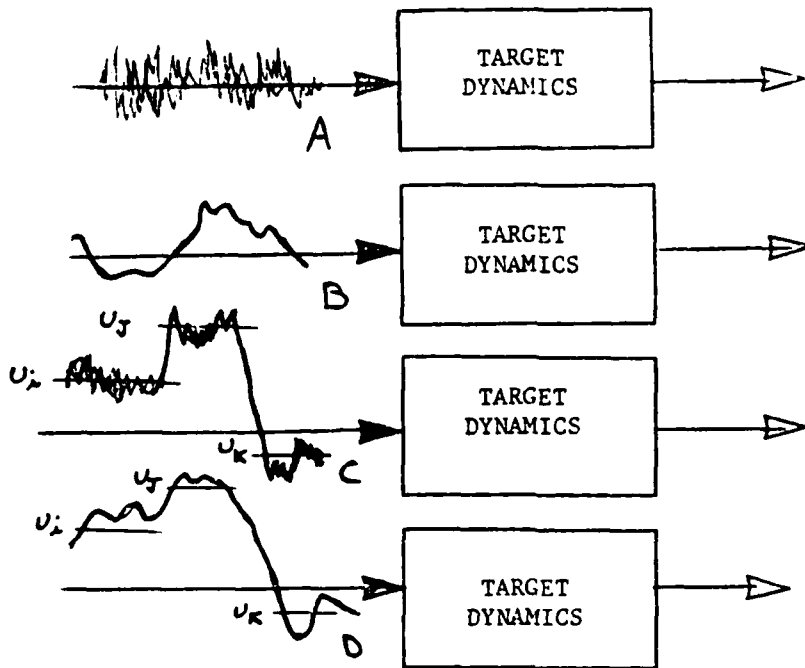


Figure 1. Historical development of maneuvering target model inputs. (A) Zero-mean white Gaussian plant disturbance. (B) Correlated, zero-mean plant disturbance. (C) White Gaussian noise with randomly switching mean. (D) Correlated Gaussian noise with randomly switching mean.

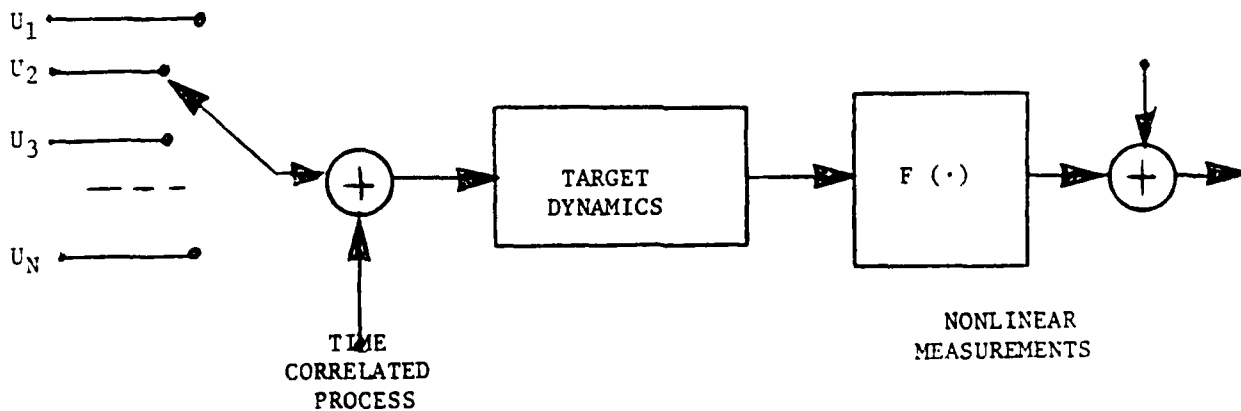


Figure 2. Target motion model.

time-correlated, randomly switching, mean-forcing function more adequately models real-world target maneuvers.

The basic target modeling ideas are shown in Figure 2. The target trajectory is generated by the random selection of an input time-correlated Gaussian process whose mean value u_i is applied to the target plant dynamics for a random duration of time. This input disturbance process lasts until a new input u_j is randomly chosen from among a finite set of n possible inputs. With this model as a background and using an appropriate choice of state variable equations to represent target dynamics, either submarine or aircraft, it is possible to develop an "optimal" (in the minimum mean-square error sense) tracking filter that adaptively learns, then quickly adjusts itself for each major alteration of target trajectory.

1.3 Incorporation of Singer Process into the Target Dynamics

In incorporating the correlated process, the linearized polar model of [6] is preserved. To this end, consider a target whose motion in rectangular coordinates is described by

$$\begin{aligned}\ddot{x} &= -\alpha\dot{x} + u_x + w'_x \\ \dot{w}'_x &= -\alpha w'_x + w_x\end{aligned}\tag{1.3.1}$$

where

α is a drag coefficient

u_x is the deterministic input in the x direction randomly chosen from a set of N possible inputs.

w'_x is the Singer correlated acceleration process acting in the x direction with a time constant $\tau_c = 1/\alpha$.

w_x is a white Gaussian random process acting in the x direction

A similar set of equations exists for the y and z directions.

Defining

$$x_1 = x$$

$$x_2 = \dot{x}$$

$$x_3 = w'_x$$

the following continuous time state variable model is obtained for

Equation (1.3.1)

$$\begin{bmatrix} \dot{x}_1 \\ \dot{x}_2 \\ \dot{x}_3 \end{bmatrix} = \begin{bmatrix} 0 & 1 & 0 \\ 0 & -\alpha & 1 \\ 0 & 0 & -a \end{bmatrix} \begin{bmatrix} x_1 \\ x_2 \\ x_3 \end{bmatrix} + \begin{bmatrix} 0 \\ 1 \\ 0 \end{bmatrix} u_x + \begin{bmatrix} 0 \\ 0 \\ 1 \end{bmatrix} w_x \quad (1.3.2)$$

Discretizing (1.3.2) in time yields

$$\begin{bmatrix} x_1 \\ x_2 \\ x_3 \end{bmatrix}_{k+1} = \begin{bmatrix} 1 & A & B \\ 0 & E & F \\ 0 & 0 & e^{-aT} \end{bmatrix} \begin{bmatrix} x_1 \\ x_2 \\ x_3 \end{bmatrix}_k + \begin{bmatrix} C \\ A \\ 0 \end{bmatrix} u_{x_k} + \begin{bmatrix} D \\ G \\ J \end{bmatrix} w_{x_k} \quad (1.3.3)$$

where

$$A = (1 - e^{-\alpha T})/\alpha$$

$$B = [1 + (\alpha e^{-\alpha T} - \alpha e^{-aT}) / (\alpha - a)] / (\alpha a)$$

$$C = (\alpha T - 1 + e^{-\alpha T})/\alpha^2$$

$$D = [T + (\alpha A - \alpha J)/(\alpha - a)]/(\alpha a)$$

$$E = e^{-\alpha T}$$

$$F = (e^{-\alpha T} - e^{-aT})/(\alpha - a)$$

$$G = (J - A)/\alpha - a$$

$$J = (1 - e^{-aT})/a$$

1.4 Development of the Polar Plant Model

The linearized polar model is developed using a modified version of the approximate modeling technique of Reference (5) except that now, the origin of the coordinate system is moving.

ρ CHANNEL MODEL

ρ_{k+1} calculation:

Referring to Figure 3.

$$\rho = [(x_s - x_o)^2 + (y_s - y_o)^2]^{1/2}$$

$$\frac{\partial \rho}{\partial x_s} = \frac{(x_s - x_o)}{\rho}$$

$$\frac{\partial \rho}{\partial x_o} = -\frac{(x_s - x_o)}{\rho}$$

(1.4.1)

$$\frac{\partial \rho}{\partial y_s} = \frac{(y_s - y_o)}{\rho}$$

$$\frac{\partial \rho}{\partial y_o} = -\frac{(y_s - y_o)}{\rho}$$

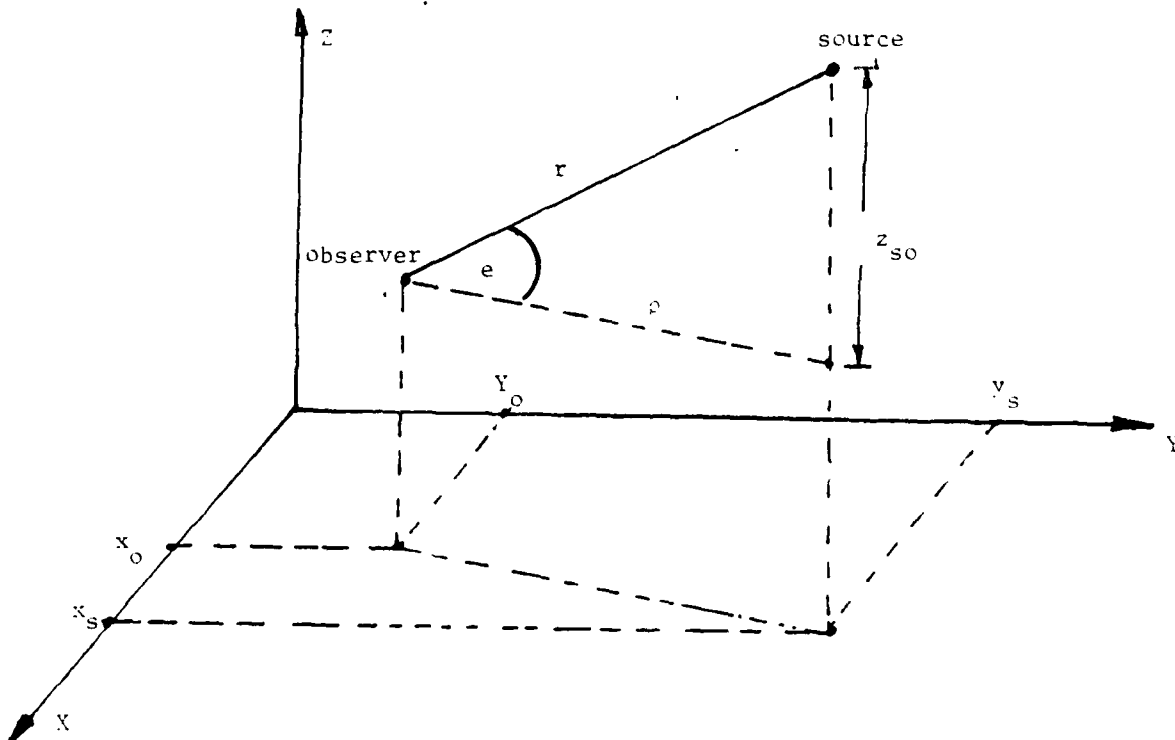


Figure 3. Geometry of the Observer-Source Scenario in Polar Coordinates

$$\dot{\rho} = \frac{(x_s - x_o)}{\rho} (\dot{x}_s - \dot{x}_o) + \frac{(y_s - y_o)}{\rho} (\dot{y}_s - \dot{y}_o) \quad (1.4.2)$$

ρ_{k+1} is expanded as follows keeping only the linear terms:

$$\begin{aligned} \rho_{k+1} = \rho_k + \frac{\partial \rho}{\partial x_s} \Big|_k (x_{s_{k+1}} - x_{s_k}) + \frac{\partial \rho}{\partial y_s} \Big|_k (y_{s_{k+1}} - y_{s_k}) \\ + \frac{\partial \rho}{\partial x_o} \Big|_k (x_{o_{k+1}} - x_{o_k}) + \frac{\partial \rho}{\partial y_o} \Big|_k (y_{o_{k+1}} - y_{o_k}) \end{aligned} \quad (1.4.3)$$

Assuming a linear drag model for the Source as given in (1.3.1), upon substituting (1.4.1) into (1.4.3) for the Source connected terms, and we get

$$(x_{k+1} - x_k) = Ax'_k + Bw'_{x_k} + Cu_{x_k}$$

$$\begin{aligned} \rho_{k+1} = \rho_k + \frac{(x_s - x_o)}{\rho} \Big|_k [Ax'_s + Bw'_{s_x} + Cu_{s_x} + Dw_{s_x}] \Big|_k \\ + \frac{(y_s - y_o)}{\rho} \Big|_k [Ay'_s + Bw'_{s_y} + Cu_{s_y} + Dw_{s_y}] \Big|_k \\ - \frac{(x_s - x_o)}{\rho} \Big|_k [x_{o_{k+1}} - x_{o_k}] - \frac{(y_s - y_o)}{\rho} \Big|_k [y_{o_{k+1}} - y_{o_k}] \end{aligned} \quad (1.4.4)$$

In the above equation and in all subsequent analysis, subscripts s and o refer to the Source and the Observer, respectively.

Now

$$(x_{o_{k+1}} - x_{o_k}) = \dot{x}_{o_k} T$$

and

$$(y_{o_{k+1}} - y_{o_k}) = \dot{y}_{o_k} T$$

(1.4.5)

Combining terms with like coefficients in (1.4.4) and making use of (1.4.5),

$$\begin{aligned}
\rho_{k+1} = & \rho_k + A \left[\frac{(x_s - x_o)}{\rho} \dot{x}_s + \frac{(y_s - y_o)}{\rho} \dot{y}_s \right] \Big|_k \\
& + B \left[\frac{(x_s - x_o)}{\rho} w'_{s_x} + \frac{(y_s - y_o)}{\rho} w'_{s_y} \right] \Big|_k \\
& + C \left[\frac{(x_s - x_o)}{\rho} u_{s_x} + \frac{(y_s - y_o)}{\rho} u_{s_y} \right] \Big|_k \\
& + D \left[\frac{(x_s - x_o)}{\rho} w_{s_x} + \frac{(y_s - y_o)}{\rho} w_{s_y} \right] \Big|_k \\
& - T \left[\frac{(x_s - x_o)}{\rho} \dot{x}_o + \frac{(y_s - y_o)}{\rho} \dot{y}_o \right] \Big|_k
\end{aligned}
\tag{1.4.6}$$

Consider the coefficient of B appearing in Equation (1.4.6)

$\frac{(x_s - x_o)}{\rho}$ and $\frac{(y_s - y_o)}{\rho}$ are the direction cosines between the X and Y axes, respectively, and the ρ direction. Hence

$$\frac{(x_s - x_o)}{\rho} w'_{s_x} + \frac{(y_s - y_o)}{\rho} w'_{s_y} \equiv w'_{s_\rho}
\tag{1.4.7}$$

is the sum of the projections of w'_{s_x} and w'_{s_y} onto the ρ direction. This sum acting in the ρ direction can be replaced by a single equivalent term denoted by w'_{s_ρ} . In a similar manner the coefficients of C and D are called u_{s_ρ} and w_{s_ρ} respectively. The coefficient of A in (1.4.6) represents the projection of the Source velocity onto the radial direction. This coefficient must be recast in a different formulation in order to complete the state model of (1.4.6). To this end Equation (1.4.2) is rewritten as follows:

$$\frac{(x_s - x_o)}{\rho} \dot{x}_s + \frac{(y_s - y_o)}{\rho} \dot{y}_s = \dot{\rho} + \frac{(x_s - x_o)}{\rho} \dot{x}_o + \frac{(y_s - y_o)}{\rho} \dot{y}_o \quad (1.4.8)$$

$$\text{using } \frac{(x_s - x_o)}{\rho} \dot{x}_o + \frac{(y_s - y_o)}{\rho} \dot{y}_o \equiv V_o \cos \beta_{so} \quad (1.4.9)$$

where V_o = observer velocity, β_{so} is the bearing between V_o and the target.

using 1.4.8 and 1.4.9 yields

$$\frac{(x_s - x_o)}{\rho} \dot{x}_s + \frac{(y_s - y_o)}{\rho} \dot{y}_s = \dot{\rho} + V_o \cos \beta_{so} \quad (1.4.10)$$

Substituting Equations (1.4.9) and (1.4.10) for the coefficients of T and A, respectively, in (1.4.6) and collecting like terms results in the following state variable model:

$$\rho_{k+1} = \rho_k + A \rho_k + B w'_{s\rho k} + C u_{s\rho k} + D w_{s\rho k} + (A-T)(V_o \cos \beta_{so}) \rho_k \quad (1.4.11)$$

A similar approach is taken to develop a state model for $\dot{\rho}_{k+1}$. By assuming that the Observer maintains a constant velocity for long periods of time, and that $w'_{s\rho}$ is a zero mean correlated GAUSSIAN random process acting in the ρ direction the following state equations are easily obtained.

$$\begin{bmatrix} \rho \\ \dot{\rho} \\ w'_{s\rho} \end{bmatrix}_{k+1} = \begin{bmatrix} 1 & A & B \\ 0 & E & F \\ 0 & 0 & e^{-aT} \end{bmatrix} \begin{bmatrix} \rho \\ \dot{\rho} \\ w'_{s\rho} \end{bmatrix}_k + \begin{bmatrix} C & (A-T) \\ A & (E-1) \\ 0 & 0 \end{bmatrix} \begin{bmatrix} u_{s\rho} \\ V_o \cos \beta_{so} \end{bmatrix}_k + \begin{bmatrix} D \\ G \\ J \end{bmatrix} w_{s\rho k} \quad (1.4.12)$$

The underlying constraint for the state model (1.4.12) requires that the Observer adopt a constant velocity profile.

Z Channel

Using a discretized version of the basic linearized drag model of Section 1.3, and letting d_T be the target depth the following state model is presented.

$$\begin{bmatrix} d_T \\ \dot{d}_T \\ w'_z \end{bmatrix}_{k+1} = \begin{bmatrix} 1 & A & B \\ 0 & E & F \\ 0 & 0 & e^{-aT} \end{bmatrix} \begin{bmatrix} d_T \\ \dot{d}_T \\ w'_z \end{bmatrix}_k + u_z \begin{bmatrix} C \\ A \\ 0 \end{bmatrix} + \begin{bmatrix} D \\ G \\ J \end{bmatrix} w_{z_k} \quad (1.4.13)$$

The state model is also subject to the constraint of a constant velocity observer.

It is interesting to observe that both state models (1.4.12) and (1.4.13) are identical although the types of manipulations involved in the derivations are quite different. For example, a Taylor series expansion is used to derive (1.4.12) whereas no such expansion is used in deriving (1.4.13).

2.1 Two Dimensional System Analysis

To develop the measurement equations use is made of Figure (4) below. Hassab (7) at NUSC developed the following set of equations for the difference in arrival times τ_1 and τ_2 . Where τ_1 represents the time delay difference between the direct path along (r) and the surface reflected path.

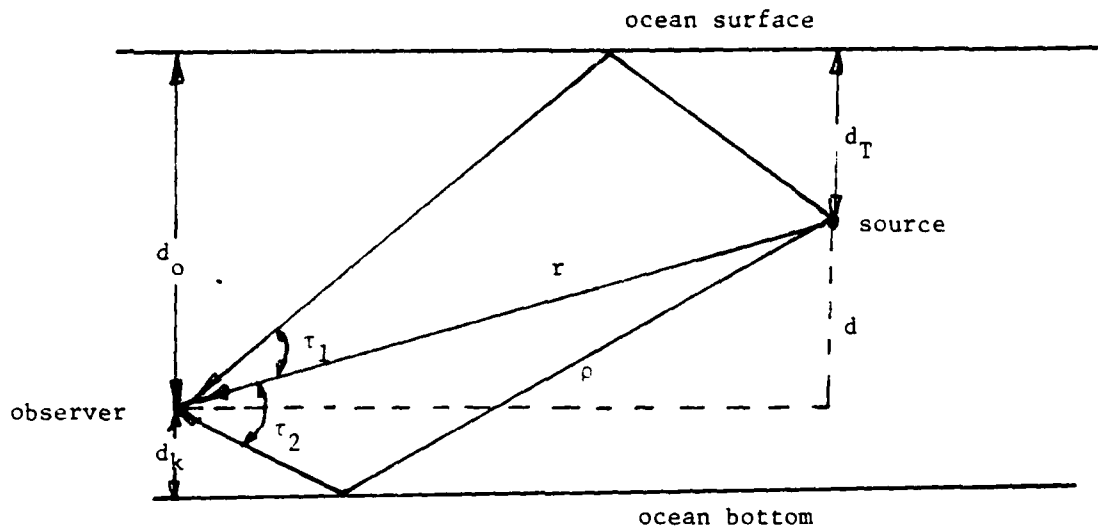


Figure 4. Two Dimensional (Range and Depth) Tracking Geometry

From Hassab we have:

$$\tau_1 = [(r^2 + 4 d_o^2 - 4 d_o d)^{1/2} - r]/C$$

$$\tau_2 = [(r^2 + 4 d_k^2 + 4 d_k d)^{1/2} - r]/C \quad (2.1.1)$$

$$\text{and } r^2 = \rho^2 + d^2$$

C = speed of sound in water

Now, by making the assumption that the square of target range (r^2) is much

larger than the observer depth squared (d_o^2) then τ_1 becomes, where ρ is the polar target range.

$$\tau_1 = \frac{2 d_o d_T}{\rho C} \quad (2.1.2)$$

If, in addition, we have the "shallow water ranging situation," i.e. that (d_k^2/r^2) is $\ll 1$. For example, if $r \geq 2.25 d_k$, our error of approximation is less than 1.4%, thus τ_2 becomes

$$\tau_2 = \frac{2 d_k (d_w - d_T)}{\rho C} \quad (2.1.3)$$

where d_w = total ocean depth.

Examining the set of equations 2.1.2 and 2.1.3, we see we have two non-linear algebraic equations in terms of our state variables ρ and d_T . At this point in the past, these equations were linearized in a Taylor's series expansion to yield a linear measurement of ρ and d_T . By doing this periodically in time, an extended Kalman filter tracking system (6) was developed and reported upon.

It was decided to eliminate the extended Kalman filters in order to reduce system complexity and computational burden, and to increase the *robustness* of the tracker against any possible filter divergence problems. This was done by developing the nonlinear prefilter discussed in the following section.

2.2 Development of the Nonlinear Prefilter

In order to *linearize* the time delay measurements, we notice that each is a nonlinear function of the system state variables polar range and target depth (ρ, d_T). By dividing τ_1 by τ_2 , and letting $a_o = (d_o/d_k)$ the ratio of observer depth to depth of water under the keel we have the following expression containing only d_T .

$$\frac{\tau_1}{\tau_2} = \frac{a_o d_T}{d_w - d_T}$$

Solving for d_T we get for the true target depth

$$d_T = \frac{\tau_1 d_w}{\tau_1 + a_o \tau_2} \quad (2.2.1)$$

To determine true target polar range ρ substitute equation (2.2.1) into equation 2.1.2 and solve for ρ . Defining the system parameter $(b_o) = 2 d_o d_w / C$ where d_w is ocean depth and C is the sound velocity, we get

$$\rho = \frac{b_o}{\tau_1 + a_o \tau_2} \quad (2.2.2)$$

In reality, we do not have τ_1 and τ_2 given to us but only the noisy set of measurements

$$z\tau_1 = \tau_1 + v_1 \quad (2.2.3)$$

$$z\tau_2 = \tau_2 + v_2$$

where v_1 and v_2 are Gaussian random processes with zero mean and variances σ_1^2 and σ_2^2 respectively. This results in the noisy set of measurements

$$zd_T = \frac{z\tau_1 d_w}{z\tau_1 + a_o z\tau_2} \quad (2.2.4)$$

$$z\rho = \frac{b_o}{z\tau_1 + a_o z\tau_2}$$

2.3 Measurement Linearization

Considering first the case of target depth, define the random process $v_d = (zd_T - d_T)$ to be the measurement error. Combining equations 2.2.1, 2.2.3 and 2.2.4 yields

$$v_d = \frac{(\tau_1 + v_1) d_w}{(\tau_1 + a_o \tau_2) + (v_1 + a_o v_2)} - \frac{\tau_1 d_w}{(\tau_1 + a_o \tau_2)}$$

or

$$v_d = \left(\frac{a_o d_w}{\tau_T} \right) \left(\frac{v_1 \tau_2 - v_2 \tau_1}{\tau_T + v_1 + a_o v_2} \right) \quad (2.3.1)$$

where $\tau_T = (\tau_1 + a_o \tau_2)$.

The target depth error term is thus the ratio of two Gaussian random processes x and y . The terms x and y are both sums and differences of the zero mean Gaussian processes v_1 and v_2 . Thus they are both strongly correlated, and in the case of the denominator y , nonzero mean, which becomes very important in determining the structure of the density function of v_d . From Figure (5) we see the structure of the linearized measurement $z d_T = (d_T + v_d)$.

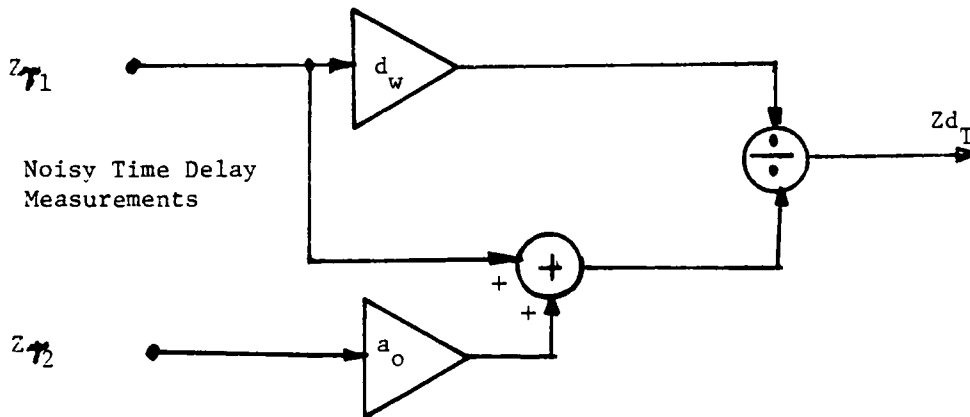


Figure 5. Nonlinear Prefilter for Target Depth Measurement

We now want to examine the measurement error v_o of the polar range equation $z_o = \rho + v_o$. Take the difference of equations 2.2.2 and 2.2.4, we find that

$$v_\rho = \frac{b_o}{(\tau_1 + a_o \tau_2) + (v_1 + a_o v_2)} - \frac{b_o}{(\tau_1 + a_o \tau_2)}$$

$$v_\rho = -\rho \frac{(v_1 + a_o v_2)}{(\tau_T + v_1 + a_o v_2)} \quad (2.3.2)$$

where $\tau_T = \tau_1 + a_o \tau_2$ and

$\rho = b_o / \tau_T$, the true polar range.

Equation 2.3.2 can be simplified considerably if we define the random process v_T to be $(v_1 + a_o v_2)$. Thus v_T is Gaussian, with zero mean and variance $\sigma_T^2 = \sigma_1^2 + a_o^2 \sigma_2^2$. The measurement error as shown in Figure (7) becomes

$$v_\rho = \frac{-\rho v_T}{v_T + \tau_T} \quad (2.3.3)$$

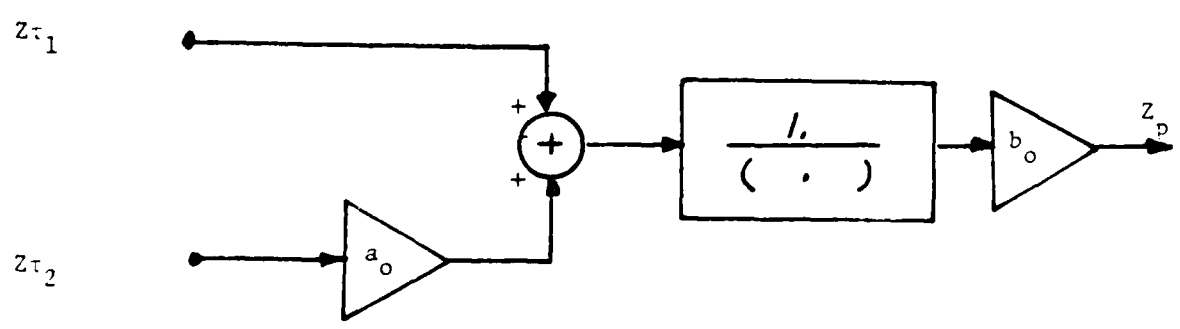


Figure 6. Nonlinear Prefilter for the Target Range Measurement

3.1 Statistical Analysis for Polar Range Measurement Error

Suppose we have a function $Y(x)$ given by $y = -ax/(x + k)$ where a and k are constants and x is a zero-mean Gaussian random process with variance σ^2 . If we sketch $Y(x)$, we see from Figure (7) that it is single valued in x . In other words, one value of x produces one unique value of y . However, there is a singularity at the point $x = -k$. In practice, there is a near-zero probability of x being in the vicinity of $-k$. For example, in shallow water with $a_0 = 1/2$, $\rho = 30,000$, $\tau_T = (9.6 + 77/2)$ msec and $\sigma_1 = \sigma_2$ equal to 5 msec, then $(-k)$ is 8.75 standard deviations away from 0. This means that the $\text{pr}[-9.25\sigma \leq x \leq 9.25\sigma] < 3.4 \times 10^{-16}$, however this number increases rapidly as target range increases.

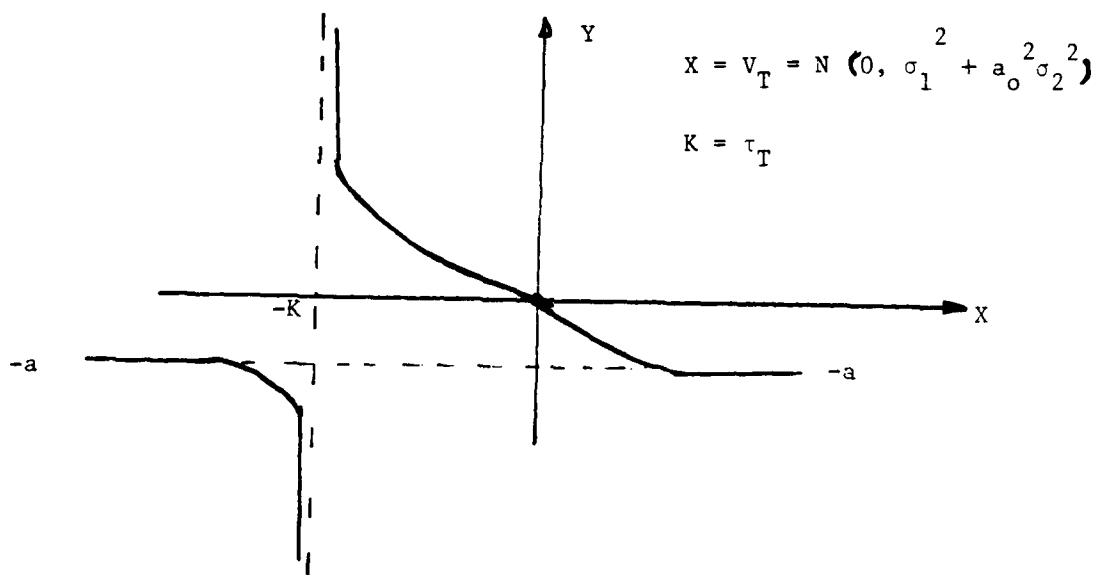


Figure 7. Plot of Nonlinear Transformation of a Gaussian Random Process

For the single valued functions $Y = g(x) = -a x/(x + k)$, the density on y , $P_2(y)$ is given by

$$P_2(y) = P_1[x = g^{-1}(y)] \left| \frac{dg^{-1}(y)}{dy} \right| \quad (3.1.1)$$

Letting $x = g^{-1}(y) = -ky/(y + a)$, and $P_1(x)$ the zero-mean Gaussian density results in

$$P_2(y) = \frac{ak}{\sigma\sqrt{2\pi} (y + a)^2} \exp \left[\frac{-k^2 y^2}{2\sigma^2 (y + a)^2} \right] \quad (3.1.2)$$

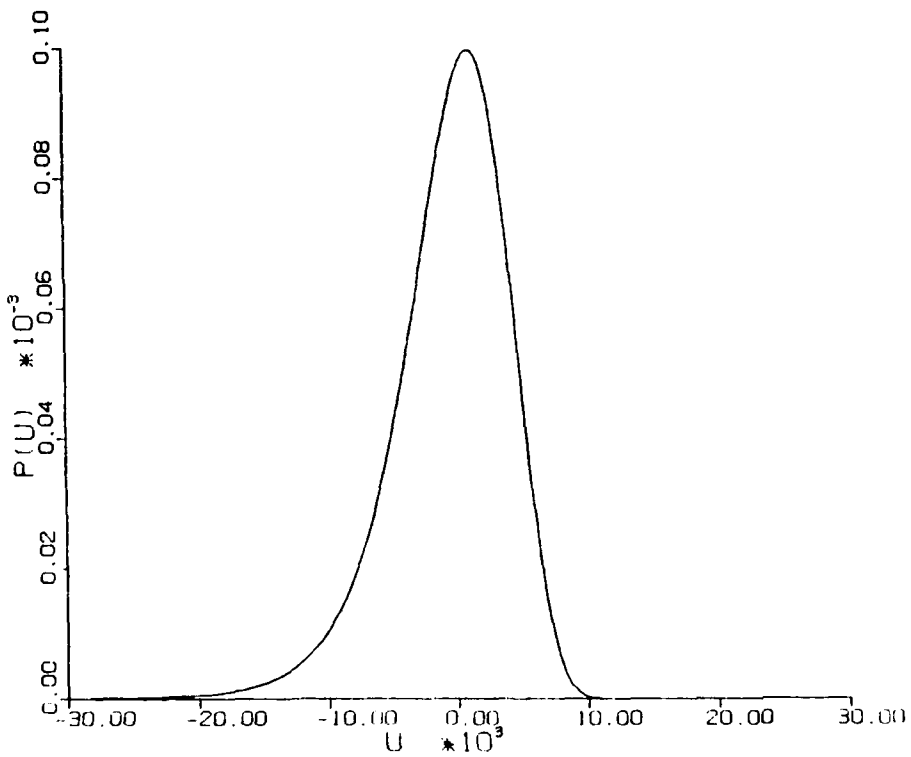
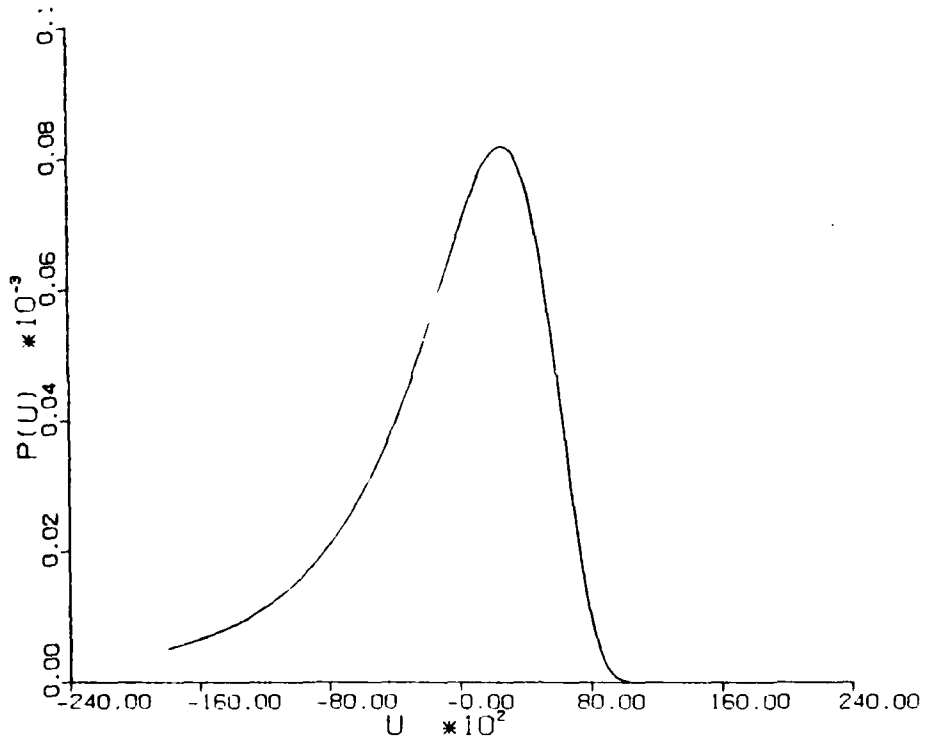
By making the substitutions $a = \rho$, $k = \tau_T$, $x = v_T$, $y = v_\rho$ the measurement error, and $\sigma_T^2 = (\sigma_1^2 + a_o^2 \sigma_o^2)$ we have for the density of the polar range measurement error

$$P_2(v_\rho) = \frac{\rho \tau_T}{\sigma_T \sqrt{2\pi} (\rho + v_\rho)^2} \exp \left[\frac{-\tau_T^2 v_\rho^2}{2\sigma_T^2 (\rho + v_\rho)^2} \right] \quad (3.1.3)$$

The nature of this density function is shown in the following figures for the target and observer at fixed depths, but closing in range.

It appears that the density function $P_2(v_\rho)$ given by equation (3.1.3) is of a form that does not appear in such complete sets of integrals as, Tables of Integrals, Series and Products, by GradshTeyn and Ryzhik, Academic Press, 1980. In addition, it does not seem likely that there is a closed form for the expected value ($v_\rho = -ax/(x + k)$), or for the expected value of $v_\rho^2 = a^2 x^2 / (x + k)^2$ where x is $N(0, \sigma^2)$. Thus one must use numerical integration in order to get an approximation for the mean and the variance of measurement error (v_ρ). Examining the density function, we see that it is a smooth continuous curve. As target range closes the mean and variance becomes smaller and the density becomes more and more symmetrical approaching a near Gaussian like density.

After several discussions with Dr. A. H. Nuttall of NUSC, New London, CT, it was decided to limit any measurements of ρ which exceeds a certain threshold. This would guarantee that the variance of the measurement error



Measurement Error Density Function for Closing Range

(Figure 7a)

v_ρ remain bounded and constant for fixed target range. This is due to the small, but finite probability (especially at long ranges of ρ) that $v_T(t_k)$ equal $-\tau_T(t_k)$ in equation (2.3.3) at some time t_k . In other words, it is possible that occasionally a bad data point will crop up and must be discarded. It was found that only a few stored values of $E(v_\rho)$ and $E(v_\rho^2)$ were needed in the tracking system as the target range closed.

3.2 Statistical Analysis of the Target Depth Measurement Error

Repeating the target depth measurement error equation 2.3.1, we have

$$v_d = \frac{a_o d_w (v_1 \tau_2 - v_2 \tau_1)}{\tau_T (\tau_T + v_1 + a_o v_2)}$$

where v_1 and v_2 are the statistically independent, zero mean, Gaussian measurement errors associated with measuring τ_1 and τ_2 .

Letting $x = (av_1 - bv_2)$ and $y = (\tau_T + v_1 + a_o v_2)$, we have $E(x) = 0$, $E(x^2) = \sigma_x^2 = (a^2 \sigma_1^2 + b^2 \sigma_2^2)$, and $E(y) = \tau_T$, $\sigma_y^2 = (\tau_1^2 + a_o^2 \sigma_2^2)$. Now define (r) to be the correlation coefficient of the linearly related random variables (x) and (y) . It will be assumed in this section that r is known and will be developed later in this report. The joint density function $P_1(x,y)$ for correlated Gaussian random variables x and y becomes

$$P_1(x,y) = \alpha \exp \left[-\beta \left(\frac{x^2}{\sigma_x^2} - \frac{2rx(y - \bar{y})}{\sigma_x \sigma_y} + \frac{(y - \bar{y})^2}{\sigma_y^2} \right) \right] \quad (3.2.1)$$

where: $r = \frac{E(xy)}{\sigma_x \sigma_y}$

$$\bar{y} = E(y)$$

$$\alpha = \left(2\pi \sigma_x \sigma_y \sqrt{1 - r^2} \right)^{-1}$$

$$\beta = (2(1 - r^2))^{-1}$$

Now let z equal x/y where the joint density function $P(x,y)$ is the known Gaussian distribution of (3.2.1). In order to find the density function of z , we need to identify the region of the x,y plane that is valid. To do this, let z_0 be any possible value of z . Then for the probability of $z = \left(\frac{x}{y}\right) \leq z_0$, we have two regions - the first for y positive, yields $x \leq yz_0$, and the second for y negative results in $x \geq yz_0$. Using Figure (8), the probability becomes for Region I and II

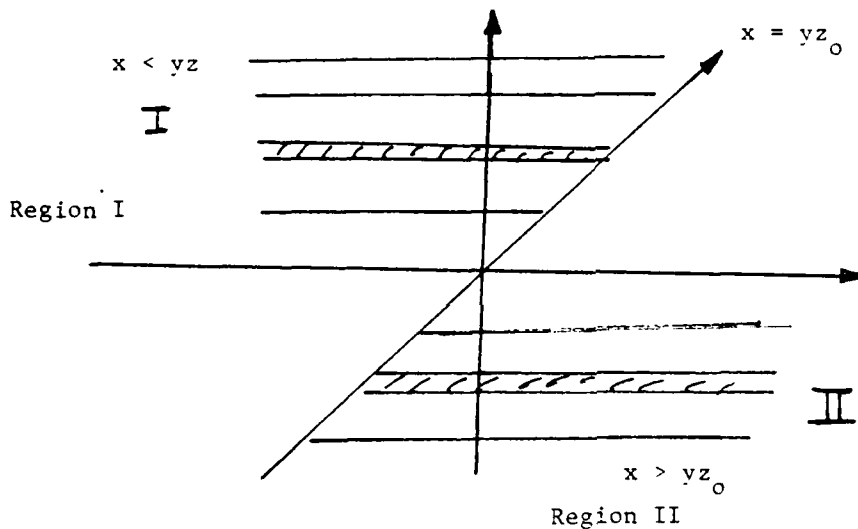


Figure 8. The Regions of Interest for $Z = X/Y$

$$P_R[z \leq z_0] = \int_0^{\infty} \int_{-\infty}^{z_0 y} P_1(x,y) dx dy + \int_{-\infty}^0 \int_{z_0 y}^{\infty} P_1(x,y) dx dy \quad (3.2.2)$$

To get the probability density functions $P(z_0)$, we must differentiate the cumulative probability distribution of equation 3.2.2. When we do this, and make the substitution $z_0 = z$, we have

$$P(z) = \int_0^{\infty} y P_1(yz, y) dy - \int_{-\infty}^0 y P_1(yz, y) dy \quad (3.2.3)$$

where $P_1(x = yz, y)$ is the joint density of x, y with yz substituted for x .

The first integral (I_1) becomes

$$I_1 = a \int_0^{\infty} y \exp \left[-\beta \left[\frac{y^2 z^2}{\sigma_x^2} - \frac{2ryz}{\sigma_x \sigma_y} (y - \bar{y}) + \frac{(y - \bar{y})^2}{\sigma_y^2} \right] \right] dy$$

Expanding, collecting terms, and letting

$$a = \left(\frac{\beta z^2}{\sigma_x^2} - \frac{2r\beta z}{\sigma_x \sigma_y} + \frac{\beta}{\sigma_y^2} \right)$$

$$b = \frac{2\bar{y}\beta}{\sigma_x \sigma_y} \left(rz - \frac{\sigma_x}{\sigma_y} \right) \quad (3.2.4)$$

I_1 becomes:

$$I_1 = \alpha e^{-\frac{\beta \bar{y}^2}{\sigma_y^2}} \int_0^{\infty} y e^{-(ay^2 + by)} dy \quad (3.2.5)$$

Noting that $\int_0^{\infty} y e^{-(ay^2 + by)} dy = \frac{1}{2a} \left[1 - be^{\frac{b^2}{4a}} \sqrt{\frac{\pi}{a}} \int_{\frac{b}{\sqrt{2a}}}^{\infty} \frac{e^{-t^2}}{\sqrt{2\pi}} dt \right]$ and that the

right hand integral is the standard normalized Gaussian probability integral

$1 - F\left(\frac{b}{\sqrt{2a}}\right)$ we have for I_1

$$I_1 = \frac{\alpha}{2a} e^{-\frac{\beta \bar{y}^2}{\sigma_y^2}} \left[1 - be^{\frac{b^2}{4a}} \sqrt{\frac{\pi}{a}} \left(1 - F\left(\frac{b}{\sqrt{2a}}\right) \right) \right] \quad (3.2.6)$$

Likewise for I_2

$$I_2 = -\frac{\alpha}{2a} e^{-\frac{\beta \bar{y}^2}{\sigma_y^2}} \left[1 + be^{\frac{b^2}{4a}} \sqrt{\frac{\pi}{a}} F\left(\frac{b}{\sqrt{2a}}\right) \right] \quad (3.2.7)$$

Combining equations 3.2.3, 3.2.6 and 3.2.7, we have for the density function of z

$$P(z) = \frac{\alpha e^{-\frac{\beta \bar{y}^2}{\sigma_y^2}}}{a} \left[1 + be^{\frac{b^2}{4a}} \sqrt{\frac{\pi}{a}} F\left(\frac{b}{\sqrt{2a}} - \frac{1}{2}\right) \right] \quad (3.2.8)$$

where α , β are defined in 3.2.1, and a , b in equation 3.2.4.

To get a physical feel for the form of the density function $P(z)$ where $z = x/y$, if we let $E(y) = \bar{y} = 0$ then $b = 0$, and $P(z)$ reduces to the following when β is replaced by $(2 - 2r^2)^{-1}$

$$P(z) = \frac{\alpha}{a} = \frac{\sigma_x \sigma_y \sqrt{1 - r^2}}{\pi \left[\sigma_y^2 \left(z - \frac{r x}{\sigma_y} \right)^2 + \sigma_x^2 (1 - r^2) \right]} \quad (3.2.9)$$

This has the form of the familiar Cauchy density function centered at $z = \frac{r x}{\sigma_y}$. Unfortunately, in our case $\bar{y} = \tau_T$ which is the weighted sum of time delays $\tau_1 + a_0 \tau_2$, and this is never zero.

If we now look at the first term of $P(z)$ in 3.2.8, we see that the Cauchy density is *weighted* by the term $\exp \left[- \frac{\beta y^2}{\sigma_y^2} \right]$. Now by taking the integral of the entire first term with respect to z we have just the previously mentioned exponential term for its contribution to the total probability distribution of z . If this contribution is large (near unity) then the second part of equation 3.2.8 contributes little, and $P(z)$ is nearly a Cauchy density. In order to compute this weight we must go back and determine the correlation coefficient r .

3.3 Determination of Correlation r in Target Depth Measurement Error

The additive measurement error v_d was previously found to be

$$v_d = \frac{a_0 d_w (\tau_2 v_1 - \tau_1 v_2)}{\tau_T (\tau_T + v_1 + a_0 v_2)}$$

When we originally substituted $z = x/y$, we let x be a Gaussian process given by $\frac{a_0 d_w}{\tau_T} (\tau_2 v_1 - \tau_1 v_2)$, and y also Gaussian is given by $(\tau_T + v_1 + a_0 v_2)$. We found that the $E(x) = 0$, $\sigma_x^2 = a^2 \sigma_1^2 + b^2 \sigma_2^2$, $E(y) = \tau_T$ and $\sigma_y^2 = \tau_1^2 + a_0^2 \sigma_2^2$. In this substitution a equals $a_0 d_w \tau_2 / \tau_T$, and b equals $a_0 d_w \tau_1 / \tau_T$. The basic definition of the correlation coefficient r is given by

$$r = \frac{E(xy) - E(x)E(y)}{\sigma_x \sigma_y} \quad (3.3.1)$$

where the expected value of $x = 0$. The first numerator term becomes

$$E(xy) = E[(av_1 - bv_2)(\tau_T + v_1 + a_0 v_2)]$$

$$E(xy) = a\sigma_1^2 - a_0 b \sigma_2^2 \quad (3.3.2)$$

With the second numerator term equal to zero and σ_x and σ_y given above the correlation coefficient r can be expressed as

$$r = \frac{\left[1 - \frac{a_0 \tau_1 \sigma_2^2}{\tau_2 \sigma_1^2}\right]}{\left[1 + \frac{\tau_1^2 \sigma_2^2}{\tau_2^2 \sigma_1^2}\right]^{1/2} \left[1 + a_0^2 \frac{\sigma_2^2}{\sigma_1^2}\right]^{1/2}} \quad (3.3.3)$$

A typical scenario might be:

$$\rho = 25,000$$

$$d_w = 3,000$$

$$d_o = 1,000$$

$$\tau_1 = 10 \text{ ms}$$

$$\tau_2 = 80 \text{ ms}$$

$$a_0 = 1/2$$

then if $\sigma_2 = \sigma_1 \Rightarrow r$ equals .838

if $\sigma_2 = 2\sigma_1 \Rightarrow r$ equals .514

indicating a strong correlation between x and y .

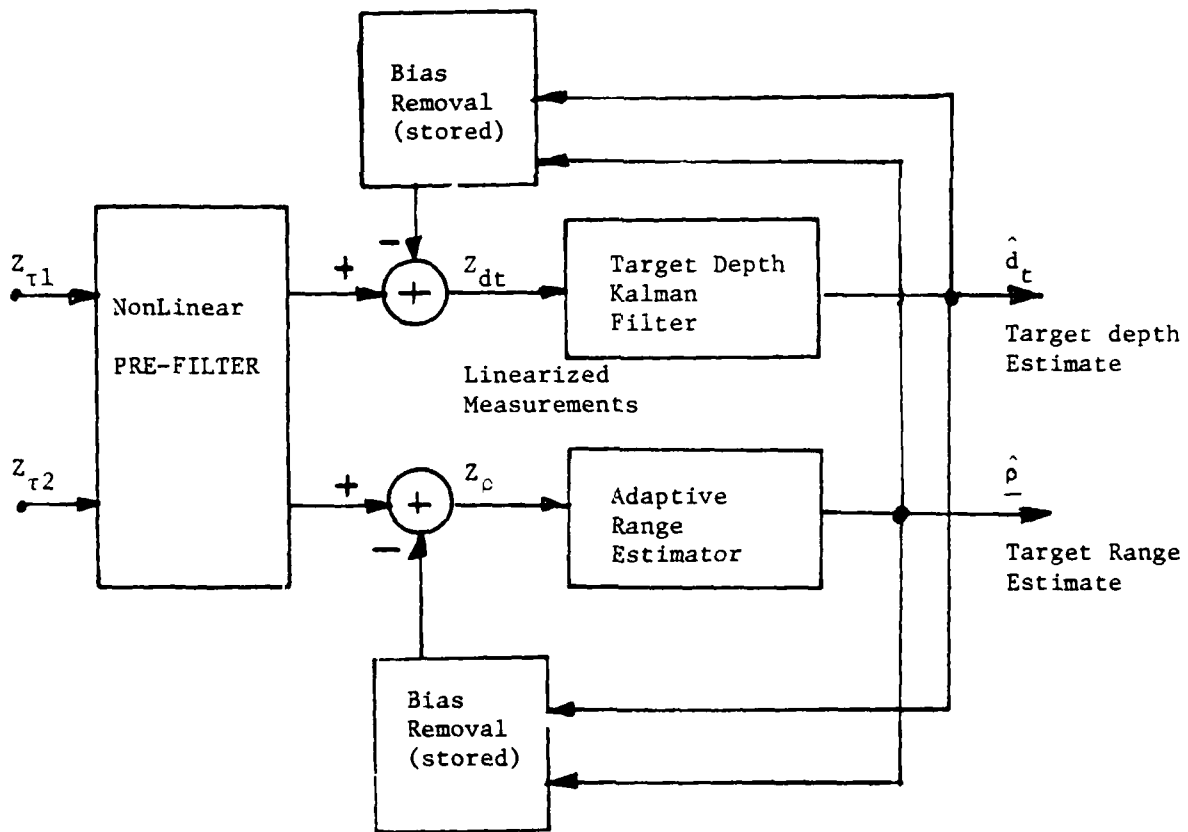
Chapter 4

State Estimation and Adaptive Tracking System Structure

4.1 Introduction

In this section, we will discuss the basic estimator system structure. We will make use of the linearized measurements containing the nonstationary, non-Gaussian, statistics that was previously discussed in Chapter 3 of the report.

Referring to Figure (9), the nonlinear time delay measurements $Z_{\tau 1}$ and $Z_{\tau 2}$ are fed into the nonlinear prefilter. This unit develops a linearized



Basic Estimation Structure

Figure (9)

measurement of target range (ρ) and depth (dt). The errors in measuring these target parameters are both non-Gaussian and nonstationary depending upon the geometry of the tracking situation. As target range closes, or opens the mean value, and variances of these errors change, and must be accounted for.

An offline computer program was developed to generate the variation in the mean value and variance of v_ρ as a function of target range ρ . Details of this work is presented in the accompanying appendix along with the outline of the pitfalls to be avoided in using numerical integration routines on functions containing an isolated singularity. Results shown in Figure (11) illustrate that, for stationary Gaussian measurement errors σ_1 and σ_2 associated with time delays τ_1 and τ_2 , it is possible to simply store offline as a small catalog the necessary values of $E(v_\rho)$ and $E(v_\rho^2)$.

In order to evaluate the mean and variance of the target depth error v_{d_T} , data was generated at fixed target ranges. It was then operated upon by the nonlinear prefilter shown in Figure (10), and then numerically

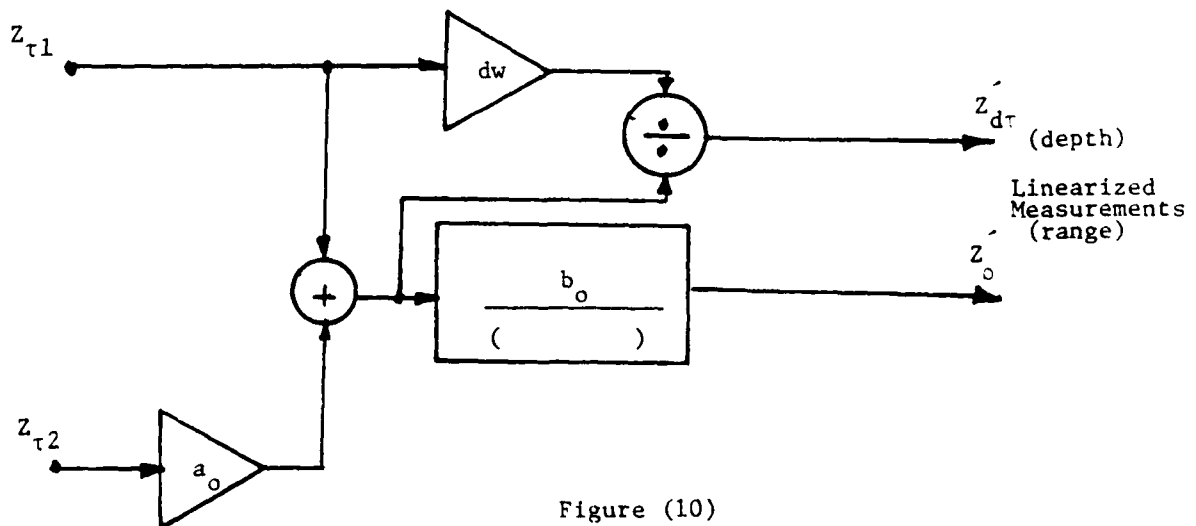
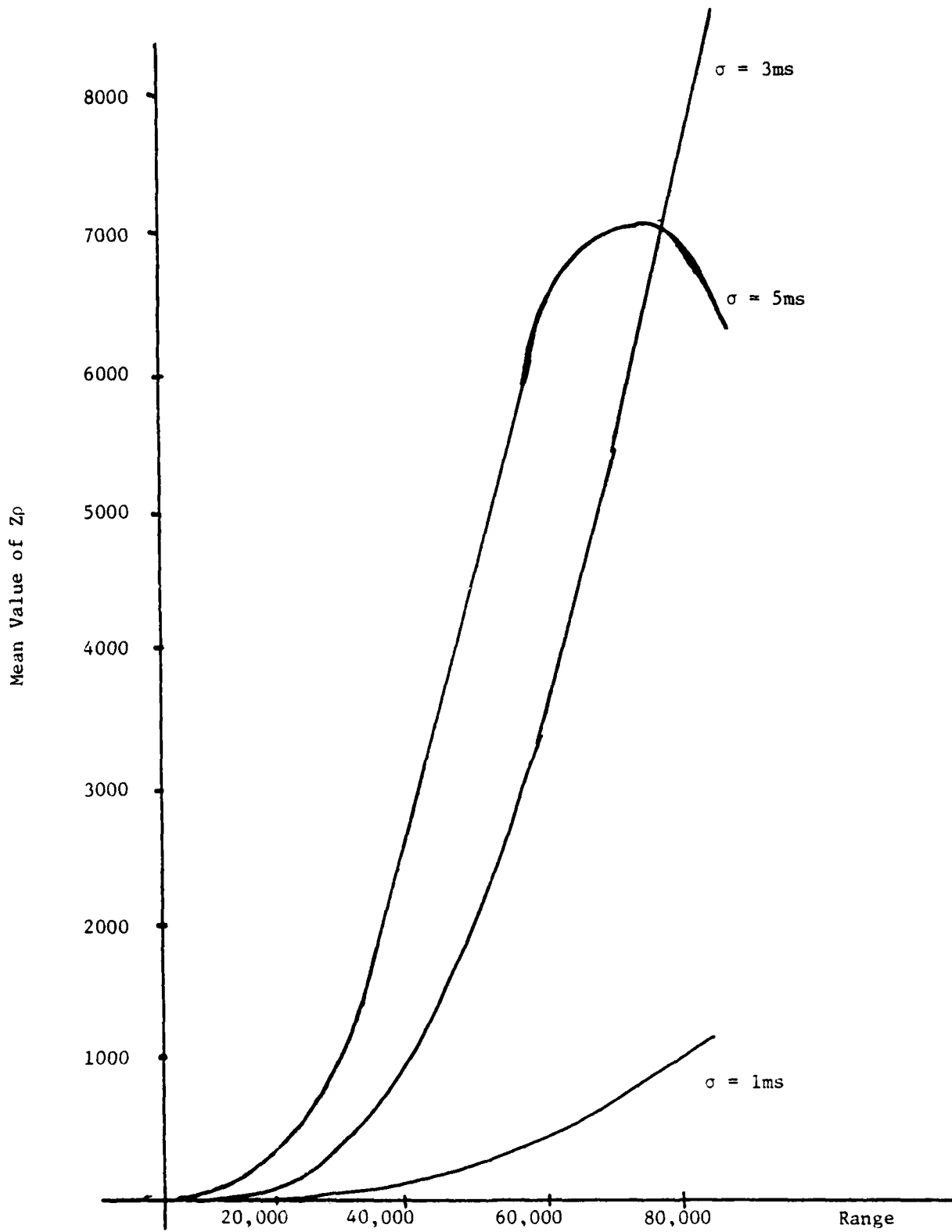


Figure (10)
NONLINEAR PREFILTER



Mean Value of Linearized Measurement Error vs Range

FIGURE 11

Range	$\sigma_{1,2} = 1\text{ms}$		$\sigma_{1,2} = 2\text{ms}$		$\sigma_{1,2} = 5\text{ms}$	
	Mean	Var	Mean	Var	Mean	Var
10,000	3.8	.209E + 05	24.	.191E + 06	62.	.549E + 06
20,000	23.	.336E + 06	175.	.323E + 07	487.	.102E + 08
30,000	72.	.172E + 07	588.	.179E + 08	1650.	.605E + 08
40,000	163.	.552E + 07	1413.	.633E + 08	3518.	.192E + 09
50,000	310.	.137E + 08	2750.	.168E + 09	5588.	.427E + 09
60,000	527.	.290E + 08	4527.	.345E + 09	6841.	.780E + 09
70,000	831.	.555E + 08	6560.	.641E + 09	7068.	.127E + 10
80,000	1238.	.972E + 08	8679.	.103E + 10	6204.	.190E + 10

Linearized Measurement Error Means and Variances vs Range

Table I

integrated to yield a set of means and variances for use in the target depth estimation portion of Figure (9).

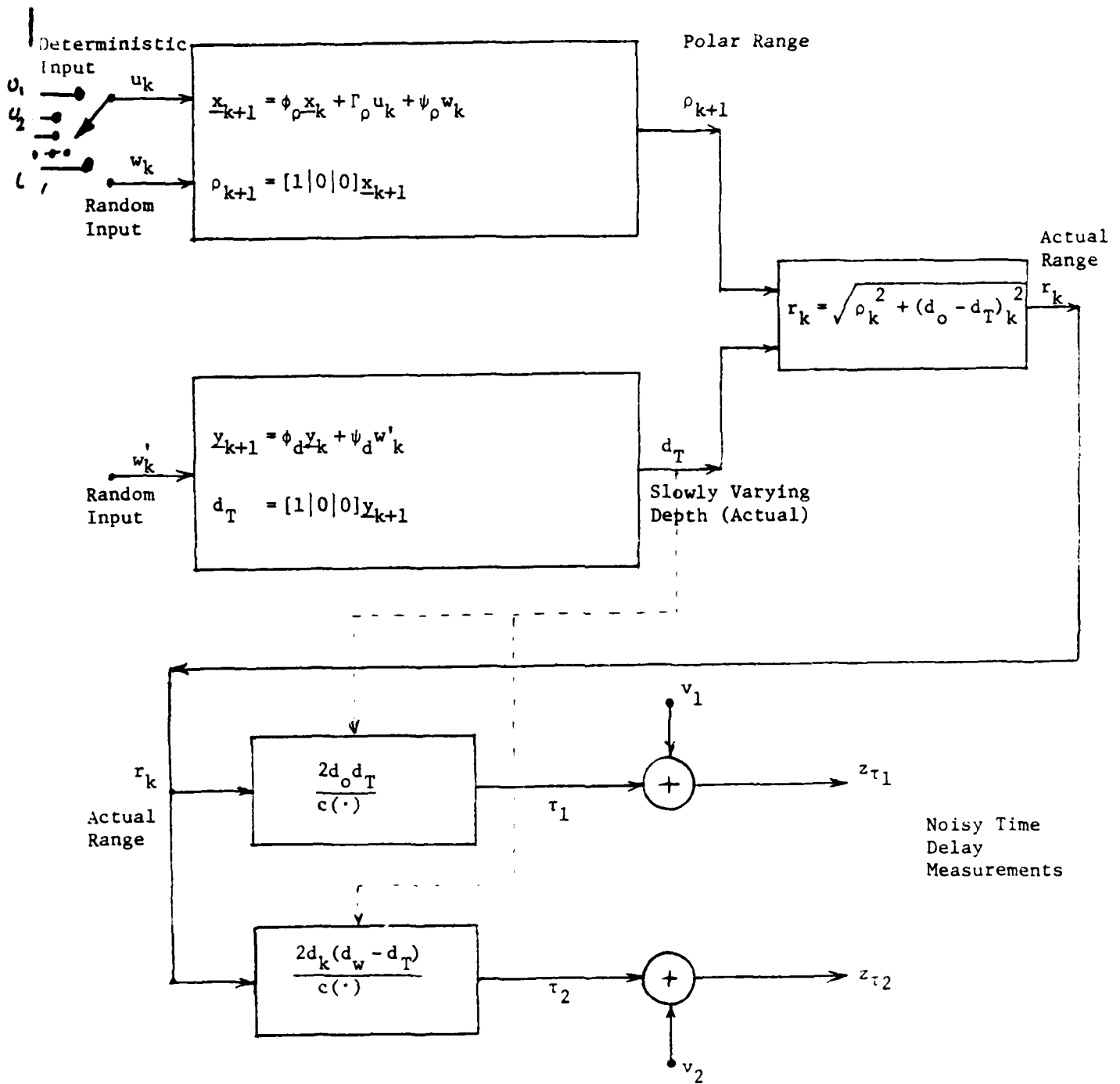
4.2 Target Depth State Estimation and Data Generation

A conventional Kalman filter was developed for the state equation $\underline{x}_{k+1} = \phi \underline{x}_k + \psi w_{zk}$ where ϕ and ψ are given by eq. 1.4.13 and 1.3.3. The filter of the form $\hat{\underline{x}}_{k+1} = \phi \hat{\underline{x}}_k + K_{k+1} [Z_{dT}(k+1) - H\phi \hat{\underline{x}}_k]$ gives estimates of the target depth $\hat{d}_T(k+1)$ which is the first or upper component of the estimated state vector $\hat{\underline{x}}_{k+1}$.

A large number of computer runs were made using noisy data generated by the following technique. In Figure 12 a discrete time system model is presented showing the development of noisy time delay measurements $Z_{\tau_1}(k)$ and $Z_{\tau_2}(k)$. The upper portion shows the generation of $\underline{x}_{k+1} = [\phi \underline{x}_k + \Gamma U_k + \psi W_k]$ where ϕ , Γ , and ψ are discussed in eq. 1.4.12 with $\cos \beta_{so} = 1.0$. The deterministic input U_k is unknown to the tracking filter and serves to generate large scale target maneuvers in velocity. A measure of randomness in target trajectory ($x_1 = \rho_k$ and $x_2 = \dot{c}_k$) is generated by applying a Gaussian random input W_k to the simulated target, exponentially correlated, forcing function component as state vector $x_3 = W_\rho(k)$.

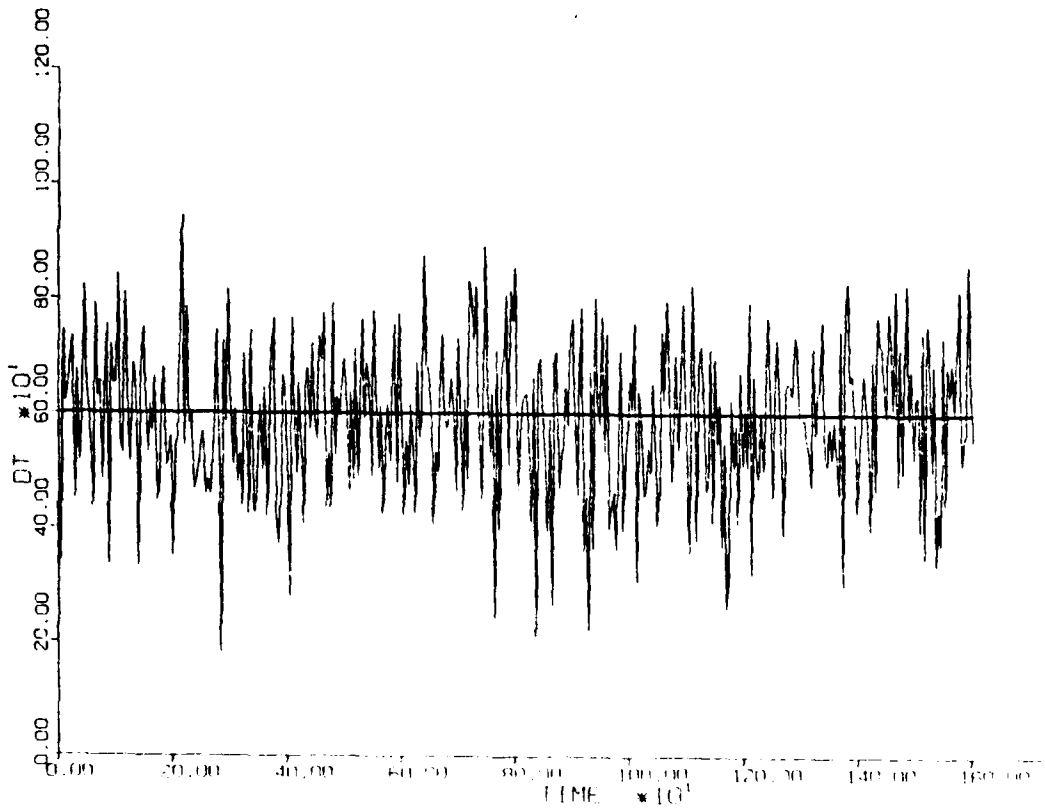
Once ρ_{k+1} is generated, it is acted upon in a nonlinear manner to generate τ_1 and τ_2 , which when added with the Gaussian random measurement errors v_1 , v_2 produce the noisy time delay measurements Z_{τ_1} and Z_{τ_2} .

With the background completed, we will now present some computer simulation. The results shown are typical of those that were observed over many trial tests. In Figure 13 (low noise case) the first figure is a plot of the linearized nonGaussian raw data $Z_{dT}(k)$. The target is at a fixed range of $\rho = 25,000$, and at a mean depth of 600 feet making slow random changes



DATA Generation
Figure (12)

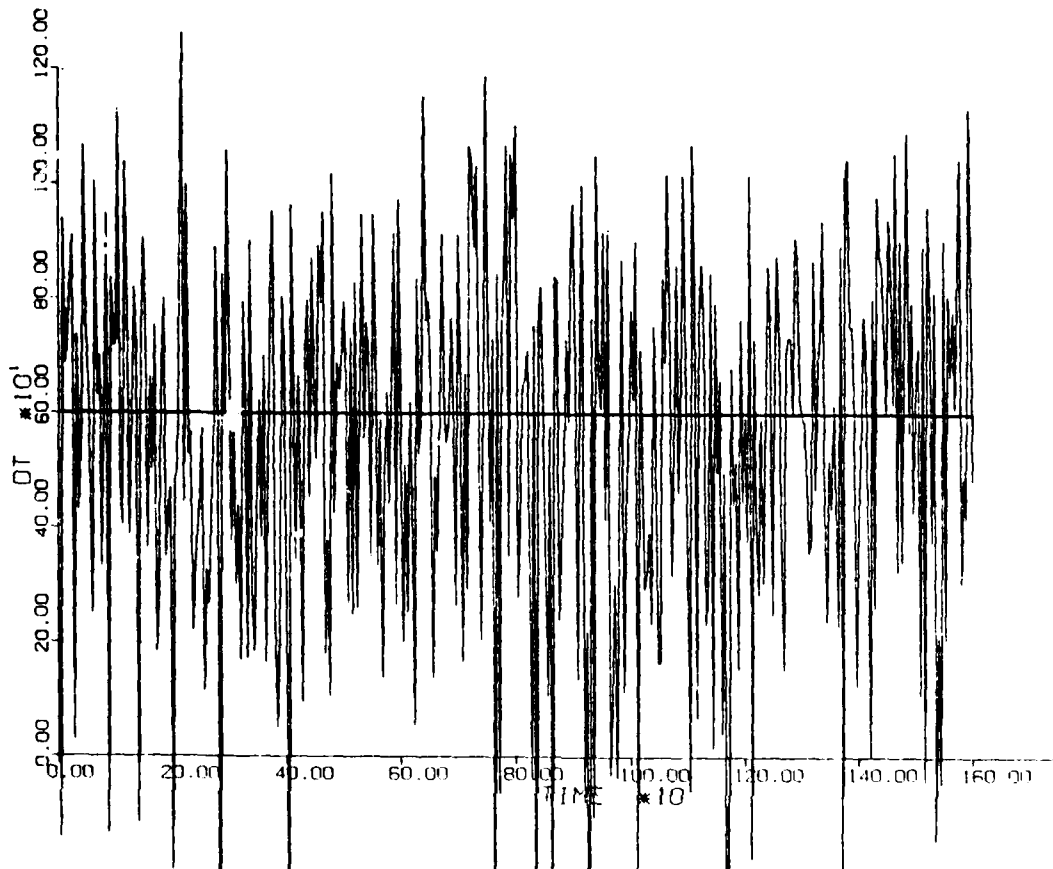
on the order of ± 30 -40 feet. Measurement errors of $\sigma_1 = 2.5$ msec and $\sigma_2 = 5$ msec were added to τ_1 and τ_2 in Figure 12.



Noisy Depth Data $Z_{dT}(k)$

Figure (13)

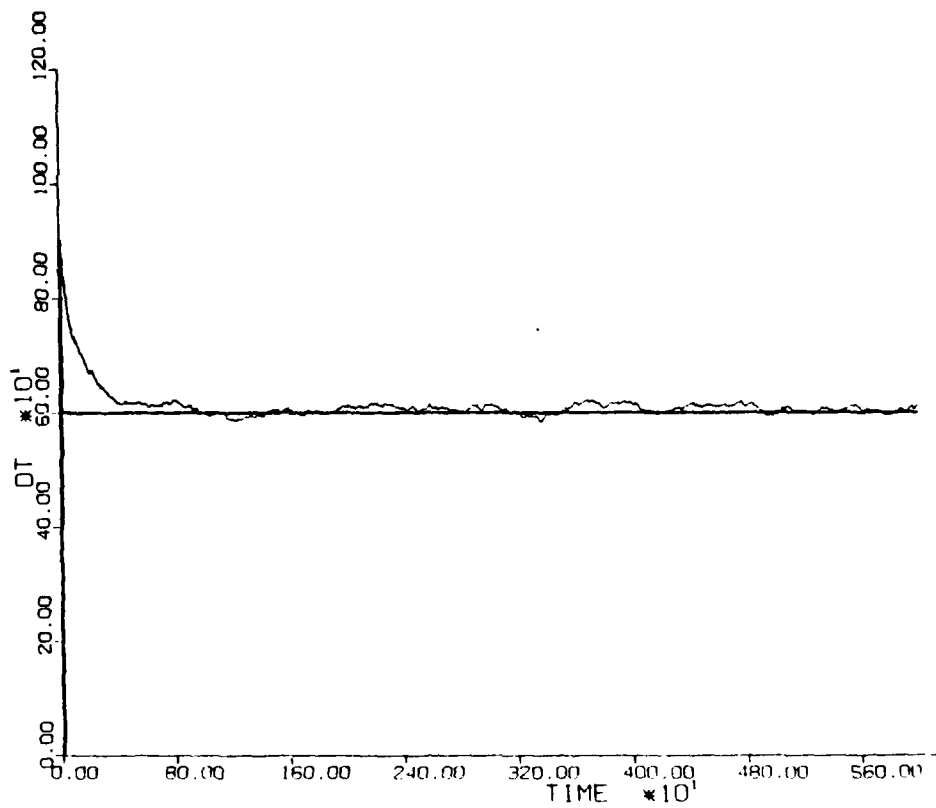
In Figure 14, the target range has been increased to 40,000 and σ_1^2 increased by a factor of 4.0. Notice the data shows a bias due to an excessive number of large positive readings. In the future, bad data points that are nonrealistic will be "windowed out."



Large Measurement Error Effect on $Z_{dT}(k)$

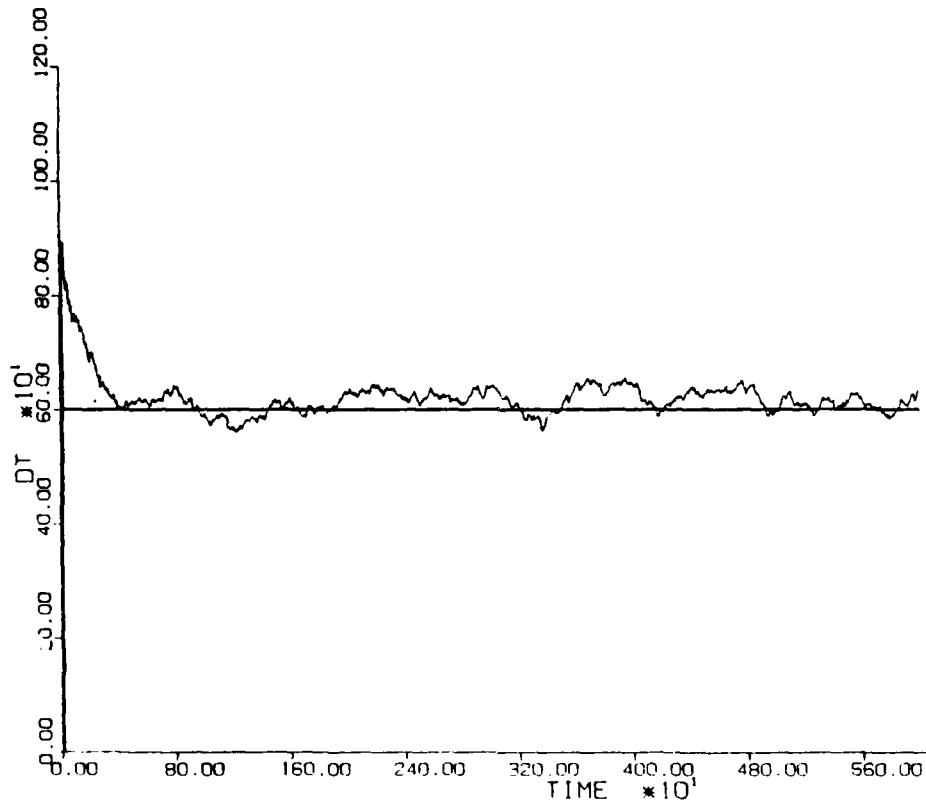
Figure (14)

Figures 15 and 16 show the convergence of the tracking filter, for the previous sets of data given by Figures 13 and 14. The depth estimators provide a good track as the target makes $\pm 1 \sigma$ random depth changes (± 30 feet) about the mean value of 600 which is unknown to the tracking filter. Again the targets range is fixed at 25,000 and 40,000 with the observer at a mean depth of 1000, target 600, and water depth $D_w = 3000$.



Depth Estimation vs Time for Low Noise Case

Figure (15)



Depth Estimation for Longer Range, Higher Noise Case

Figure (16)

4.3 Depth Estimation for Variable Range Targets

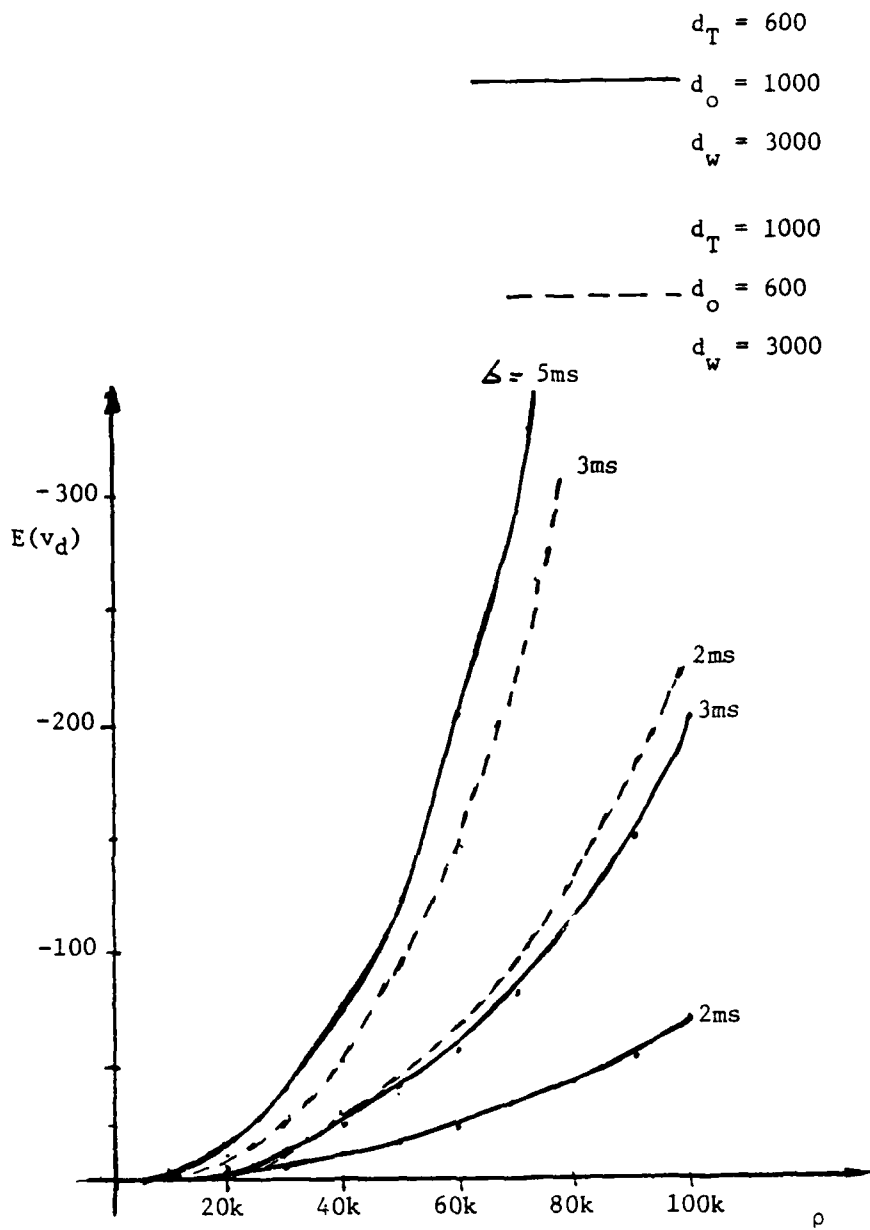
The work presented in the previous section dealt only with targets at fixed ranges, which for most scenarios is a very unrealistic situation. In order to provide depth estimation for a target whose range is time varying, and with an initial estimate of range and depth, a study was performed to analyze the effects of range and noise variances on the depth estimates previously developed.

It has been determined that both range and depth estimation improve as the observer increases his depth. Now with target depth initially unknown, and this being an exploratory engineering study we have decided to investigate two scenarios. The first has observer at 1000 ft and the target at 600, the ocean depth shallow at 3000 ft. The second is a reversal of magnitudes with target at 1000 and observer at 600. Values obtained then would allow the estimator to perform anywhere within this range without going to a new set of tabulated means and variances.

What we need as the target's range varies, is to compensate for the changing bias introduced in the nonlinear data operation of the nonlinear prefilter of figure (10) page 26. Now, the data generation system of figure (12) page 29 was exercised at a series of discrete target ranges $\rho_i = 5K, 10K, 15K, \dots, 90K$. Additive Gaussian noises v_1 and v_2 were generated from a series of ten independent random generators. The noisy measurements z_{τ_1} and $z_{\tau_2}(\rho_i)$ were then fed into the nonlinear prefilter. Taking the output and subtracting ρ_i the measurement error was obtained. By averaging a sequence of 250 noisy measurements a value of mean and variance of v_d was obtained, for each target range ρ_i . This was repeated for each of the ten random sequences to produce a good "Monti-Carlo" set

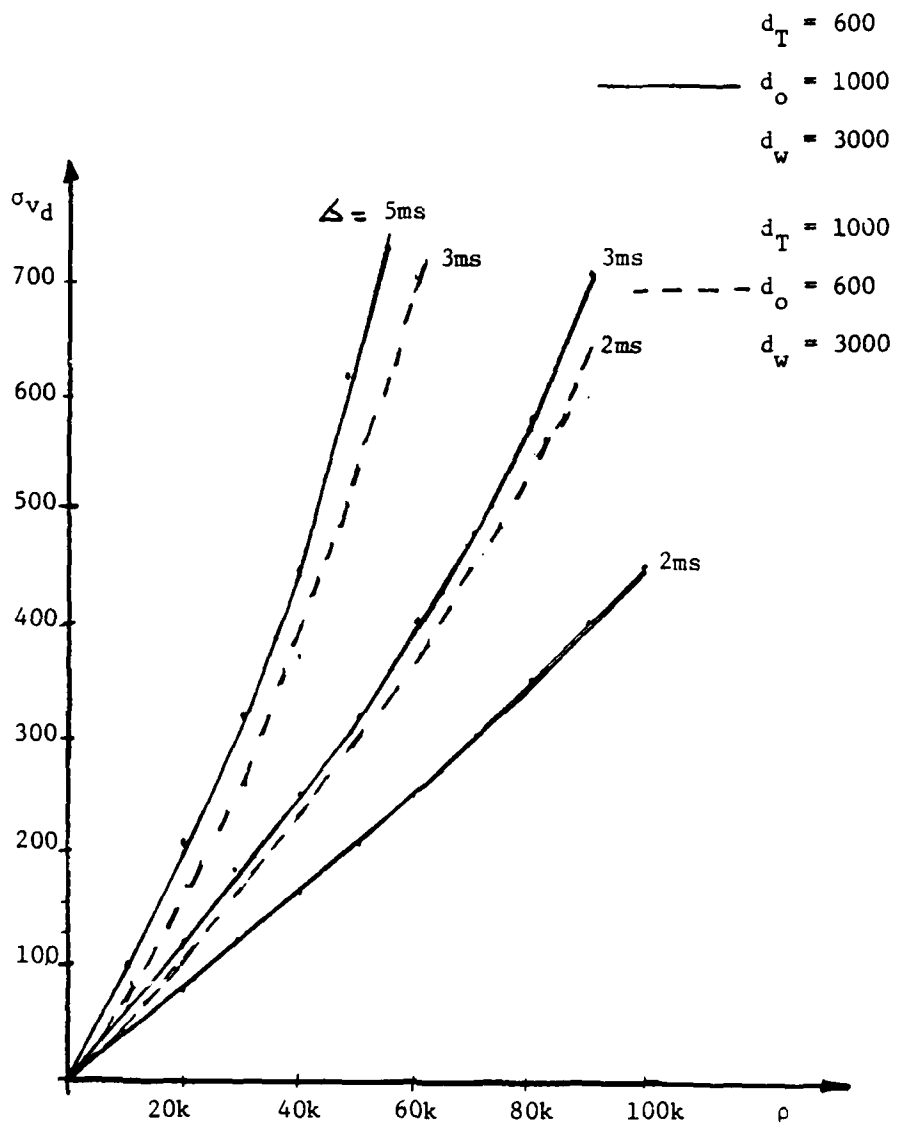
of mean values and variances. The results are shown in figures 17 and 18. It is to be noted that the curves also show the effect of increasing the variance of the Gaussian measurement errors v_1 and v_2 from 2 to 5 ms.

Figure 19 gives an idea of the form of the density function of the additive noise v_d . The range (ρ) is fixed at 50K and the scenario of $d_o = 1000$ and depth of target equal to 600 is used. If the area under the curve $\int_{-\infty}^{\infty} v_d P(v_d) dv_d$ is integrated, a value very close to the desired value of -50 feet is obtained.



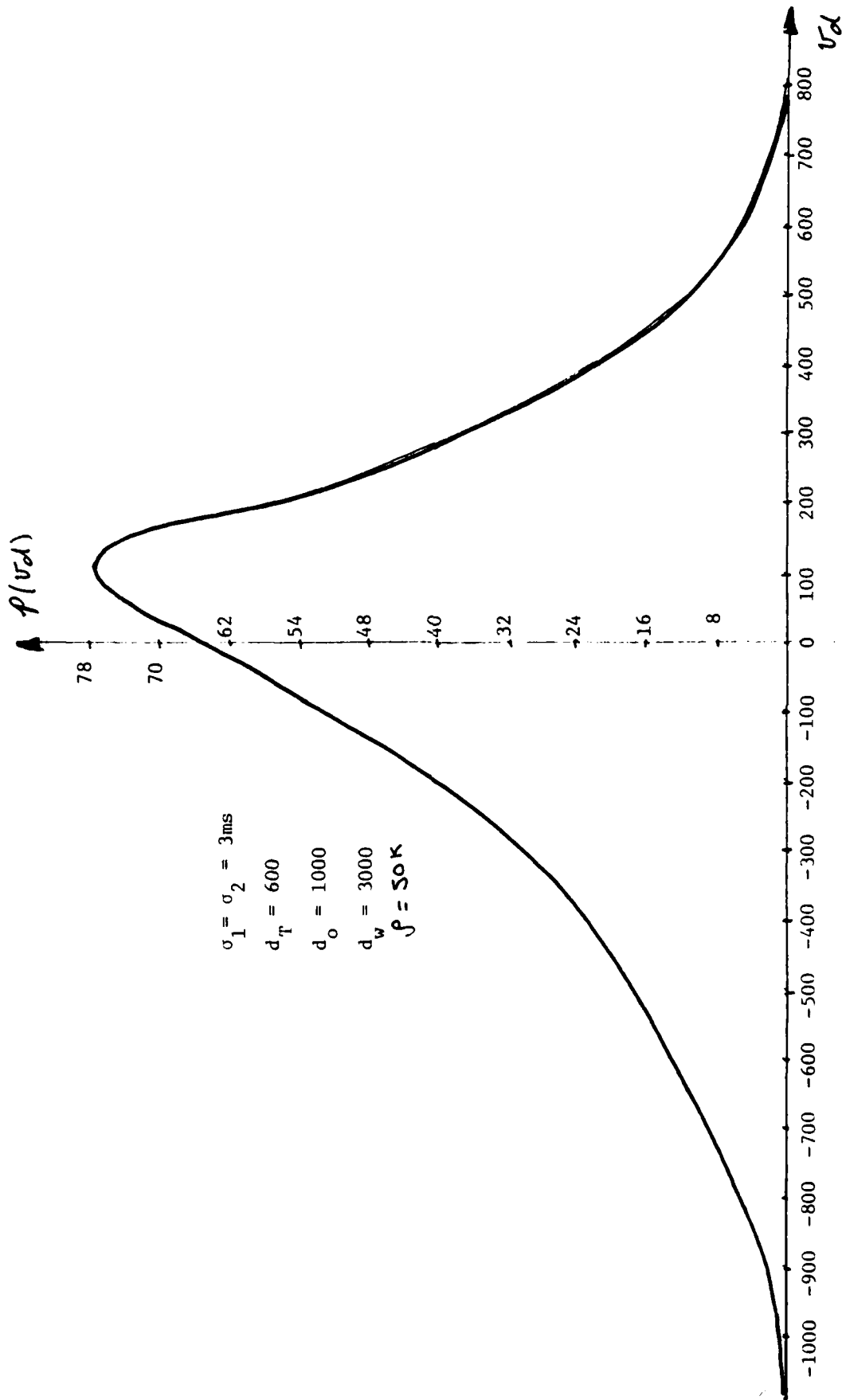
Mean Value of Measurement Error vs Range

Figure 17



Standard Deviation of Depth Error vs Range

Figure 18



Normalized density of depth measurement error.

Figure 19

Results for Depth Estimation

In figure 20, the target is closing the range from $\rho = 80\text{K}$ to 20K at a constant depth of 900 . An initial depth estimate $\hat{d}_T(0)$ equal to 200 was chosen with the observer at 600 , and ocean depth 3000 . The standard deviation of 3 ms was chosen for additive noises v_1 and v_2 . In this, and the figures to follow raw depth measurements z_{dT} out of the nonlinear prefilter are shown. Note the decay (on the average) of the noisy measurements as the target closes the range, making the received signal to noise ratio increase.

Figure 21, illustrates the case of higher noise power $\sigma_1 = \sigma_2 = 5$ msec and target closing from 50K to 20K . The initial depth estimate is again chosen to be 200 with target at an unknown fixed depth of 900 .

In figure 22, a target closes from 10K to 1K and makes large-scale random changes in depth. The estimate is initialized at $\hat{d}_T(0) = 200$ and appears to follow very accurately. Note the fact that the unfiltered measurements are not very noisy. This is due to the close range, high signal to noise ratio that is in effect even though $\sigma_1 = \sigma_2 = 3$ msec.

Figure 23 is the same scenario as the previous figure, but with target range increased from 50K to 20K and depth still making major random variations. Tracking is still quite good with the exception of the tracker lag that develops, which introduces an offset of 100 or more feet. This ability of the tracker is primarily due to the addition of the Singer correlated acceleration which was previously built in to the filter. It is also to be pointed out that the tracker continually uses new stored values of the mean and variance of the nonGaussian measurement and error since the target is constantly changing range.

SIGMA EQUALS 3NSEC

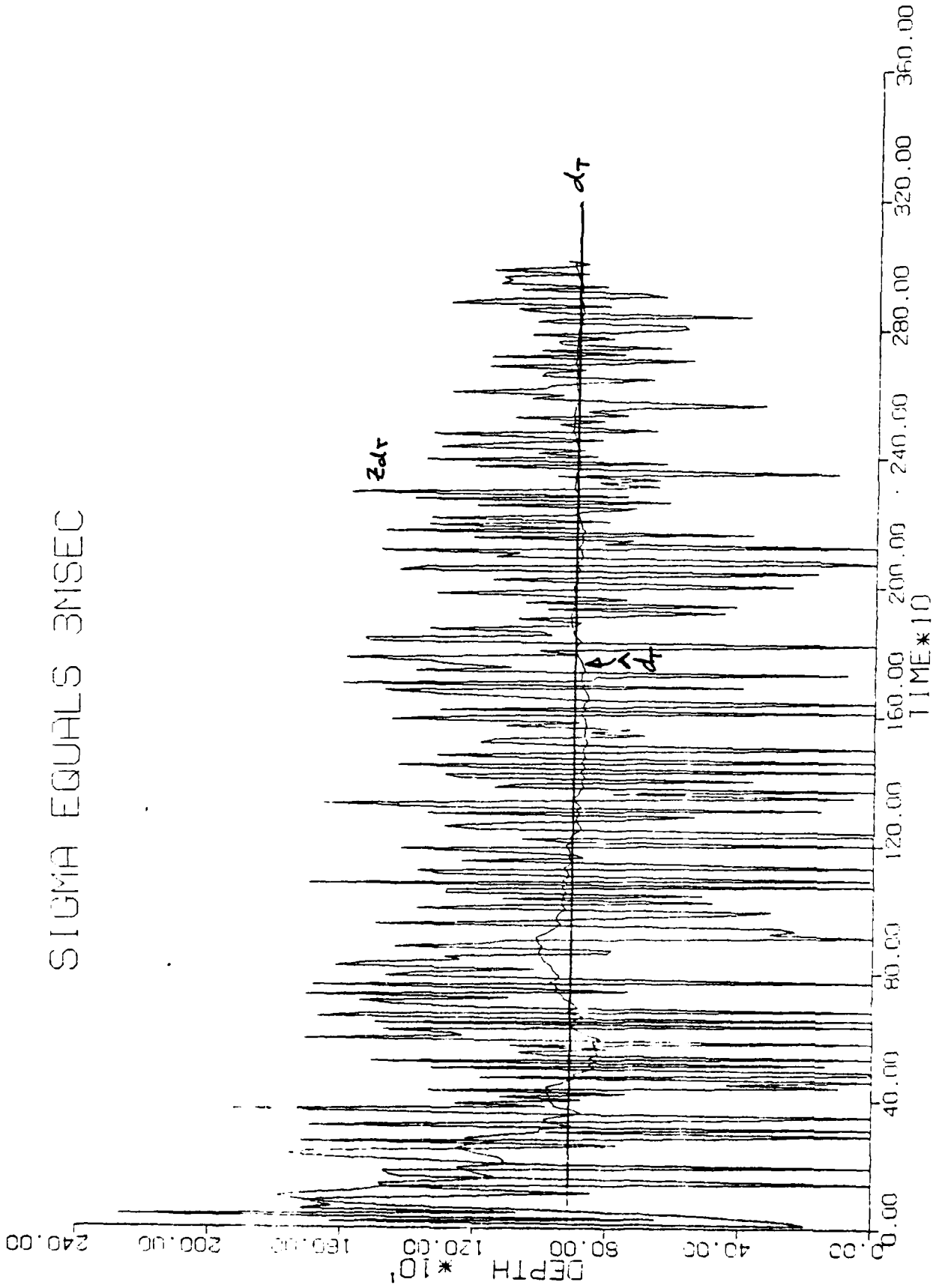


Figure 20: Depth Estimate vs Time for Target Closing, (80K to 20K) Range.

SIGMA EQUALS 5MSEC

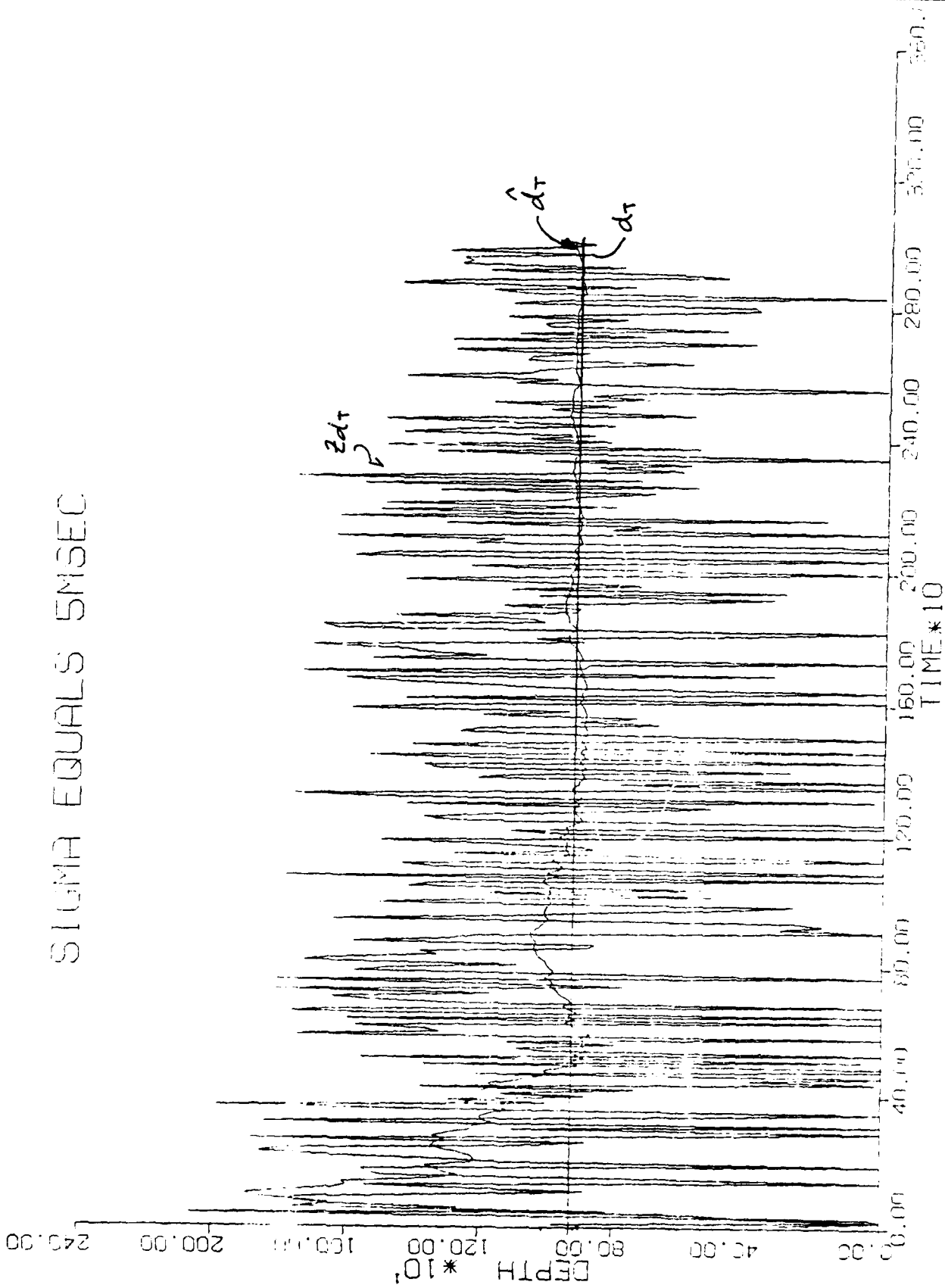


Figure 21: Depth Estimate vs Time for Target Closing 50K to 20K, High Noise Core.

SIGMA EQUALS 3MSEC

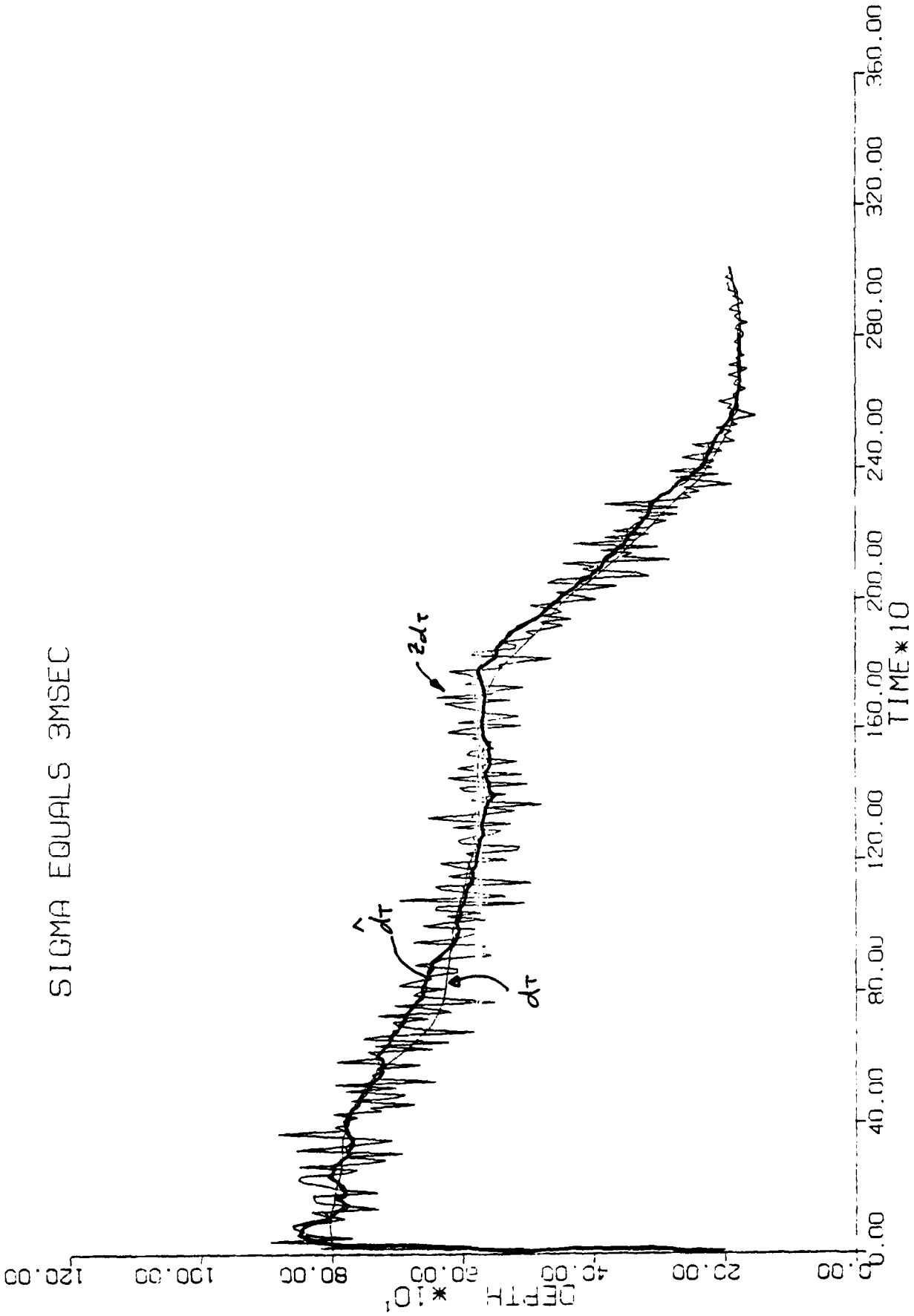


Figure 22: Short Variable Range, Variable Depth Target and Estimator Output vs Time

SIGMA EQUALS 3MSEC

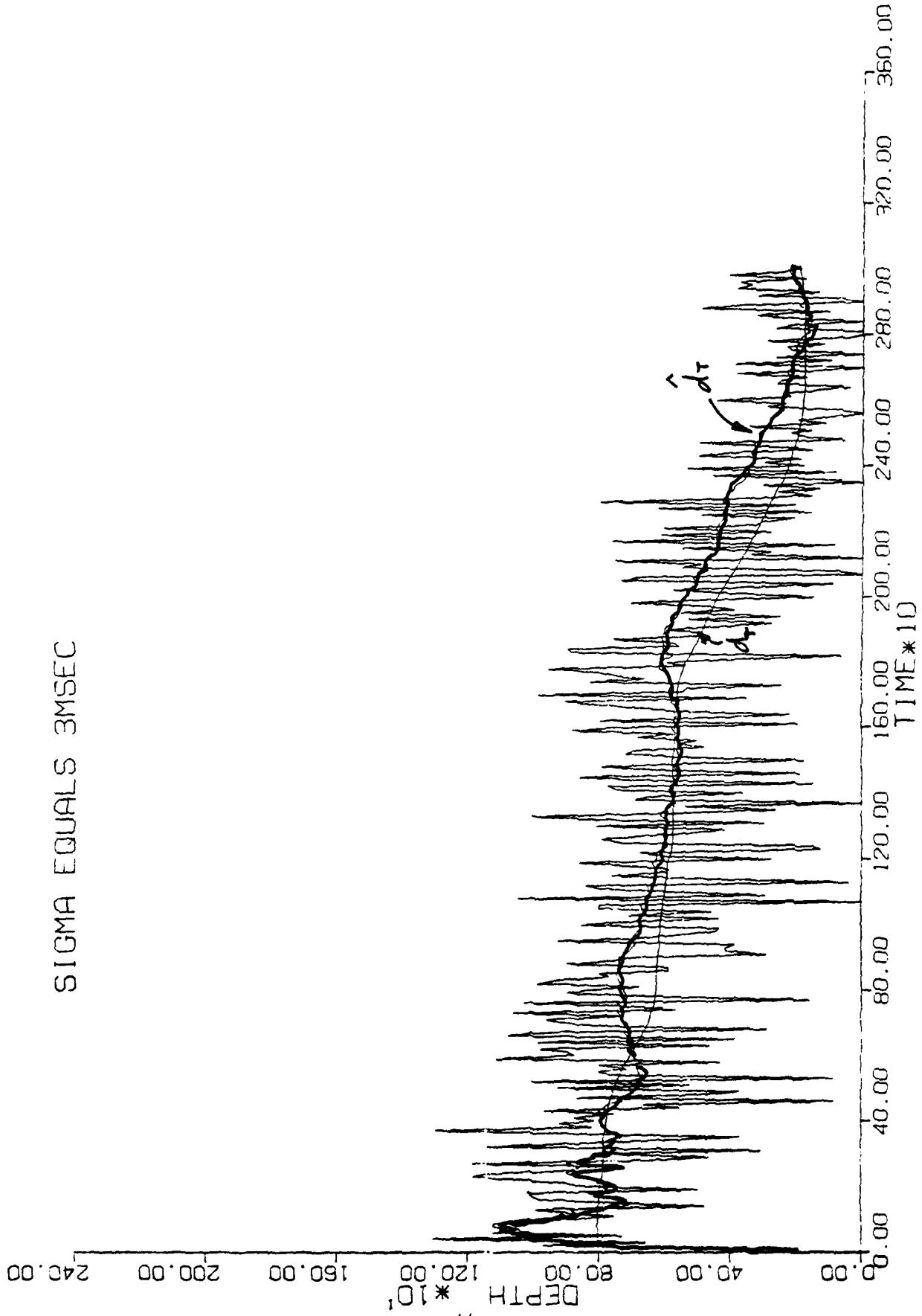


Figure 23: Variable Range 50K to 20K and Variable Depth Target.

A final set of runs were made to study some different scenarios that might be of interest to the Navy. The first, shown in figure (24) is a tracking situation where the observer is maintaining a fixed range of $\rho = 30$ K, and the target is making rapid large scale random depth changes. The filter was initialized at a depth estimate of 200 feet for the target. Target depth (d_T) is shown as the light curve, and the depth estimate (\hat{d}_T) as the heavy curve. The raw data (z_{dT}) out of the nonlinear prefilter is also shown. The worst errors were on the order of 100 feet lasting for about 30 time samples, or 300 sec of data.

Figure (25) shows the target at a fixed range of $\rho = 30$ K proceeding at a constant depth of 250 feet. The observer is at 1000 maintaining the 30 K fixed range, and using the old catalogue set of means and variances for the target at a fixed 600 foot depth. A fixed bias is observed of about 60 to 70 feet, gradually decaying towards zero as a new set of means and variances were automatically changed in the filter.

SEISMIC LOGS 3MSEC

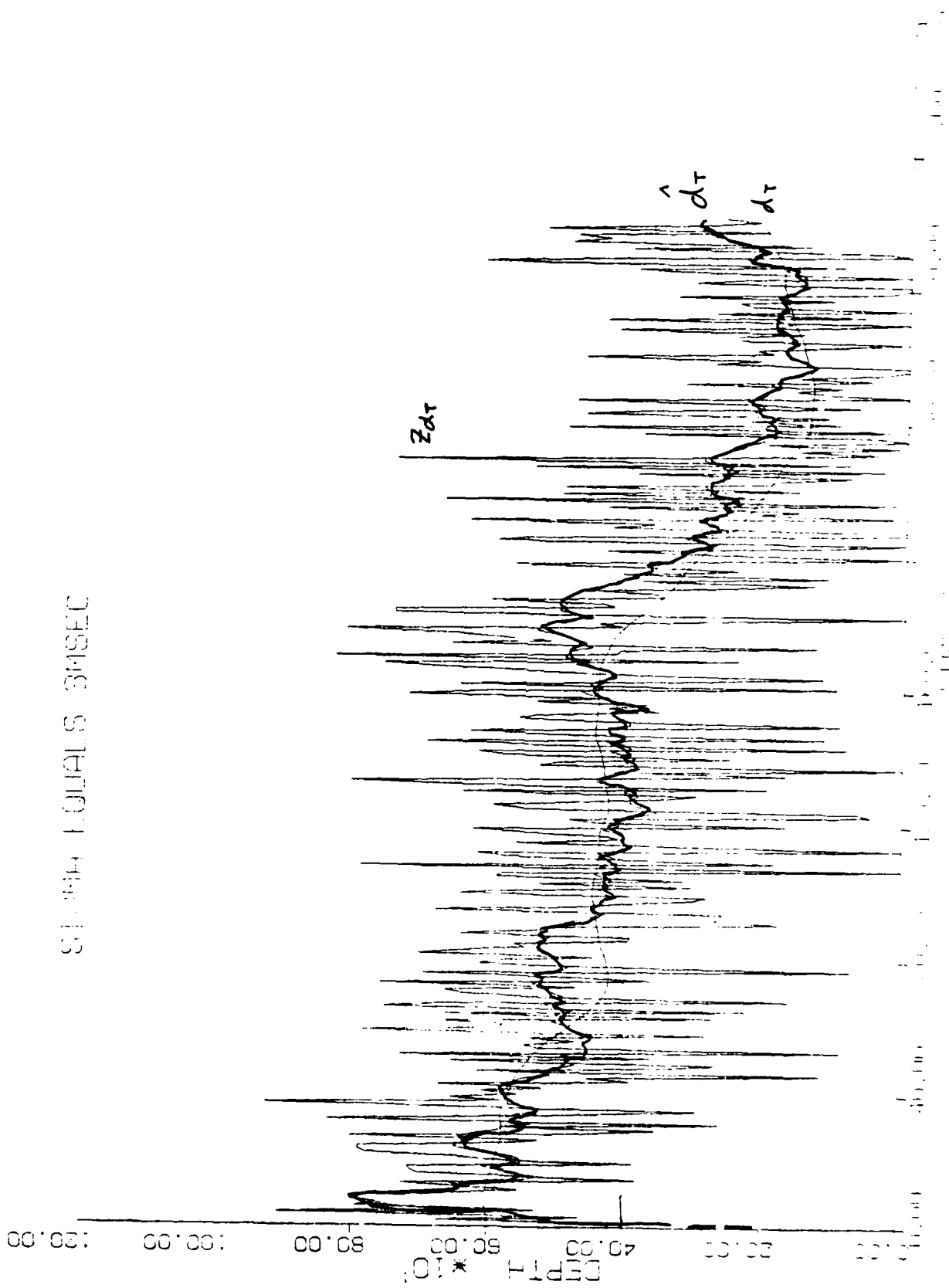


Figure 24

SIGMA EQUALS 3MSEC

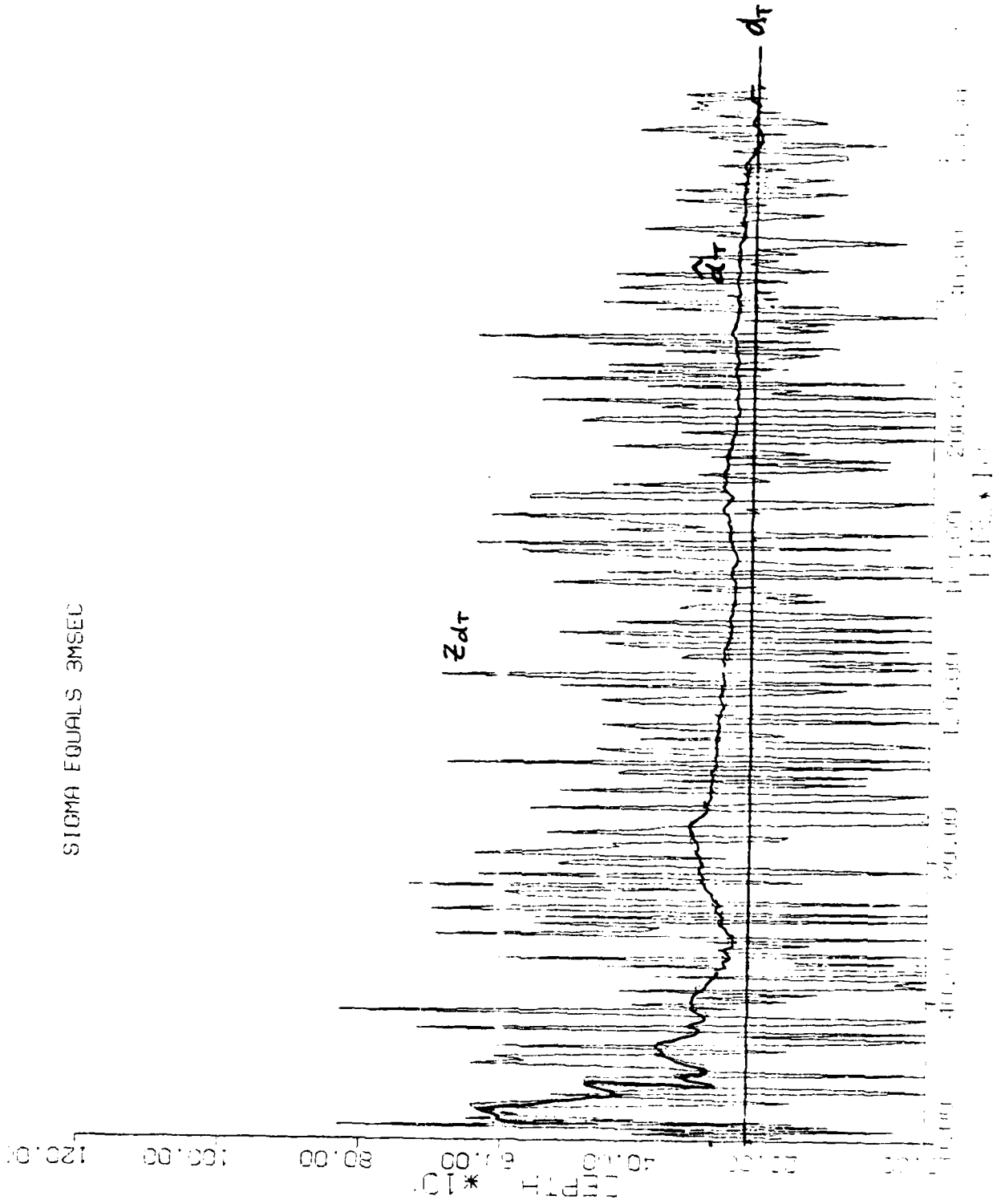
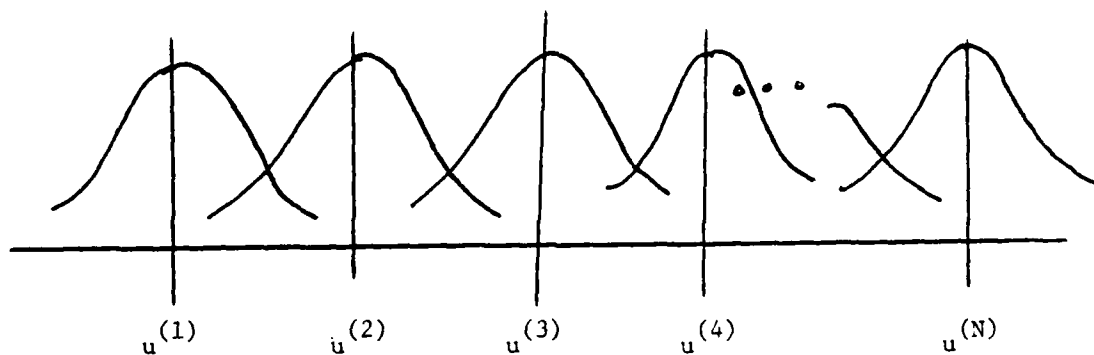


Figure 25

Chapter 5

The Polar Range Adaptive State Estimator

The heart of the adaptive filter summarized in this report, is in the forming of the total estimate of the target states, from a weighted sum of state estimates conditioned on the N possible discrete input levels $u_{\rho}^{(i)}$. Consider the state model (1.4.12). This state model views the target input acting in the polar direction as being derived from a time correlated Gaussian density having a mean value u_{ρ} . Next consider a series of N such Gaussian curves with displaced mean values $u_{\rho}^{(i)}$, $i = 1, 2, \dots, N$ and partially overlapping "tails" as shown in Figure 26. If a bank of N Kalman filters is formed, each filter based on the state equations of equation (1.4.12) with the deterministic input u_{ρ} being a different one of these N



Series of N Partially Overlapping Gaussian Curves with Mean Values $u^{(i)}$

Figure (26)

mean values, then a series of N estimates is obtained, each conditioned on a different Gaussian curve. Next a weighted sum of these estimates is

obtained in a manner to be disclosed below, and this weighted sum is taken to be the total unconditioned estimate of the target states given by equation 5.1.

$$\hat{\underline{x}}(k+1) = \sum_{i=1}^N \hat{\underline{x}}^{(i)}(k+1) W_i(k+1) \quad (5.1)$$

Now as the target executes a series of evasive maneuvers in the polar channel, the changing input necessary to produce these maneuvers is viewed as randomly switching among the N Gaussian curves. By applying semi-Markov statistics to this switching process a series of N probabilities W_i , $i = 1, 2, \dots, N$ is generated where

$$W_i \equiv \Pr \{ \text{target input is being derived from the Gaussian curve whose mean value is } u_{\rho}^{(i)} \} \quad \text{OR,}$$

$$W_i(k+1) = \Pr \{ u_{\rho}(k) = u^{(i)} | Z(k+1) \} \quad (5.2)$$

and

$$\hat{\underline{x}}^{(i)}(k+1) = E\{ \underline{x}(k+1) | u_{\rho}(k) = u^{(i)}, Z(k+1) \}.$$

Equation (5.1) is a total probability expression developed from the basic relation that

$$\hat{\underline{x}}(k+1) = E\{ \underline{x}(k+1) | Z(k+1) \}$$

is the optimal mean-squared estimate. It is well known that the optimal input-conditioned estimates are provided by suitably matched Kalman filters. In particular, for the i^{th} filter

$$\begin{aligned} \hat{\underline{x}}^{(i)}(k+1) = & \Phi \hat{\underline{x}}^{(i)}(k) + \Gamma u^{(i)} + K(k+1) [z(k+1) \\ & - H \Phi \hat{\underline{x}}^{(i)}(k) - H \Gamma u^{(i)}] \end{aligned}$$

where

$$K(k+1) = M(k+1) H^T [HM(k+1) H^T + R]^{-1},$$

$$M(k+1) = \phi P(k) \phi^T + \psi Q \psi^T$$

and

$$P(k+1) = [I - K(k+1)H] M(k+1).$$

The matrices ϕ , Γ and ψ are used to denote the respective coefficient matrices in (1.4.12).

The following (repeated here for completeness) is an outline of the analysis given in [5] to calculate the recursive weighting coefficients W_i , $i = 1, 2, \dots, N$. Defining $Z(k+1) = \{Z(k), z(k+1)\}$, apply Bayes Theorem to (5.2) and we obtain

$$W_i(k+1) = \frac{\Pr\{u(k) = u^{(i)} | Z(k)\} p\{z(k+1) | u(k) = u^{(i)}, Z(k)\}}{p\{z(k+1) | Z(k)\}} \quad (5.3)$$

The time varying denominator is independent of i and is therefore common to each $W_i(k+1)$ as a normalizing constant. The first numerator factor is determined from the semi-Markov input process. Expanding this factor in a total probability expression,

$$\Pr\{u(k) = u^{(i)} | Z(k)\} = \sum_{j=1}^N \Pr\{u(k) = u^{(i)} | u(k-1) = u^{(j)}, Z(k)\} W_j(k)$$

And since $Z(k)$ has no influence on the Markov state transitions,

$$\Pr\{u(k) = u^{(i)} | Z(k)\} = \sum_{j=1}^N \vartheta_{ji} W_j(k) \quad (5.4)$$

where the semi-Markov probability is

$$\vartheta_{ji} = \Pr\{u(k) = u^{(i)} | u(k-1) = u^{(j)}\}$$

is near unity for $j = i$ and near zero for $j \neq i$.

Combining (5.3) and (5.4)

$$W_i(k+1) = C_k p\{z(k+1) | u(k) = u^{(i)}, Z(k)\} \sum_{j=1}^n \theta_{ji} W_j(k) \quad (5.5)$$

where C_k is a normalizing constant

is the desired recursive relation for W_i . The required density p is approximately normally distributed and has distribution

$$P\{z(k+1) | u(k) = u^{(i)}, Z(k)\} \sim N\{m_i(k+1), V(k+1)\}, \quad (5.6)$$

where

$$m_i(k+1) = H[\phi \hat{x}^{(i)}(k) + \Gamma u^{(i)}(k)]$$

and

$$V(k+1) = [HM(k+1) H^T + R]$$

These probabilities can thus be expressed in a vector recursive form as

$$\underline{W}_{k+1} = C_k \underline{P}_k \phi^T \underline{W}_k \quad (5.7)$$

where \underline{P}_k is a time varying diagonal matrix whose elements have been previously computed in each of the (N) Kalman filters from eq. (5.6) we have

$$P_{ii} = N [m_i(k+1), V(k+1)]$$

The term C_k is a normalizing constant computed at each iteration to ensure that the sum of probabilities equals unity. The matrix $\underline{\theta}$ is a

precomputed matrix whose elements contain statistical knowledge of the randomly switching plant inputs. In practice, the diagonal elements are nearly unity and the off diagonal terms are set equal.

Although it might appear from equation (5.1) that an entire Kalman filter algorithm is being executed N times (for each of the possible inputs) at each time iteration, such is not the case, since the process and measurement covariances Q and R are the same for each filter.

What differentiates the different target "states" is the discrete levels u_i ; however, the target dynamics remain unchanged! The entire covariance, and gain analysis of the Kalman filter algorithm becomes identical for each state in a given channel and, consequently, need be executed just once rather than N times. The adaptive filter structure is shown in Figure 27.

5.2 Computation of Additional Required Covariance Term

After an initial investigation, it has been found necessary to compensate for the lack of *exact statistical* knowledge concerning target maneuver commands. In other words, the u_i of the filter bank rarely, if ever, match exactly that of the plant.

The mathematical basis for the error compensation technique is based upon the following statistical analysis.

In the state estimation algorithm, for a system with an unknown to the tracking filter deterministic input u_k , and random disturbance w_k ,

$$x(k+1) = \phi x(k) + \Gamma u(k) + \Psi w(k) \quad (5.8)$$

the predicted covariance matrix $P(k+1/k)$ is given by

$$P(k+1/k) = \phi P(k/k) \phi^T + \Psi Q(k) \Psi^T. \quad (5.9)$$

However, this is true only if the deterministic input to the plant is known exactly. Consider the situation when a mismatch exists between the plant input u_k and the deterministic input u^i used in the filtering algorithm. Assuming a linear estimator of the Kalman variety, we seek to optimize the estimate

$$\hat{x}(k+1/k+1) = \hat{x}(k+1/k) + K(k+1)[z(k+1) - H\hat{x}(k+1/k)] \quad (5.10)$$

where $\hat{x}(k+1/k)$ is the one step predicted estimate of x . The gain matrix $K(k+1)$ is as yet unspecified.

Let $\hat{x}(k+1/k) = \phi\hat{x}(k/k) + \Gamma u^i$

$$\therefore \hat{x}(k+1/k+1) = [I - KH][\phi\hat{x}(k/k) + \Gamma u^i] + KH[\phi x_k + \Gamma u_k + \Psi w_k] + K v_{k+1}$$

where $K \equiv K(k+1)$.

Defining the estimation error at time $(k+1)$ as $\tilde{x}_{k+1} = \hat{x}_{k+1} - x_{k+1}$ we have

$$\tilde{x}(k+1/k+1) = [I - KH][\phi(\hat{x}(k/k) - x(k)) + \Gamma(u^i - u_k) - \Psi w_k] + K v(k+1) \quad (5.11)$$

The error covariance matrix becomes

$$\begin{aligned} P(k+1/k+1) &= E(\tilde{x}_{k+1} \tilde{x}_{k+1}^T) \\ &= [I - KH][\phi P(k/k)\phi^T + \Psi Q \Psi^T + D][I - KH]^T + KRK^T \end{aligned}$$

+ cross terms which go to zero under the expectation operator. The new additional quantity D has the value

$$\begin{aligned} D &= \Gamma E\{(u^i - u_k)(u^i - u_k)^T\}\Gamma^T + \Gamma E\{u^i - u_k\}(\hat{x}(k/k) - x(k))^T\phi^T \\ &\quad + \phi E\{(\hat{x}(k/k) - x(k))(u^i - u_k)^T\}\Gamma^T. \end{aligned} \quad (5.12)$$

The condition for choosing $K(k+1)$ is to minimize

$$\text{trace } [P(k+1/k+1)]$$

To find this value for $K(k+1)$ it is necessary to take the partial derivative of $P(k+1/k+1)$ with respect to $K(k+1)$ and equate it to zero.

The optimum value for $K(k+1)$ is found to be of the standard form

$$K(k+1) = P(k+1/k) H^T [HP(k+1/k)H^T + R]^{-1} \quad (5.13)$$

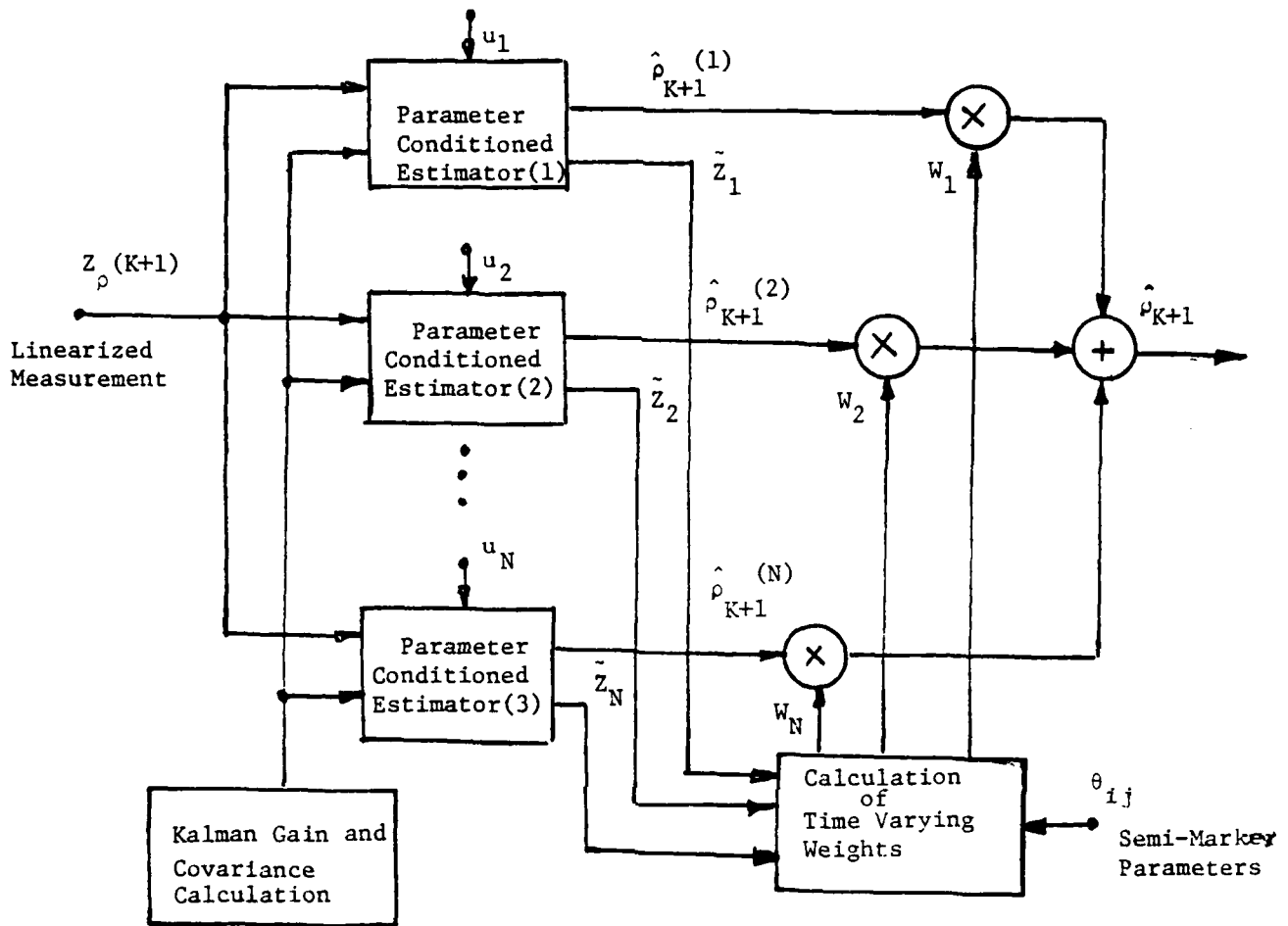
where

$$P(k+1/k) = [\phi P(k/k)\phi^T + \psi Q \psi^T + D] \quad (5.14)$$

where $P(k+1/k)$ is computed using the new additional error term. The subsequent calculations are identical with those for the Kalman filter. Thus the effect of the mismatch in the two inputs is propagated throughout the entire Kalman filter algorithm. From earlier work, we have found the estimates of the target states to be close enough to allow the assumption that $E\{\hat{x}(k/k) - x(k)\} \approx 0$. In other words, our estimator is an unbiased estimator. Thus D reduces to $\Gamma E\{(u^i - u(k))(u^i - u(k))\} \Gamma^T$.

Let δu be a uniformly distributed random variable equal to $(u_k - u^i)$. Now by setting the range of the random variable equal to $-\frac{\Delta u}{2} \leq \delta u \leq +\frac{\Delta u}{2}$ the variance is easily shown to equal $\frac{\Delta u^2}{12}$. Here Δu is the spacing between adjacent pairs of levels u_i, u_{i+1} . This analytic result turns out to equal very closely the experimentally obtained values in the 1979 ONR Report of Moose and McCabe. Thus the one step predicted covariance matrix

$$P(k+1/k) = [\phi P(k/k)\phi^T + \psi Q \psi^T + \Gamma \frac{\Delta u^2}{12} \Gamma^T]. \quad (5.15)$$



ADAPTIVE POLAR RANGE ESTIMATOR

Figure (27)

5-3 Range Estimation Results

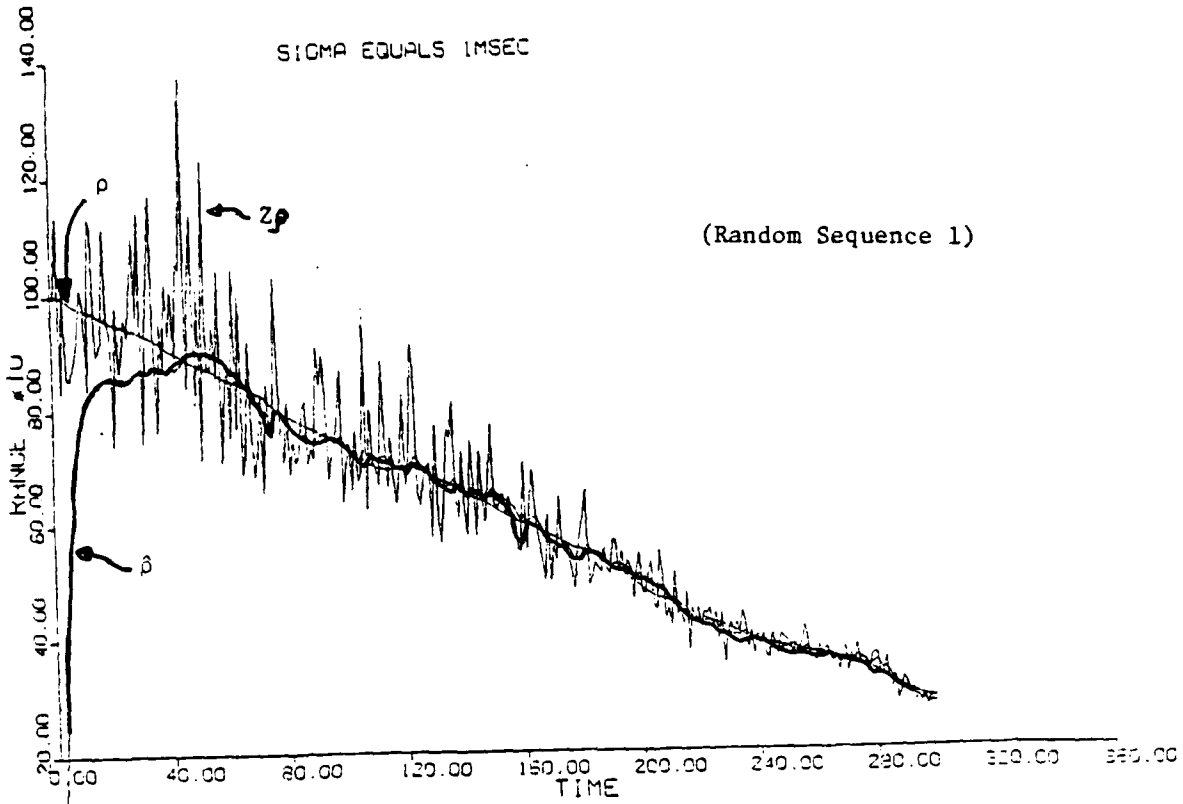
In order to have a *benchmark* with which to compare the adaptive estimator's performance the following scenario was devised. A target at the extreme range of 100,000 was generated on a closing trajectory of 25 ft/sec at a depth of 600. The target's plant model was matched exactly with that of the filter. This was done to simulate and test the performance of the optimal (non-realizable) tracking filter. In addition, it also provided a test of the nonlinear prefilter and the adaptive state estimator whose weights were all set at zero for the unmatched filters and unity for the single matched filter.

Target tracking results are shown in figures 28 and 29 for additive noises of 1 and 5 m sec, respectively. Examining the figures we see that for each, two different simulations are shown. They represent the performance that one would expect out of the unrealizable filter when two widely different sequences of random numbers are used in the data simulator that is shown in figure 12 on page 29. Notice that the vertical scale has been changed in figure 29 to show the effect of the nonlinear prefilter. The range estimates ($\hat{\rho}$) are shown darker than the actual range (ρ).

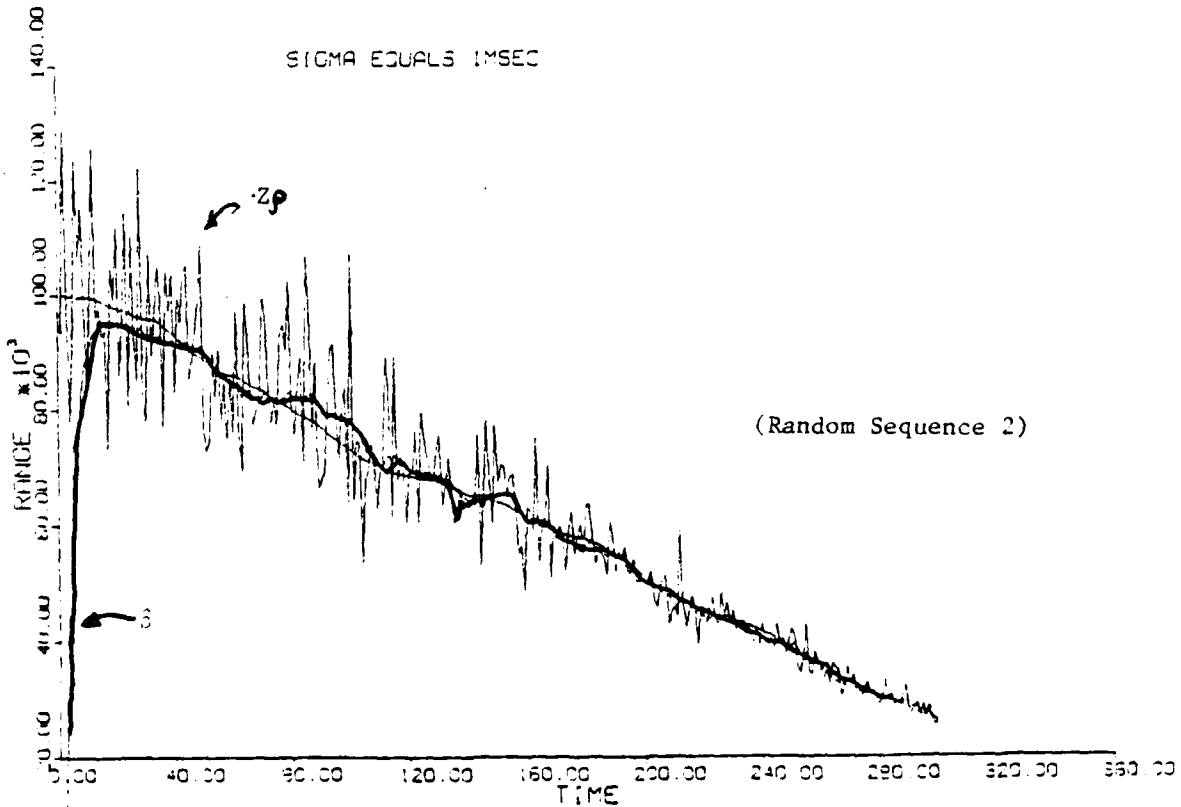
The data simulation of Figure 12, page 29 made use of the following parameters: the maneuver time constant ($1/\alpha$) was chosen as 25 seconds, the singer correlated acceleration time constant ($1/a$) in equation 1.3.1 was selected to be 40 sec, and the data rate was chosen to be one sample every 10 seconds. Although studies were made indicating a marginal increase in tracking performance, for sample intervals of 2 and 5 seconds, the sample interval was retained at 10 seconds in order to reduce the computation burden for real world applications.

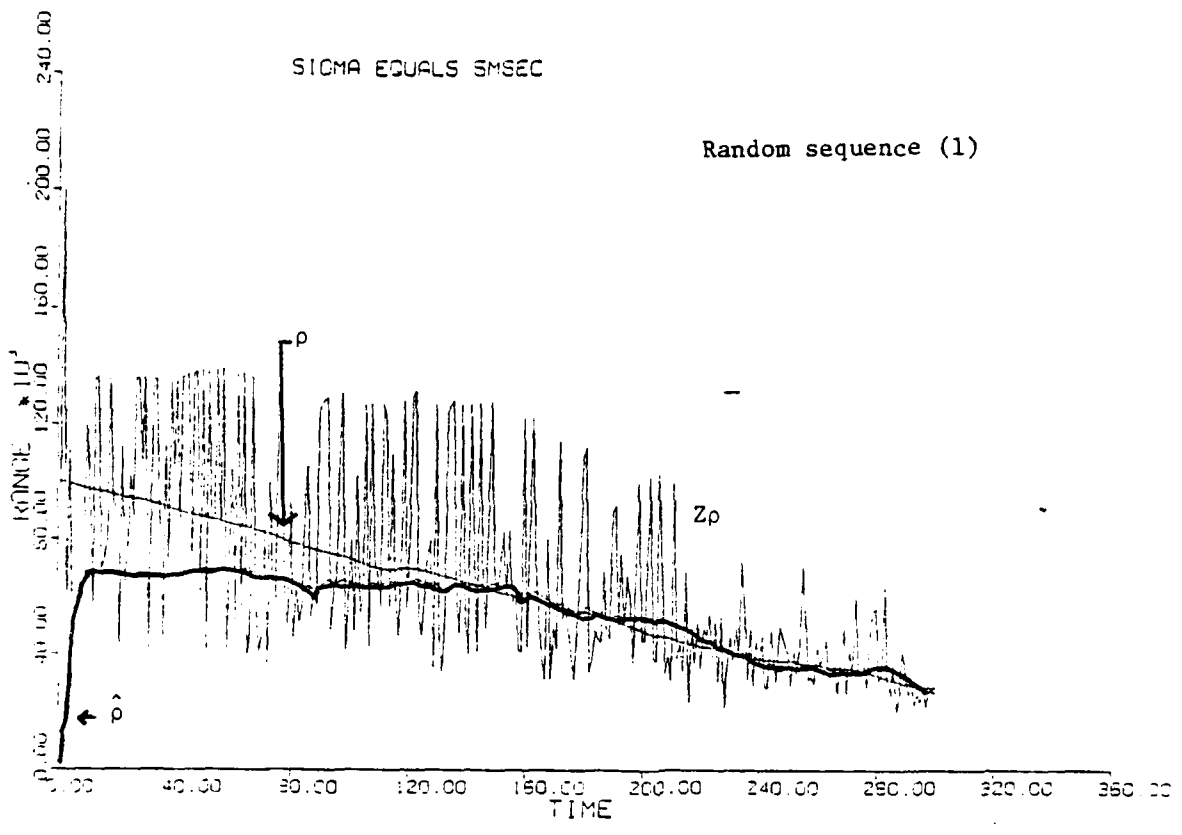
In the adaptive estimator of Figure (27), 6 levels of input u_i were chosen to span the expected target velocity range of +30 (ft/sec) for an opening target and -45 (ft/sec) for a closing target. If the velocity ranges were greater than this number N , could be increased slightly. The u_i 's were chosen to model +30, +15, 0, -15, -30, -45 (ft/sec).

The next figure (30) shows the realizable adaptive filter tracking in the presence of high noise (5 m sec). The target makes a random step change in velocity at time $k = 150$, which corresponds to 1500 seconds into the sceario. The raw data out of the nonlinear prefilter is shown almost filling the plot. Notice though, that the variance becomes smaller with

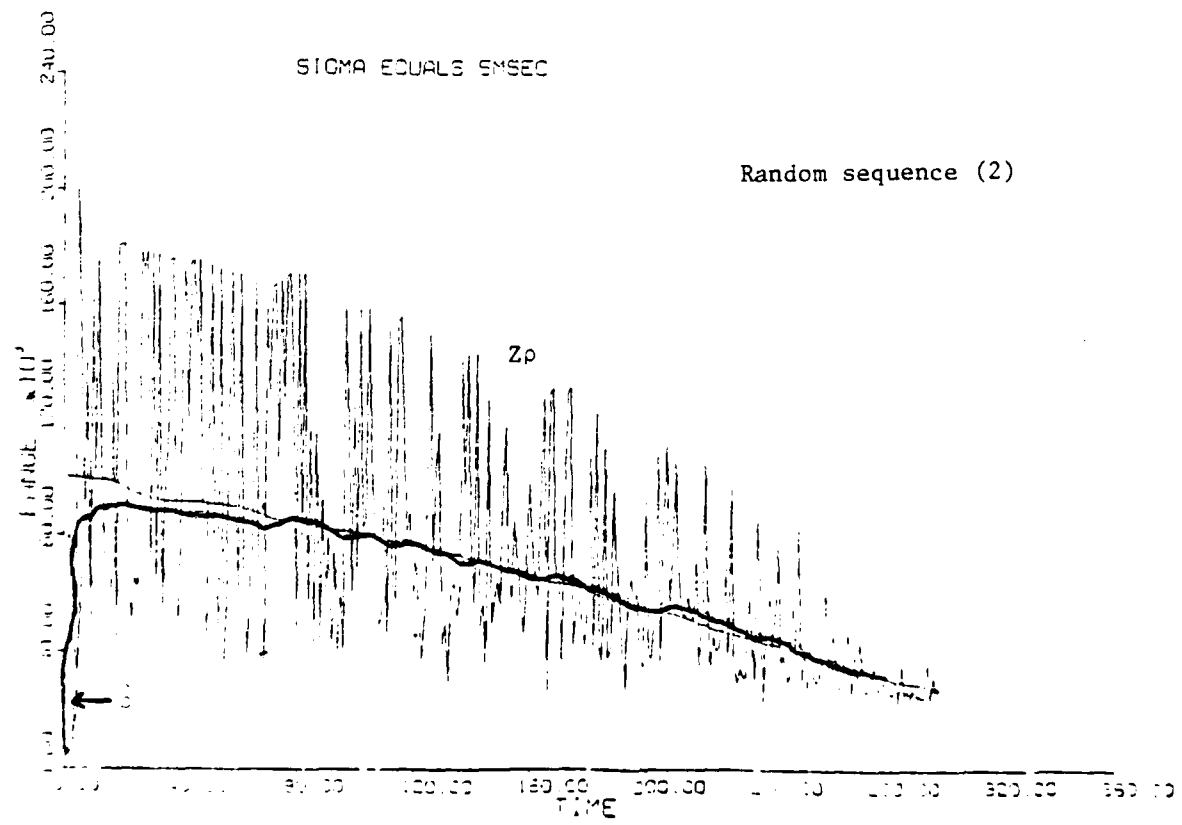


Range Estimate of Nonrealizable Tracking Filter (Figure 28)

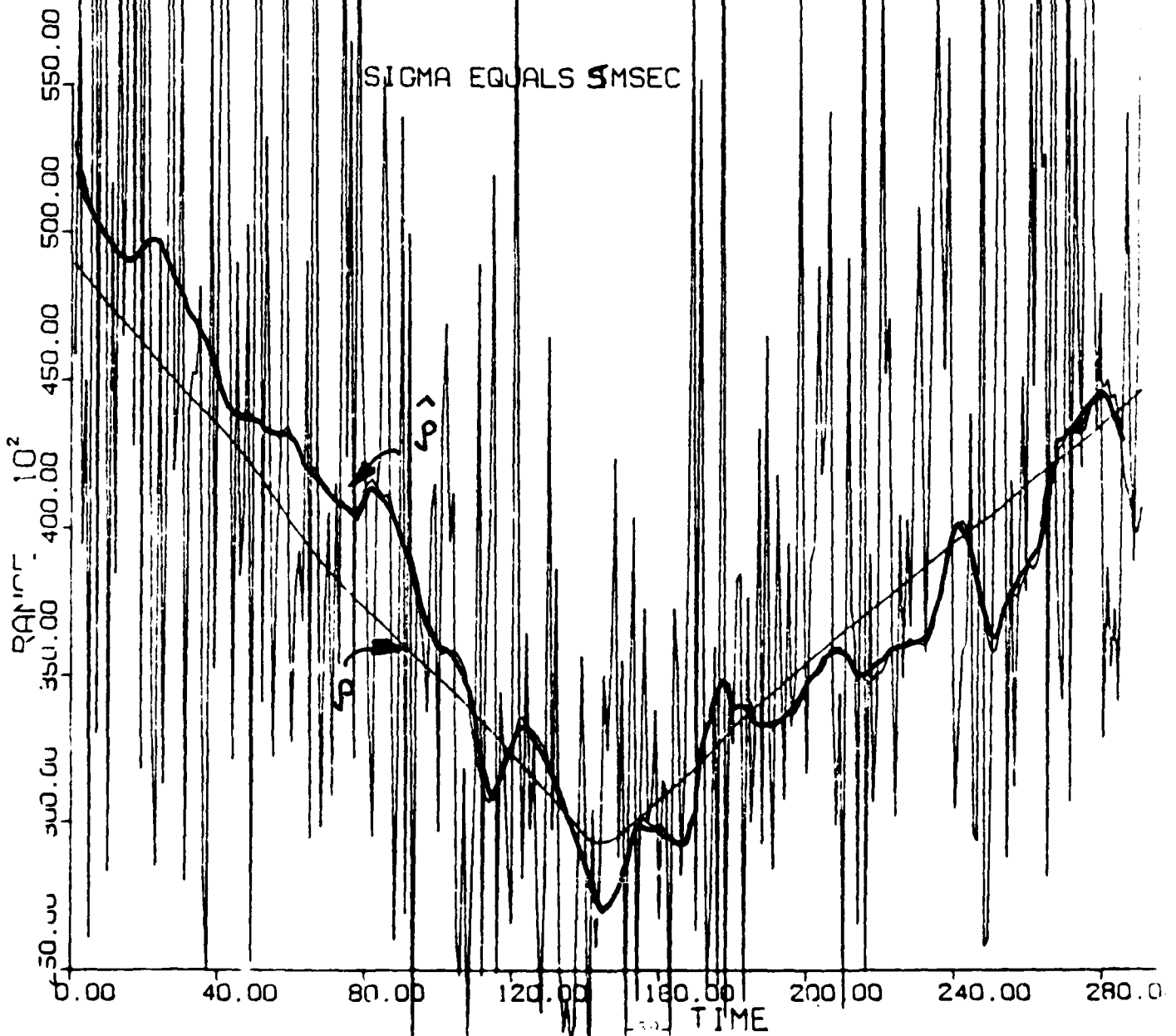




Range Estimate of Non-realizable Tracking Filter Figure (29)



Range Estimation of Adaptive Filter in the Presence of High Noise (Figure 30)



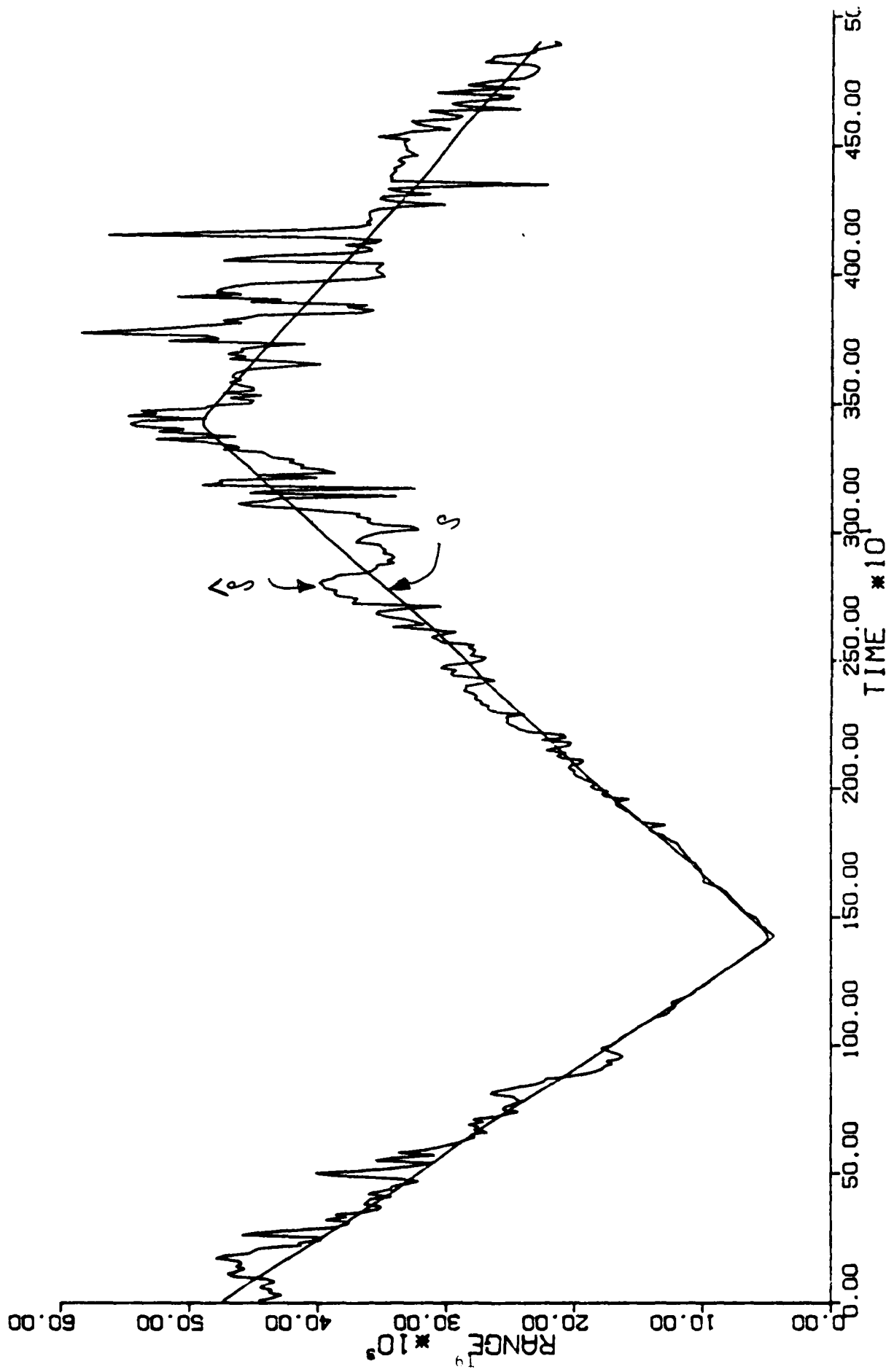
decreasing range then grows as range increases. This is typical of all simulations in this report, and point out the nonstationary random processes involved. Output of the estimator (darkline) is seen to fluctuate about the true value of range with *maximum* errors on the order of 5000 which corresponds to 10-15%. From this point on, in the presentation of the results of the ranging portion, the noisy measurements Z_p will not be shown.

In figure 31, we see the results of tracking a medium range (0-45k) target as it undergoes a maneuver at $k = 140$ and $k = 340$. The target is on a closing trajectory then reverses its velocity at 140 and 340. The estimate $\hat{\rho}$ tracks very well at close ranges and progressively gives noisier estimates as the targets range increases. This is due to the variance of the measurements, which are not shown, increasing with range. The additive time delay noise is $\sigma_1 = \sigma_2 = 3$ m sec.

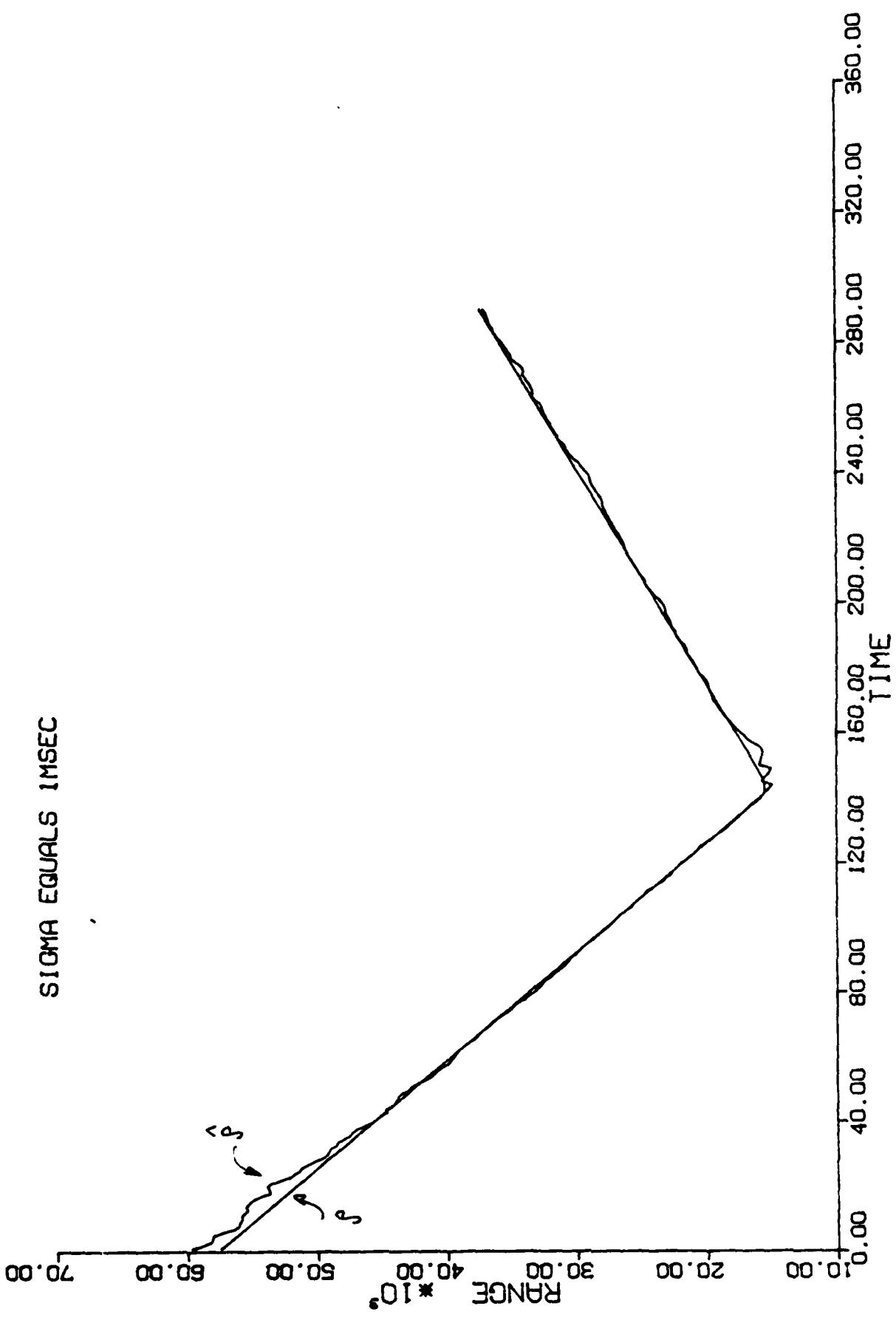
Several conclusions can be drawn from figure 31. The first is that we need to limit ourselves to close proximity targets, or smooth the estimate $\hat{\rho}(k)$, or operate in an environment with smaller additive noises.

Figure 32 shows the effects of decreasing the measurement error to a standard deviation of 1 m sec. The target makes a maneuver at $k = 140$ and the estimate $\hat{\rho}$ tracks extremely well throughout the scenario. The next figure (33) shows the weighting coefficients u_i and u_j as they vary due to the target maneuver. It is seen that the weights switch appropriately from 0 to unity as required.

The last figure (34) in this section illustrates velocity estimation $\hat{\dot{\rho}}$ vs time for a target that abruptly reverses velocity at $k = 140$. The adaptive state estimator very quickly maintains track as shown. The additive time delay measurement noise has been increased back to 3 m sec. The process noises driving the plant (target) model is excessive and will be reduced in the following work.

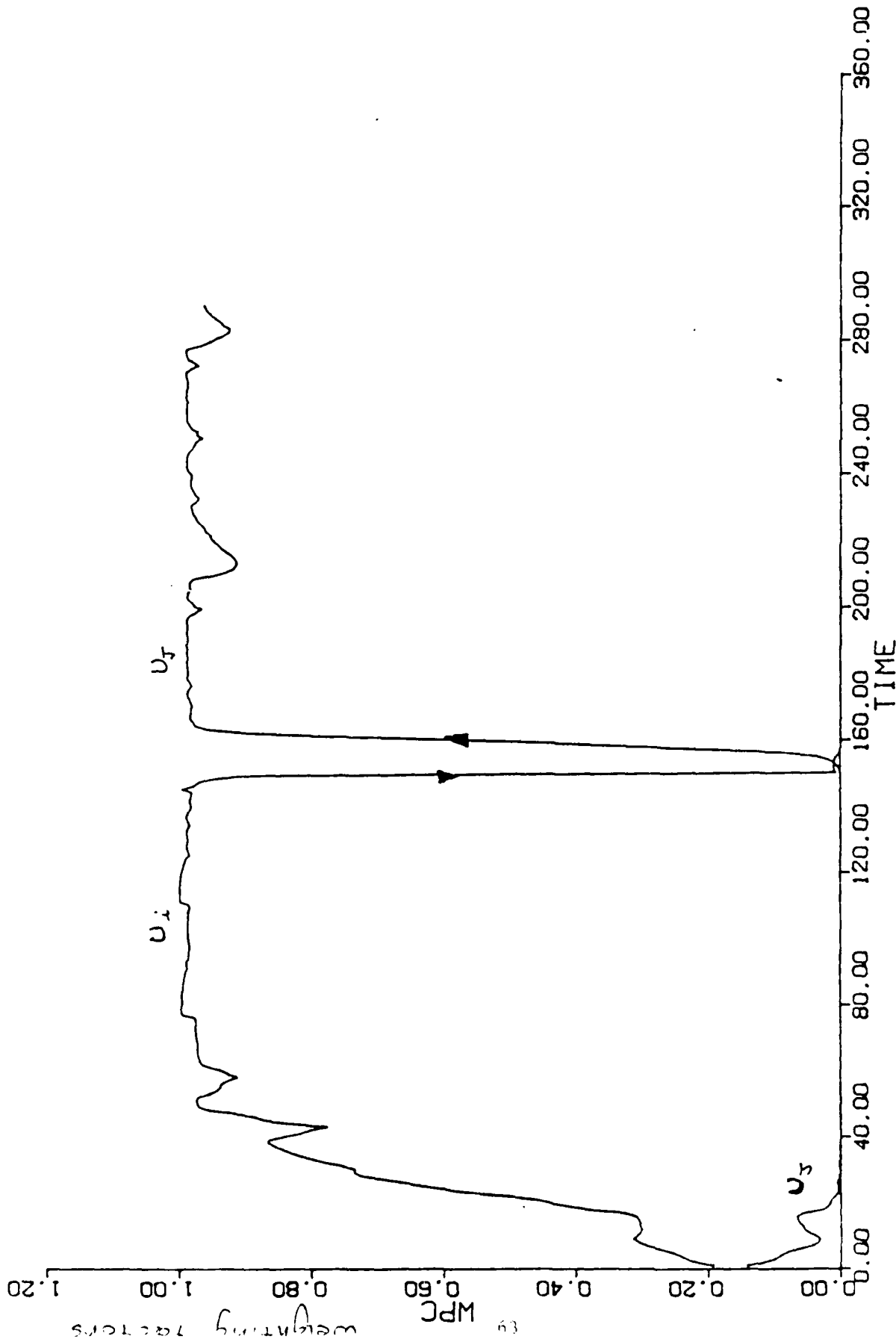


Target Tracking in the Event of Multiple Maneuvers
(Figure 31)



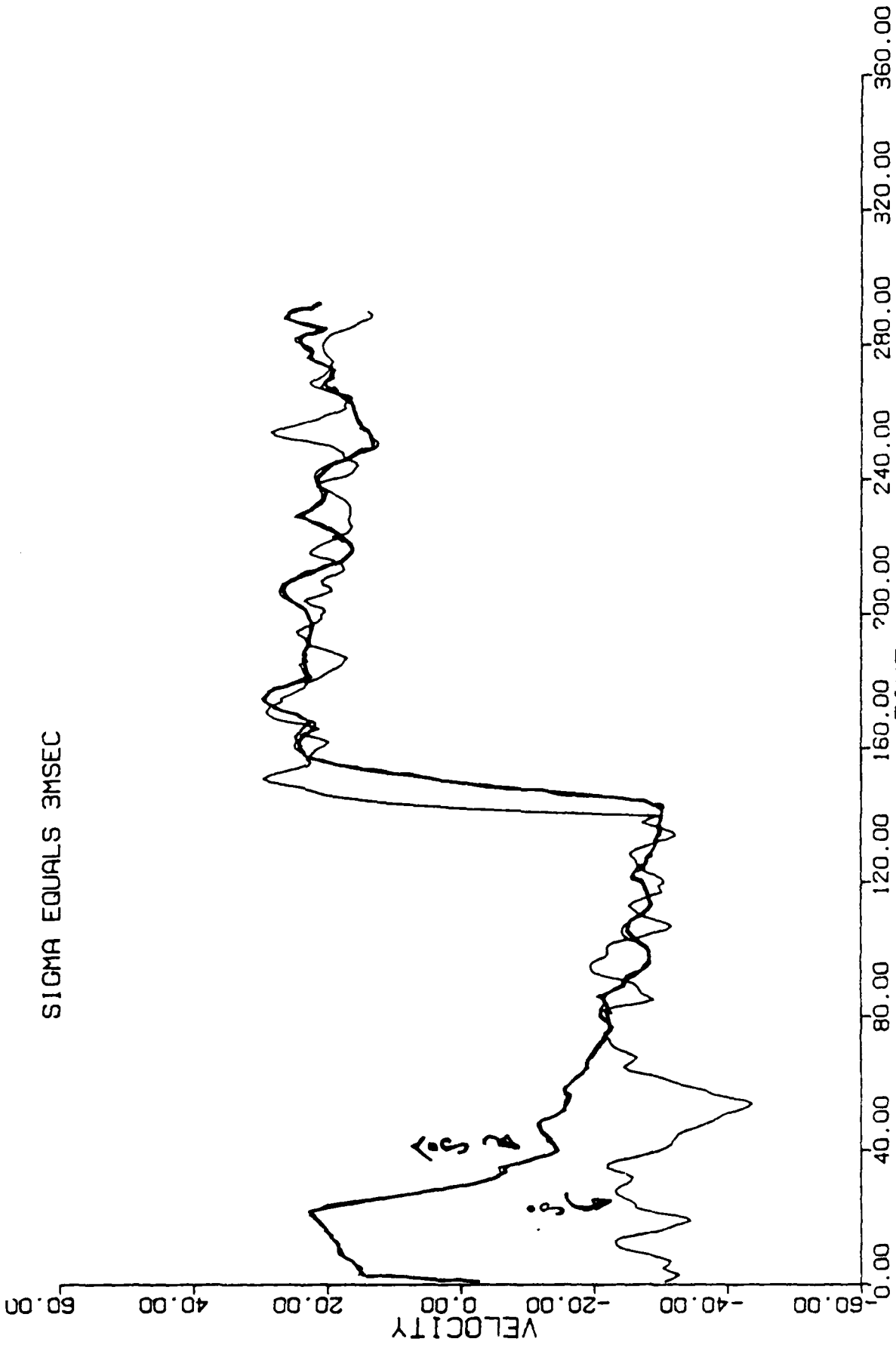
SIGMA EQUALS 1MSEC

Target Tracking for the Low Noise Case
(Figure 32)



Plot of Weighting Factors vs Time Illustrating Effects of Target Manuever (Figure 33)

SIGMA EQUALS 3MSEC



Velocity Estimation for an Abruptly Maneuvering Target
(Figure 34)

5-4 Modification to the Adaptive State Estimator

In order to operate in a noisy environment where the additive measurement errors attached to τ_1 and τ_2 are greater than or equal to 3 m sec, it becomes necessary to smooth both the weighting coefficients and/or the output estimate $\hat{\rho}_{k+1}$. It was found that a simple first order digital filter of the form

$$\tilde{\rho}_{k+1} = a\tilde{\rho}_k + b\hat{\rho}_{k+1} \quad (5.4.1)$$

was successful for good smoothing and small lag in tracking maneuvers. The term $\tilde{\rho}_{k+1}$ represents the smoothed output range estimate at t_{k+1} and $\hat{\rho}_{k+1}$ the "rough" filter input. Coefficients a and b were set at 0.9 and 0.1 respectively.

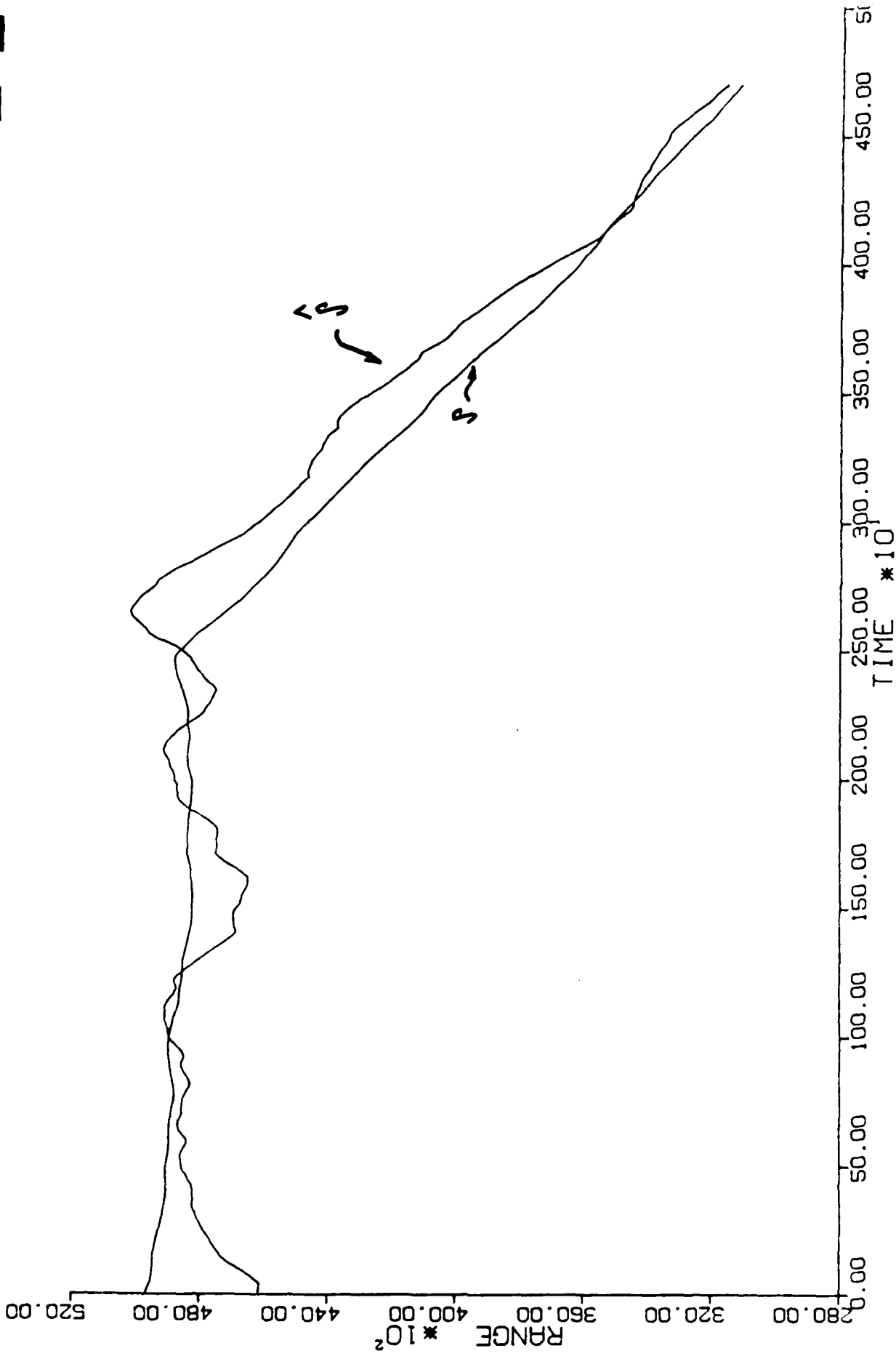
In addition, to output smoothing the weighting coefficients $w_i(k)$ $i = 1, 2, \dots, 6$ were averaged as follows:

$$\tilde{w}_i(k) = \frac{1}{N} \sum_{j=0}^{N-1} w_i(k-j) \quad (5.4.2)$$

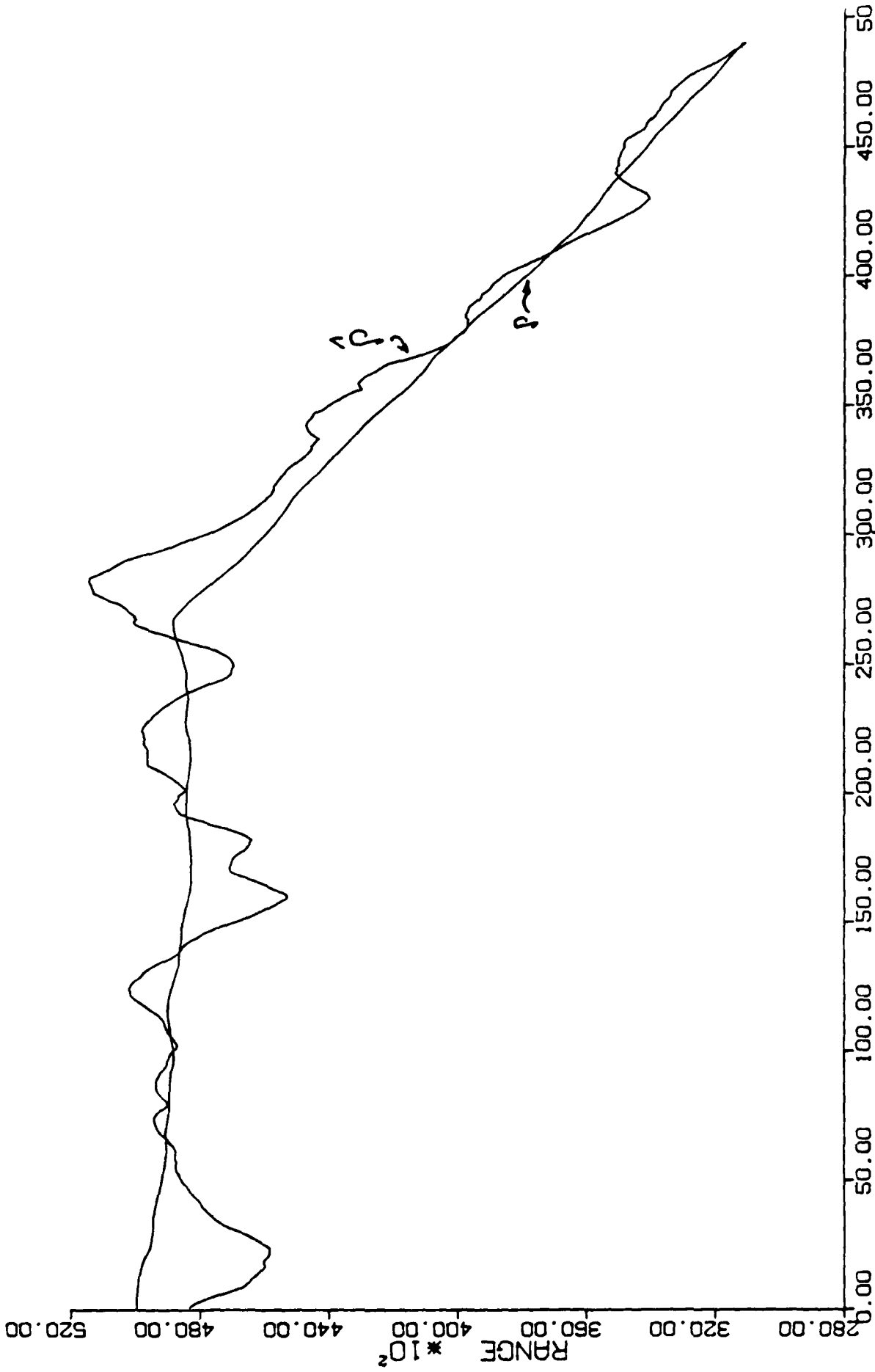
Here $\tilde{w}_i(k)$ represents the time averaged output of the moving window averager equation 5.4.2. Numerous simulations were performed as N was changed from 10 to 30. The results follow.

Figures (35 and 36) illustrate the filters range tracking performance for the case of low signal to noise ratios (long ranges), and the effect of averaging the probability weighting coefficients $w_i(k)$ on the smoothness of the filters output. The scenario used to generate figures (35,36) starts the target at a constant range of 50,000 feet with zero closing velocity and then changes the target velocity to -15 ft/sec after 2,500 seconds. Figures 35 and 36 show the filters range estimate superimposed on the target range output with 30 and 10 data points averaged respectively. It is easily seen that as the number of averaged data points decreases the smoothness of the range estimate also decreases.

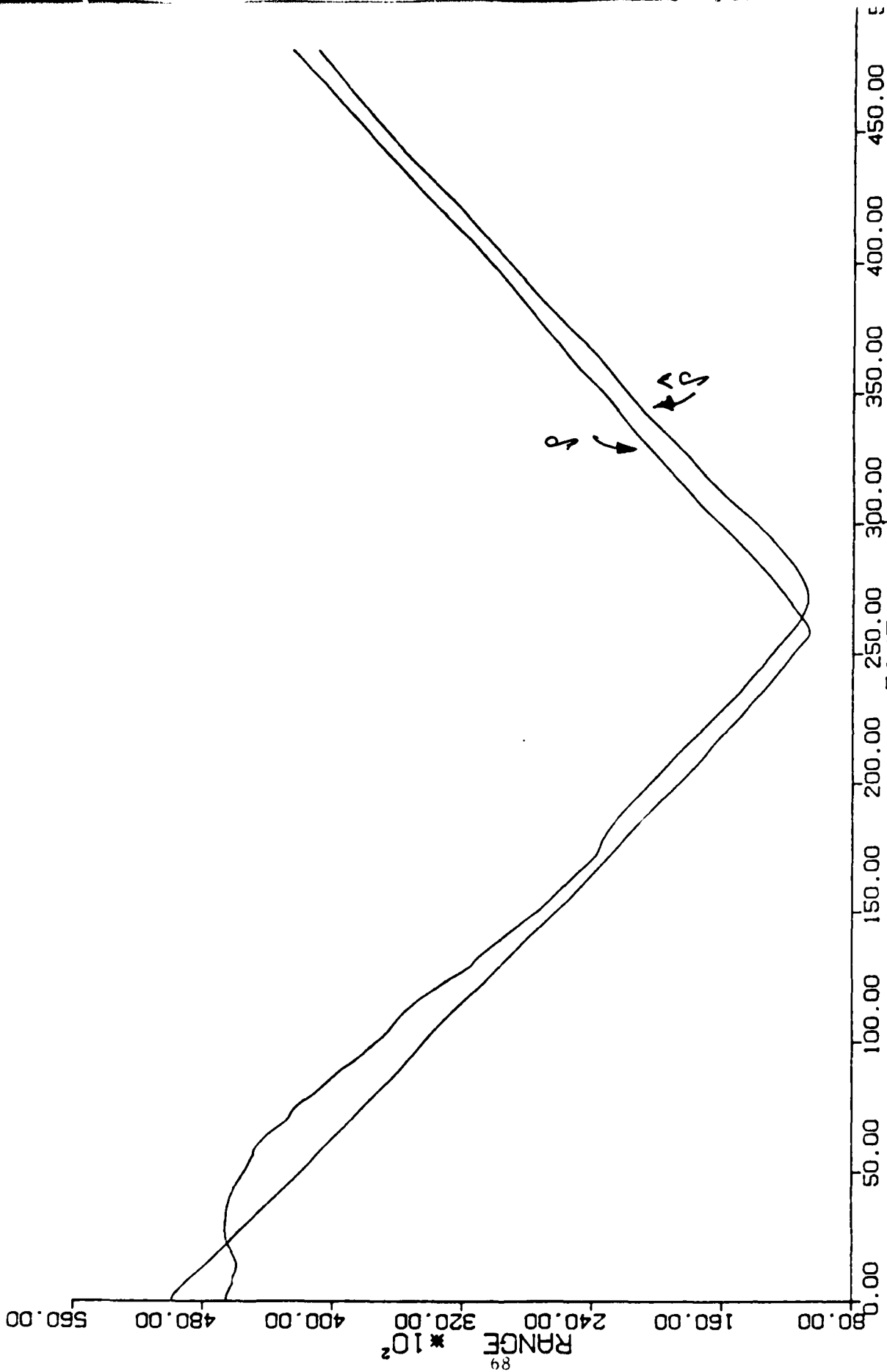
Figures (37 and 38) illustrate the performance of the filter's range and velocity estimates and the adaptive nature of the weighting functions. The figures also show how the number of averaged data points $\tilde{w}_i(k)$ effects all of the above mentioned parameters. The scenario used to generate figures (37, 38) starts the target at a range of 50,000 ft. and a velocity of -30 ft/sec (-means toward observer) and changes the targets velocity to +30 ft/sec after 2,500 seconds. Figures 37 and 40 show range estimates superimposed over the



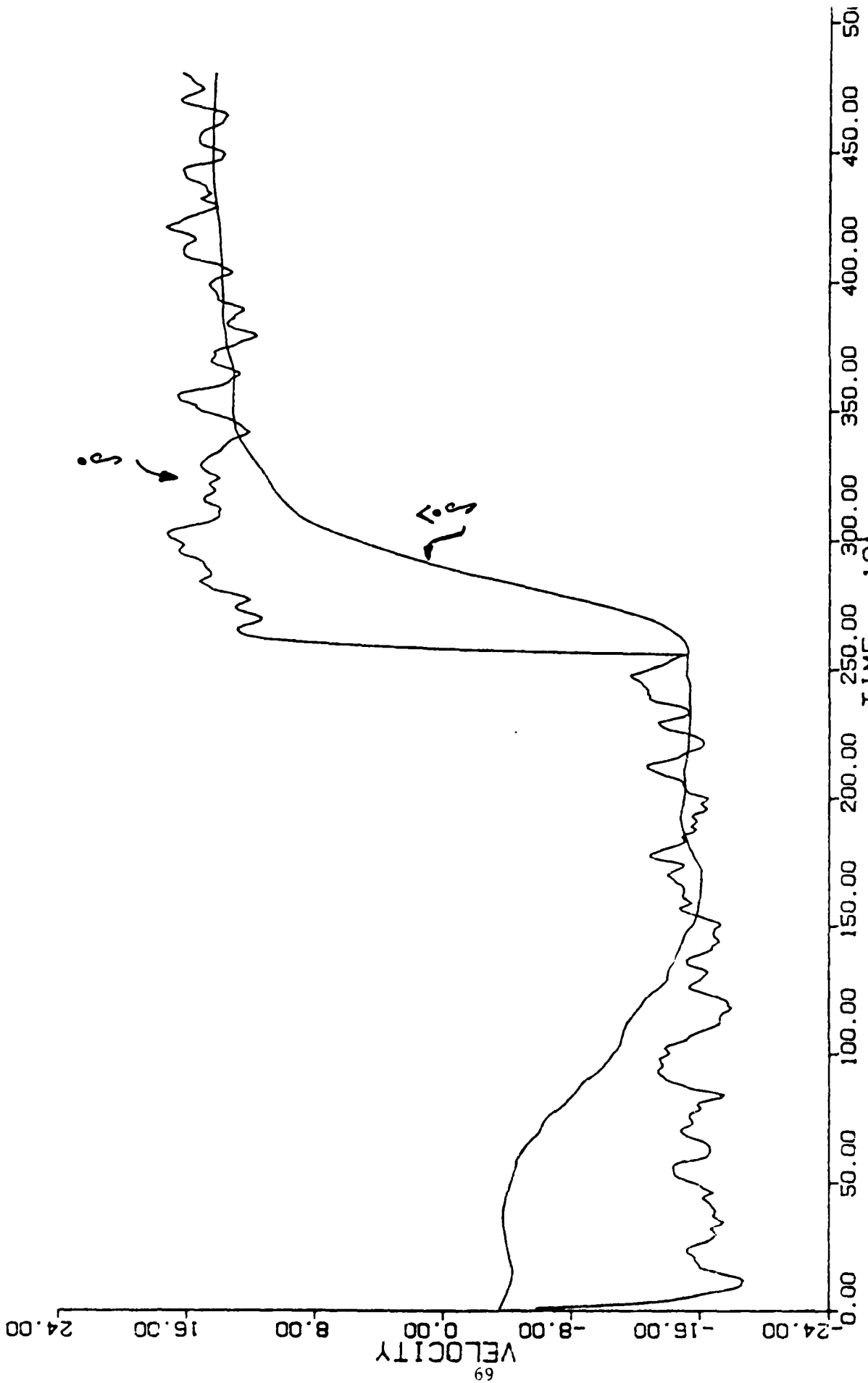
State Estimation with Output Smoothing and (30) Averaged Weights
(Figure 35)



State Estimation with Output Smoothing and (10) Averaged Weights
(Figure 36)



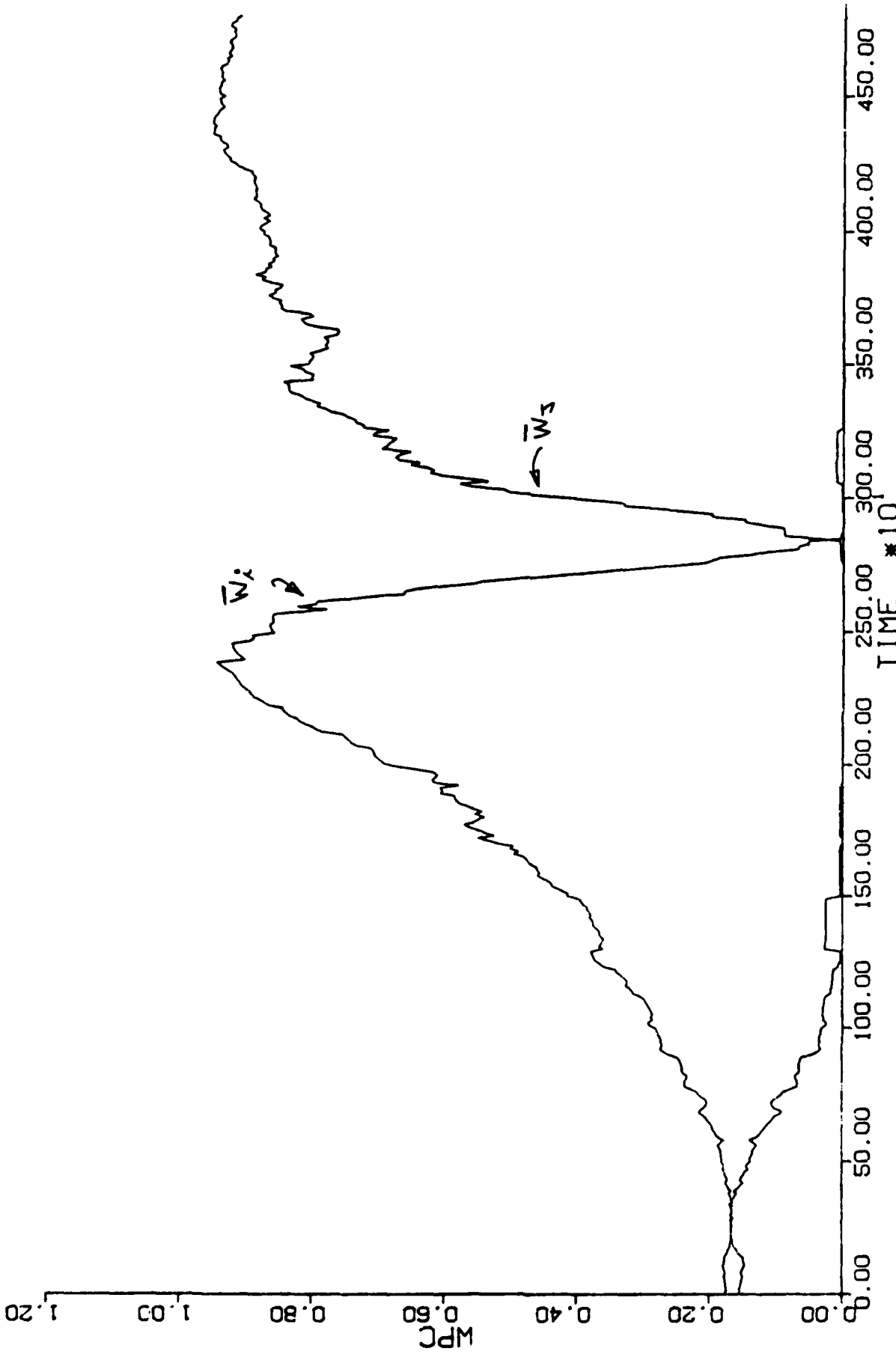
Estimate of Range for Approaching / Opening Target (20 points) Averaged
 (Figure 37)



Estimate of Velocity for Maneuvering Target (20 points) Averaged
(Figure 38)

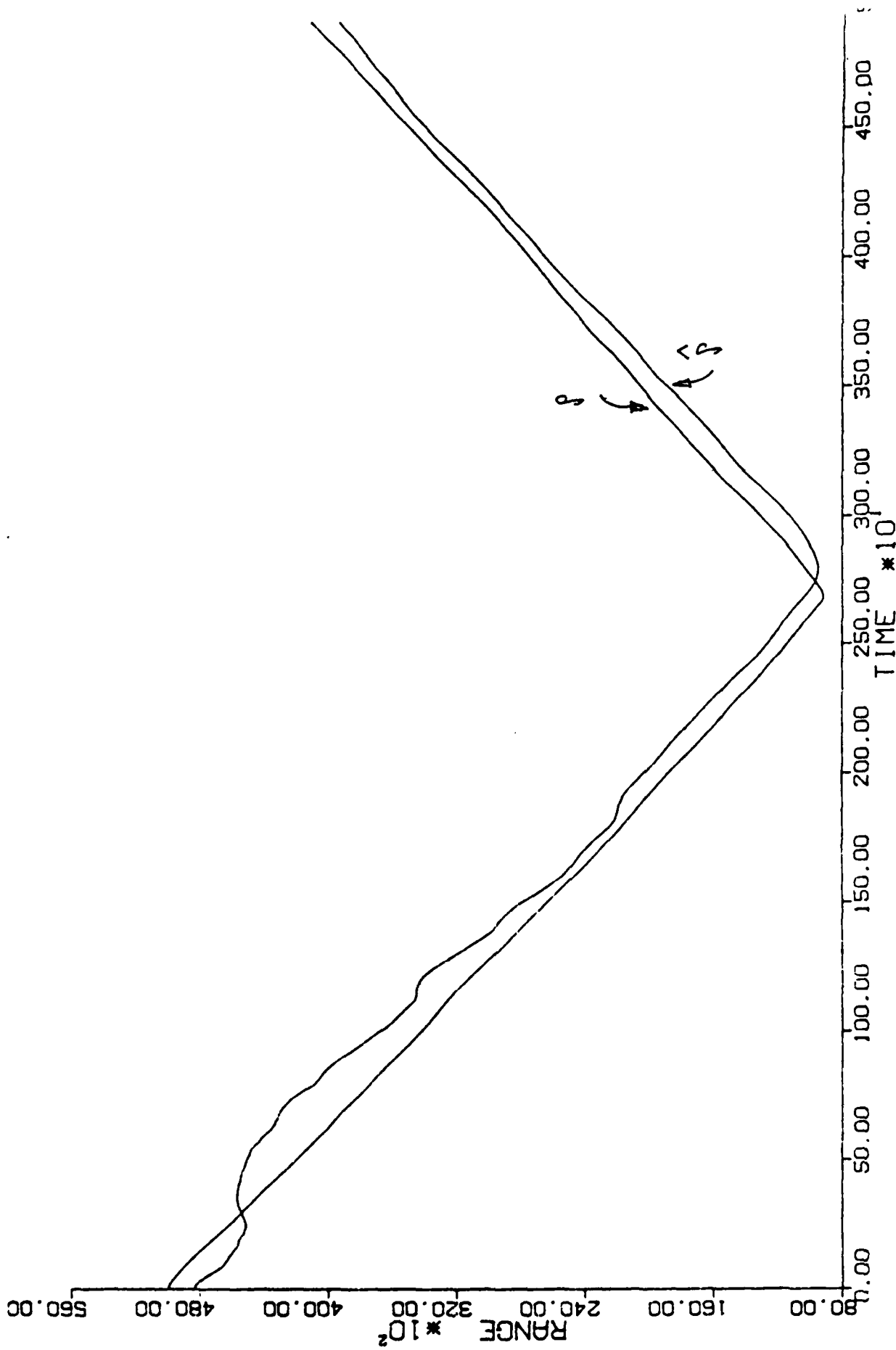
plant range output with 20 and 10 data points averaged respectively. Figures 38 and 41 show velocity estimates superimposed on the plant velocity output with 20 and 10 data points averaged respectively. Figures 39 and 42 show the learning performance of the weighting factors associated with the filters whose deterministic inputs (u_i) most nearly matches that of the plot output. Figures 39 and 42 average 20 and 10 data points respectively. In all of these types of curves shown in figures (37-42), the curves become smoother as the number of averaged data points increases.

Figure 43 shows the range estimate superimposed over the target range output for a scenario with a number of velocity changes. The scenario starts the target at 50,000 ft. with a closing velocity of -30 ft/sec. At 1,500 seconds a maneuver is made with velocity changing to +30 ft/sec, and then again changing to -30 ft/sec at 3,500 seconds. The adaptive tracking filter quickly determines that a maneuver has been made and adjusts itself to provide a good estimate.

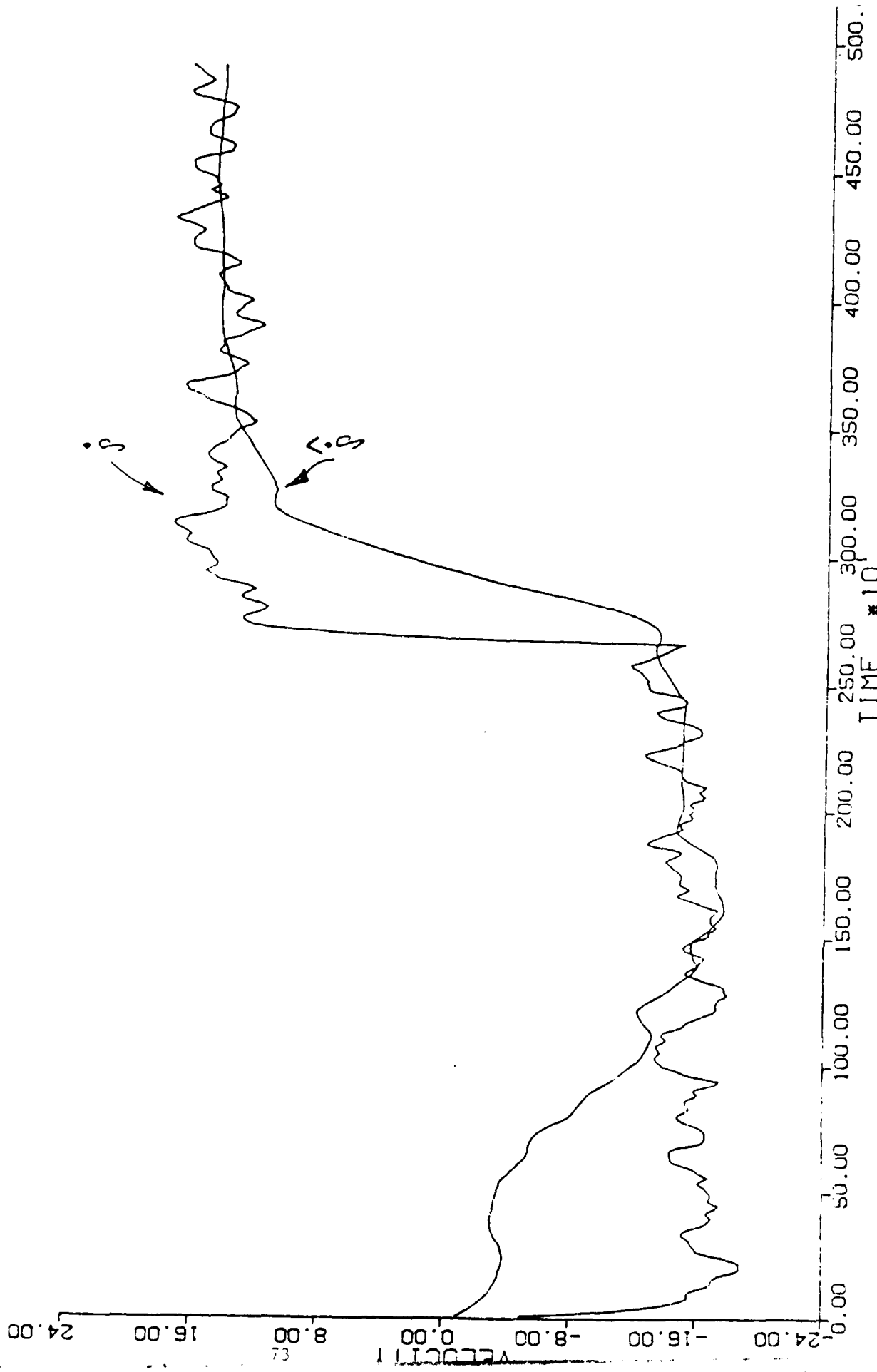


Weighting Coefficients vs Time Showing Learning Ability (20 points) Averaged

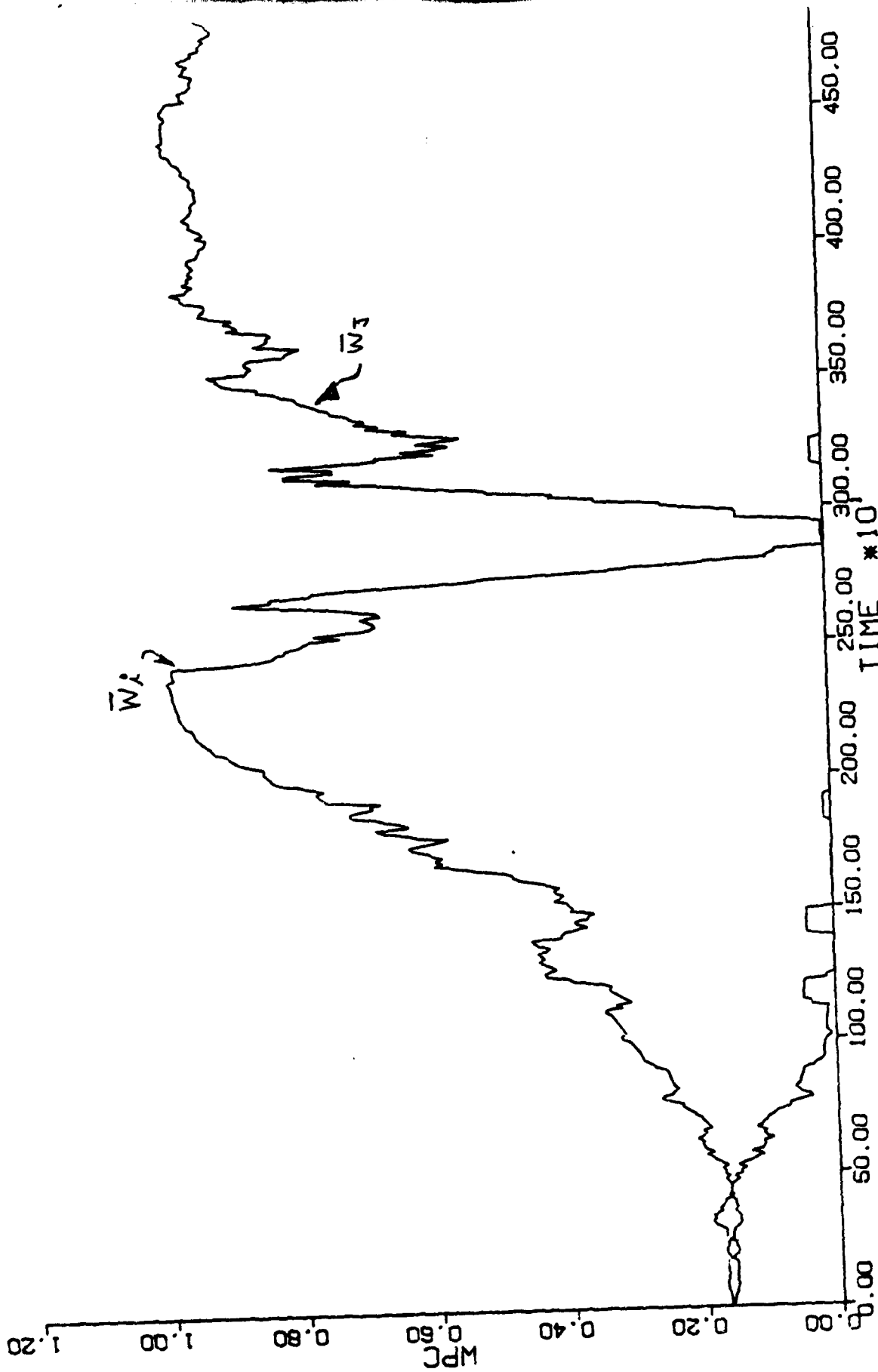
(Figure 39)



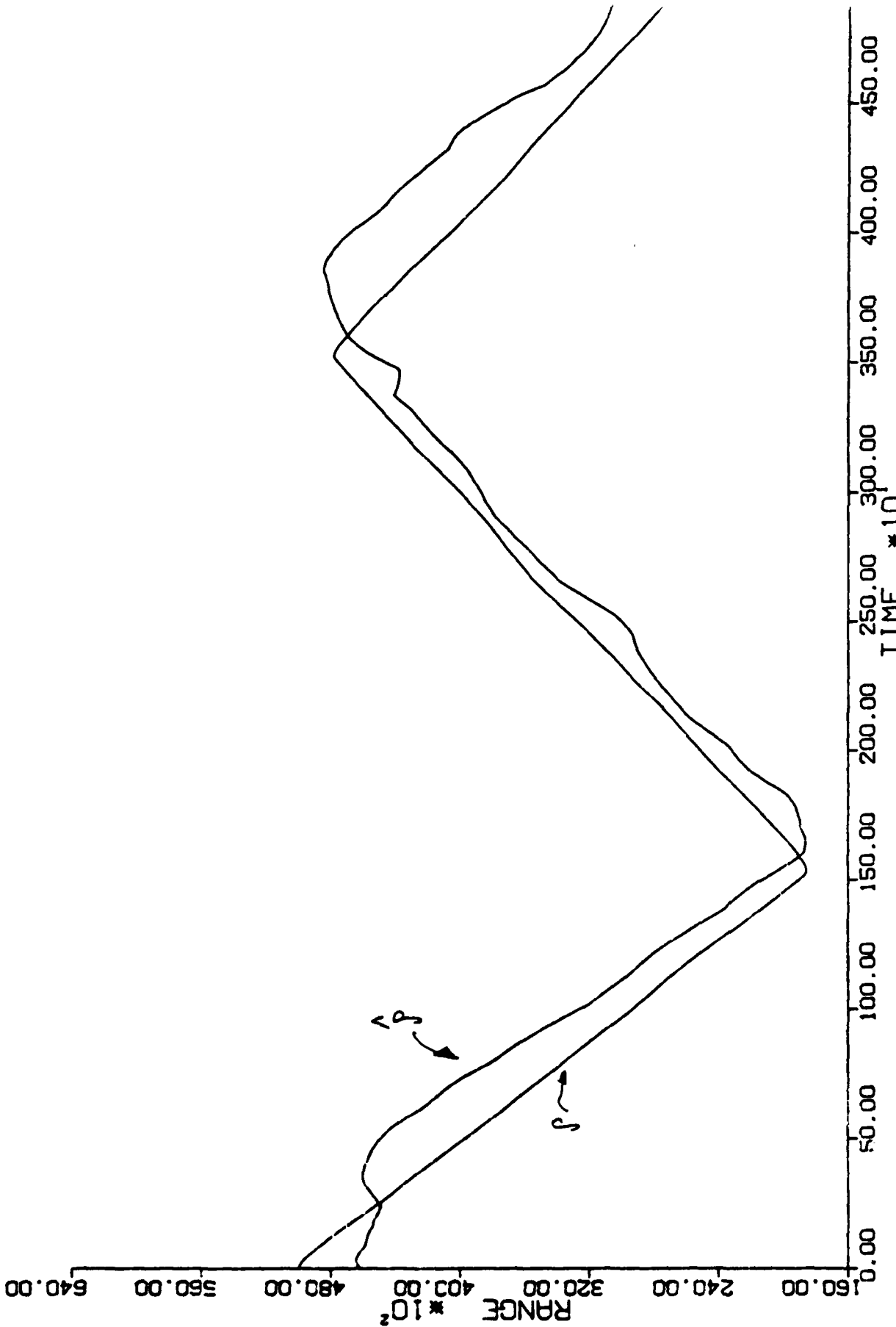
Range Estimation vs Time for (10 points) Averaged
(Figure 40)



Velocity Estimation vs Time with Maneuver at $K = 260$
 (Figure 41)



Weighting Coefficients vs Time Showing Learning Ability (10 points) Averaged
(Figure 42)



Multi Maneuver Situation with Target Undergoing Maximum Velocity Changes
(Figure 43)

6 Conclusion

An adaptive state estimator has been developed and extensively tested to track a target making random large scale maneuvers in velocity and random depth variations as well. The target/observer scenario is constrained to the vertical plane in the ocean environment. This was intentionally done so as not to compete with well established bearing tracking programs.

The adaptive estimator made use of a nonlinear prefilter to *uncouple* the state variables that model target motion in both depth and range. An additional benefit was the elimination of all extended Kalman filters in the tracking system. This results in a more *robust* tracker and significantly fewer computations. The cost of doing this, is that the linearized measurements contain nonstationary and non-Gaussian measurement errors.

System inputs to the tracking system consists of noisy time difference measurements of bottom/direct, and surface/direct multipath time delays. The adaptive tracker pre-filters the noisy multipath measurements in a nonlinear operation and then transmits the new linearized depth and range measurements into their respective filtering channels. The depth channel gave good estimates as the target underwent random depth changes. The range channel was more complex, in that since the target is free to make major random velocity changes it required six Kalman filters and an adaptive weighting technique to span the expected range of all target velocities. Computationally this was quite easily done since each filter was only third order, and had the same Kalman gain and covariance matrix which only required one basic computation common to all six filters. The filters differed only in the deterministic input u_i , $i = 1, 2, \dots, N$ built into each. As the target changed range in 5k increments new means and variances were programmed into the filter bank thus compensating for the effect of nonstationary linearized measurement errors.

Overall tracking results seem quite good, especially in the low signal to noise ratio cases. An on-going effort is underway to study techniques of averaging data to Gaussianize the measurement errors and will be reported upon in a later report.

Appendix

Problem: Find the mean and variance of the density function at the output of a non-linear filter whose input is $N(0, \sigma_T^2)$ using numerical integration techniques.

$$v_T = \frac{N(0, \sigma_T^2)}{\frac{-p v_T}{v_T + \tau_T}} \rightarrow v_p$$

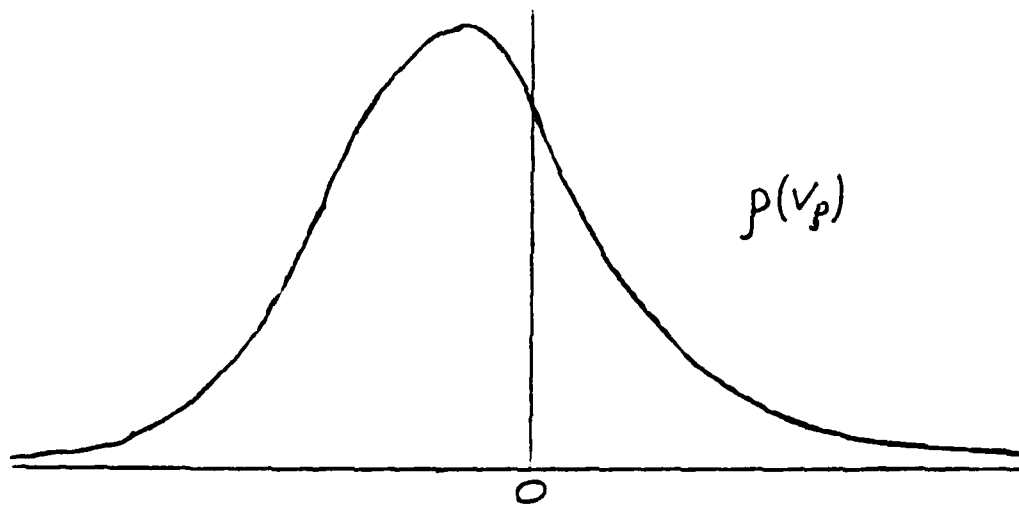


Fig. 1

The mean and variance of $p(v_p)$ can be computed using the following two methods:

A) Calculate the output density function from the input which produces $p(v_p)$ and integrate as usual.

$$p(v_p) = \frac{p \tau_T}{(v_p + p)^2 \sigma_T \sqrt{2\pi}} e^{-\frac{\tau_T^2 v_p^2}{(v_p + p)^2}}$$

$$\text{mean} = \int_{-\infty}^{\infty} v_p p(v_p) dv_p = m$$

$$\text{variance} = \int_{-\infty}^{\infty} (v_p - m)^2 p(v_p) dv_p$$

(4)

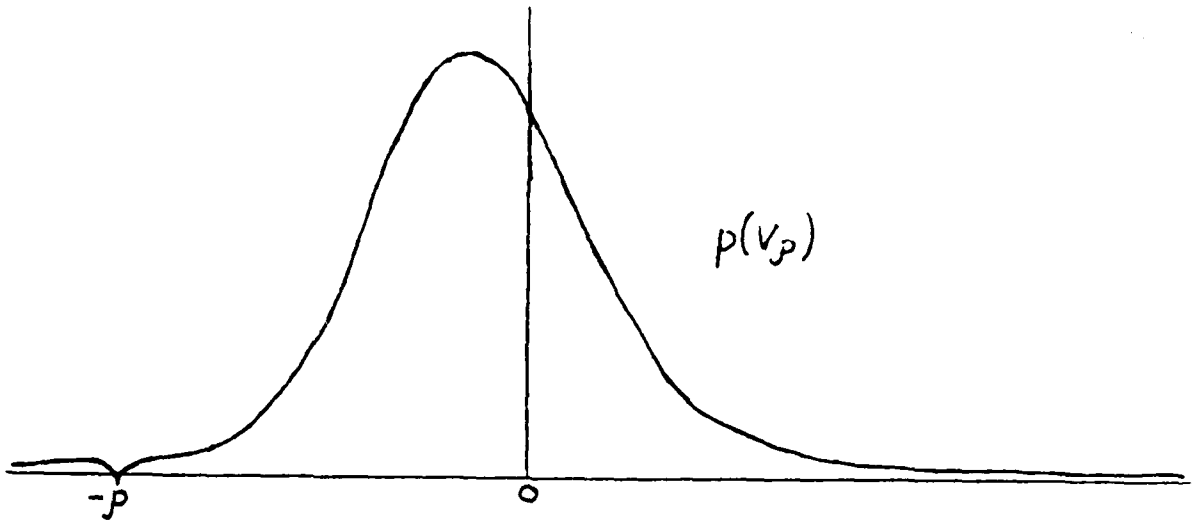


Fig. 2

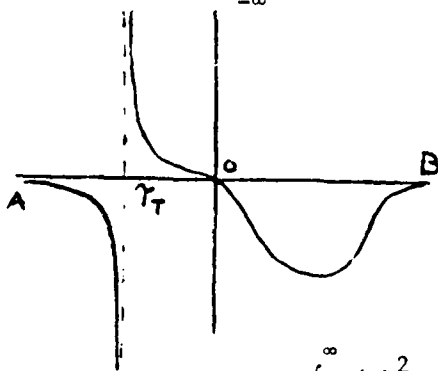
Note: 1) The tails of this function decrease slowly enough to cause problems in the calculation of the variance.

2) There is a singularity at $-p$ which must be dealt with.

These problems will be discussed in further detail latter on.

B) Let $\frac{-p v_T}{v_T + \tau_T} = g(x)$ and calculate the mean and variance as follows:

$$\text{mean} = \int_{-\infty}^{\infty} g(x) p(x) dx \quad \text{where } p(x) = N(0, \sigma^2)$$



$$\text{variance} = \int_{-\infty}^{\infty} g(x)^2 p(x) dx - m^2$$

$$\text{mean} = \int_{-\infty}^{\infty} \frac{-p v_T e^{-\frac{v_T^2}{2\sigma_T^2}}}{(v_T + \tau_T) \sigma_T \sqrt{2\pi}} dx \quad (B)$$

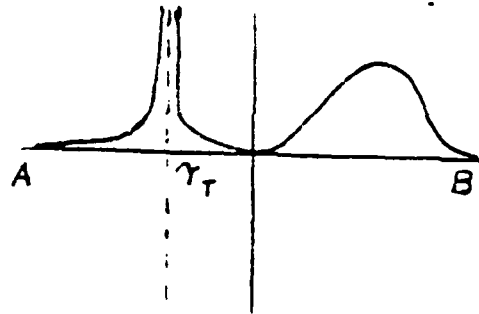


Fig. 3

Note: Both mean and variance functions have singularities at $-\tau_T$.

Calculation of Mean and Results

The mean of $p(v_p)$ was calculated using both methods A and B. The numerical integration was performed by the IMSL routine DCADRE which uses cautious Romberg extrapolation.

The singularity in eq. A caused the program to halt due to exponent underflow (i.e. $p(v_p) < 10^{-99}$). To avoid this problem, $p(v_p)$ was defined as 0 whenever it's value was less than 10^{-99} .

The singularity in equ. B caused the program to halt due to exponent overflow (i.e. $g(x) p(x) > 10^{99}$). In this case, it was assumed that the area under $g(x) p(x)$ from $-(\epsilon + \tau_T)$ to τ_T was equal to that from τ_T to $-(\tau_T - \epsilon)$ for small ϵ ($\epsilon < 10^{-6}$).^{*} Since these two areas are of opposite sign, they should cancel each other allowing integration from A to $-(\epsilon + \tau_T)$ and from $-(\tau_T - \epsilon)$ to B without affecting the final answer. (See Fig. 4.)

The mean was calculated using different values of p and τ_T , where $P * \tau_T = 500$. Method A and B produced corresponding answers whose differences were limited to the 3rd and 4th significant digit. The values of the mean associated with each p are listed in Table 1.

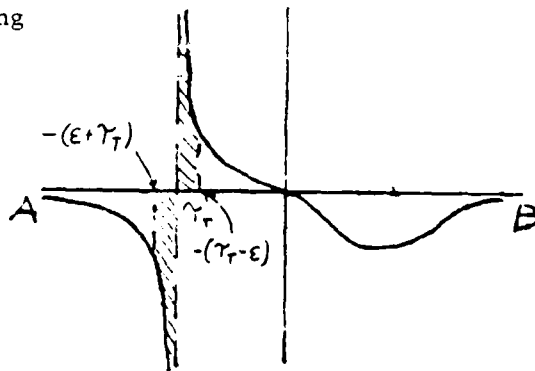


Fig. 4

^{*} ϵ was chosen as small as possible without causing exponent overflow.

Calculation of the Variance and Results

The variance was calculated using method A.

$$\text{var} = \int_{-\infty}^{\infty} \underbrace{\frac{v^2 p \tau_T}{(v+p)^2 \sigma_T \sqrt{2\pi}} e^{-\frac{v^2 \tau_T^2}{(v+p)^2 \sigma_T^2}}}_{F(v)} dv$$

One can see that the $\lim_{v \rightarrow \infty} F(v) = \frac{p \tau_T}{\sigma_T \sqrt{2\pi}} e^{-\frac{\tau_T^2}{2\sigma_T^2}} = \text{const.}$ This is due to

the fact that $\lim_{v \rightarrow \infty} \frac{v^2}{(v+p)^2} = \frac{v^2}{v^2} = 1.$

So at large values of $|v|$ the integral is that of a constant which becomes unbounded as the limits of integration increase in magnitude. Therefore a practical integration interval of $-100 * P$ to $100 * P$ was selected to produce a bounded and useful variance.

The variance associated with each p are listed in Table 1.

BIBLIOGRAPHY

- [1] A. H. Jazwinski, "Limited memory optimal filtering," IEEE Trans. Automat. Contr., vol. AC-13, Oct. 1968.
- [2] J. S. Thorp, "Optimal tracking of maneuvering targets," IEEE Trans. Aerosp. Electron. Syst., vol. AES-9, July 1973.
- [3] R. A. Singer, "Estimating optimal tracking filter performance for manned maneuvering targets," IEEE Trans. Aerosp. Electron. Syst., July 1970.
- [4] R. L. Moose, "Adaptive estimator for passive range and depth determination of a maneuvering target (U)," U. S. Naval J. Underwater Acoustics, July 1973.
- [5] N. H. Gholson and R. L. Moose, "Maneuvering target tracking using adaptive state estimation," IEEE Trans. Aerosp. Electron. Syst., May 1977.
- [6] R. A. Howard, "System analysis of semi-Markov processes," IEEE Trans. Mil Electron., vol. MIL-8, pp. 114-124, April 1964.
- [7] J. C. Hassab, "Passive Tracking of a Moving Source by a Single Observer in Shallow Water," Journal of Sound and Vibration (1976) 44 (1).
- [8] R. L. Moose, H. F. VanLandingham, D. H. McCabe, "Modeling and Estimation for Tracking Maneuvering Targets," IEEE Trans. on AES, vol. AES-15-No 3., pp. 448-456, May 1979.
- [9] D. H. McCabe and R. L. Moose, "Passive Source Tracking using Sonar Time Delay Data," IEEE Trans. on Acoustic Signal Processing, June 1981.

